NEW METHODOLOGIES FOR MEASURING AND MONITORING NUCLEAR DECAY PARAMETERS FOR TIME DEPENDENT BEHAVIOR

A Thesis

Submitted to the Faculty

of

Purdue University

by

Matthew J. Kay

In Partial Fulfillment of the

Requirements for the Degree

of

Doctor of Philosophy

December 2018

Purdue University

West Lafayette, Indiana

THE PURDUE UNIVERSITY GRADUATE SCHOOL
STATEMENT OF THESIS APPROVAL

Dr. Ephraim Fischbach, Chair

Department of Physics and Astronomy

Dr. Andrew S. Hirsch

Department of Physics and Astronomy

Dr. Virgil E. Barnes

Department of Physics and Astronomy

Dr. Dennis E. Krause

Department of Physics and Astronomy

Approved by:

Dr. John P. Finley

Department Head, Physics and Astronomy

For Willy and Dave.

ACKNOWLEDGMENTS

I woulld like to extend my heartfelt gratitude and appreciation to Ephraim Fischbach but for whom none of this would have been possible. Ephraim is an incredible source of light in an often dark world.

I would like to thank Dr. Virgil Barnes for his insightful contributions and patience, Dr. Dennis Krause for his support, and finally Dr. Andrew Hirsch who with the aforementioned participated on my thesis commitee. I would like to thank Sandy Formica for all her assitance and support with the day to day bureaucracy of graduate school, as well as being a wonderfully kind individual. I am indebted to the NSWC Crane Ph.D. program for its financial support and providing the oppurtunity to return to graduate school and finish my degree.

I would like to thank Jeff Titus for providing guidance and expertise in analog measurement, and for picking up the phone when I call. In addition, I would like thank Lt. Colonel Dan Javorsek Ph.D. for his contributions to this work.

To my parents, I love you. I cannot enumerate all things you have done for me. It has been quite a journey. Finally, Brandi, Aidan, and Noah what you mean to me is ineffable.

TABLE OF CONTENTS

Page

LIST OF TABLES

Table Page

LIST OF FIGURES

Figure Page

Figure Page

Figure Page

SYMBOLS

$t_{1/2}$	half-life for a given radioisotope
e	magnitude of electron's charge
α	alpha particle (^{4}He nucleus)
β	beta particle
$m_{\bar{\nu_e}}$	mass of electron antinuetrino
$\beta^{\pm}$	beta particle emitted as a decay product
λ	nuclear decay paramter for a radioactive sample
d	day
c	speed of light
V_{app}	applied voltage biad
R_{s}	betavoltaic series resistance
R_{SH}	betavoltaic shunt resistance
I_{rs}	reverse saturation current
n	diode ideality factor
A_{pn}	cross-sectional area of the p-n junction
T	absolute temperature in Kelvin
I_{rad}	radiation induced drift current
k_{B}	is the Boltzmann constant
W_t	depletion region width of the of p-n junction
L_p	diffusion length for hole minority carriers
L_n	diffusion length for electron minority carriers
G_{ss}	beatvoltaic conversion efficiency
g	conversion factor for lectron-hole pairs per cubic centimeter per rad (Si)
$\dot{\gamma}_{ss}$	steady state dose rate measured in rad (Si)

E_{convert}	conversion efficiency factor
$\dot{A}_0$	initial activity of beatavoltaic

ABBREVIATIONS

SID	self-induced decay
NIST	National Institute of Standards and Technology
ROI	Region Of Interest
HEB	High Energy Background
DUT	Device Under Test
DIP	Dual Inline Package
PMU	Physical Measurement Unit
EMI	Electromagnetic Interference
ESD	Electrostatic Discharge
UPS	Uninterruptible Power Supply
CAHV	Context of Accepted Half-life Value
MOU	Memorandum of Understanding
APS	Auxiliary Power Supply
RMS	Root-Mean-Square

ABSTRACT

Kay, Matthew J. Ph.D., Purdue University, December 2018. New methodologies for measuring and monitoring nuclear decay parameters for time dependent behavior. Major Professor: Ephraim Fischbach.

In this work new methodologies for measuring and monitoring nuclear decay parameters is explored. A determination of the tritium half-life by measuring the current of a betavoltaic device is presented. The benefits of this approach in exploring the possibility of time dependence of nuclear decay parameters is discussed.

1. INTRODUCTION

In order to understand the value and impact of a scientific work, it is best to have some historical context. The following section will provide a brief overview of the early history of the discovery and study of radioactive materials and the subsequent events that led to the fields of atomic and nuclear physics and the theory of quantum mechanics. Particular attention will then be given to signficant works in the formulation of a theory of beta decay.

2. HISTORY OF RADIOACTIVE DECAY

This historical overview will focus on many of the events taking place near the turn of the 20th centruy, a period of great innovation and achievement. The multitude of experimental discoveries that occurred from 1895 to 1919 laid the basic foundation for our understanding of the basic building blocks of matter. Perhaps one of the first major discoveries during this time is that of Wilhem Röntgen in 1895. Röntgen, while conducting experiments with a "well-exhausted Crookes' or Leonard's tube," often referred today as cathode ray tube, discovered a penetrating agent which he would refer to as X-rays, and his collegues would referred to as Röntgen rays (1). Röntgen would win the 1901 Noble Prize in Physics for his dicovery. The following year in 1896 Antoine Henri Becquerel, while studying phospherescence, discovered what would come to be known as spontaneous radioactivity(2). Becquerel's initial interest was studying the role X-rays, discovered by Röntgen one year earlier, played in phospherescence. Becquerel conducted numerous experiments with photographic plates and various phosphorescent materials. The idea being that the flourescence of the material and these x-rays were related and would develop photographic plates. This was determined not to be the case upon discovering that uranium salts developed the photographic plates in the absence of sunlight. Futher work with various materials containing uranium allowed Becquerel to conclude that emissions from uranium were responsible. Becquerel went on to show that these rays could be deflected by a magnetic field as well as ionized gases. The following year in 1897 J. J. Thompson discovered the electron and made the first measurements of the charge-to-mass ratio of this newly discovered particle (3). The discovery of the electron earned Thompson the 1906 Noble Prize in Physics.

A year after the discovery of the electron in 1897, Pierre and Marie Curie determined thorium produced emissions much like uranium. They went on to discover

the elements polonium and radium while studying the uranium ore pitchblende. It was the Curies who first described the elements of thorium and uranium as being "radioactive." For their investigations of radioactive materials the Curie's shared the 1903 Noble Prize in Physics with Henri Becquerel (4). Madame Curie would eventually go on to win the 1911 Nobel Prize in Chemistry for the discovery polonium and radium.

While J. J. Thompson was studying cathode rays and the Curies were investigating the emissions thorium, Ernest Rutherford, perhaps one of the greatest experimental physicists of the 20th century was begining to lay down much of the framework for our understanding of the radioactivity. The following is a list of the key contributions Rutherford, as well as his collaborator Fredrick Soody, made in the area of radioactivity(8; 9; 10; 11; 12; 13; 16):

- Uranium emits three types of radiation with varying penetrating characteristics which he went to label as α -radiation, β -radiation, and γ -radiation.
- The positive and negative charge was determined for α -radiation and β -radiation respectively, as well as the absence of charge for γ -radiation.
- The elements radium, thorium, and uranium are radioactive and produce new types of matter which are radioactive as well. This leads to the idea of decay chains
- The elements undergo spontaneous transformations to produce new elements, and the energy emitted during these transformations originate from inter-atomic sources as opposed to chemical ones. This emitted radiation characterizes this transformation.
- The rate at which a collection of atoms of a given radioactive element transforms is a fixed fraction of the number of atoms remaining. This fraction is a function

of the radioactive element. This gives rise to the following exponential decay law:

$$\frac{dN}{dt} = -\lambda N \Rightarrow N = N_0 e^{-\lambda t} \tag{2.1}$$

- α- rays are positively charged and are over a 1000 times more massive than that of an electron

- The emission of a α ray or β ray is required during the transformation process.

The begining of the twentieh century saw an explosion of discovery and atomic theory that would provide the foundation for quantum mechanics. In 1910 Rutherford, Hans Geiger, and Harry Bateman studied and developed the mathematical theory of the distribution of the number of emitted particles from a radioactive source for a given time interval. Fredrick Soddy went on to conjecture existence of isotopes in 1911. Two years later Bohr postulated that atoms exist in descrete energy states, which set the stage for Erwin Schrödinger and Werner Heisenberg to develop quantum mechanics in the mid 1920's. The theory was futher development of by Nobel Prize winning Physicists such as Wolfgang Pauli, Paul Dirac, Albert Einstein, Enrico Fermi, and Richard Feynman (4). It is this quantum mechanical framework that serves as the toolset to explore the subatomic processes and phenomena of nuclear decay.

3. OBSERVED TIME DEPENDENCE IN DECAY RATES OF RADIOISOTOPES

Radioactive decay has been shown to follow the exponential decay law regardless of the species of radioisotope. However numerous researchers have observed small periodic fluctations of the order of 10^{-3} riding on top of the familiar exponential decay. Periodicities of approximately 1, 2, 11.7, 12.1, and 13.5 cycles per year have been observed across numerous isotopes with annual periodicities being the most common observed periodicity. These isotopes range in nuclear complexity from ^{3}H to that of ^{239}Pu. These periodicities have been measured using an array of radiation detection devices. The variety of experiments with observed annual periodicity over a range of isotopes may indicate that a common mechanism is responsible for the observed behavior. Whether this common mechanism is systematic error induced by seasonal changes in the environment and instrumentation, or a possible unknown interaction with solar neutrinos and radioisotopes has yet to be determined. Table 3.1 provides list of modern experiments where time varying nuclear decay rates have been observed.

Table 3.1.
Various experiments in which time-dependent nuclear decay rates have been observed (29). For each entry the observed nuclides and their dominant decay modes are exhibited. Observed periodicities in the decay rates are noted.

Isotope	Decay Type	Detector Type	Radiation Measured	Effect/Periodicity Observed	Reference
^{3}H	β^-	Photodiodes	β^-	1 yr^{-1}	(17)
^{3}H	β^-	Liquid Scintillator	β^-	1 d^{-1}, 12.1 yr^{-1}, 1 yr^{-1}	(18)
^{3}H	β^-	Liquid Scintillator	β^-	$\sim$ 12.5 yr^{-1}	(19)
^{3}H	β^-	Solid State (Si)	β^-	$\sim$ .5 yr^{-1}	(20)
^{22}Na/^{44}Ti	β^+, κ	Solid State (Ge)	γ	1 yr^{-1}	(25)
^{36}Cl	β^-	Proportional	β^-	1 yr^{-1}, 11.7 yr^{-1}, 2.1 yr^{-1}	(26; 28; 27)
^{36}Cl	β^-	Geiger–Müller	β^-	1 yr^{-1}	(31)
^{54}Mn	κ	Scintillation	γ	Solar flare	(32)
^{54}Mn	κ	Scintillation	γ	1 yr^{-1}	(33)
^{54}Mn	κ	Scintillation	γ	1 yr^{-1}	(34)
^{60}Co	β^-	Geiger–Müller	β^-, γ	1 yr^{-1}	(35; 36)
^{60}Co	β^-	Scintillation	γ	1 d^{-1}, 12.1 yr^{-1}	(37)
^{85}Kr	β^-	Ion Chamber	γ	1 yr^{-1}	(38)
^{90}Sr/^{90}Y	β^-	Geiger–Müller	β^-	1 yr^{-1}, 11.7 yr^{-1}	(35; 36; 39)
^{108m}Ag	κ	Ion Chamber	γ	1 yr^{-1}	(38)
^{133}Ba	β^-	Ion Chamber	γ	1 yr^{-1}	(40)
^{137}Cs	β^-	Scintillation	γ	1 d^{-1}, 12.1 yr^{-1}	(37)
^{152}Eu	β^-, κ	Solid State (Ge)	γ	1 yr^{-1}	(41)
^{152}Eu	β^-, κ	Ion Chamber	γ	1 yr^{-1}	(38)
^{154}Eu	β^-, κ	Ion Chamber	γ	1 yr^{-1}	(38)
^{222}Rn	α, β^-	Scintillation	γ	1 yr^{-1}, 11.7 yr^{-1}, 2.1 yr^{-1}	(42; 44)
^{226}Ra	α, β^-	Ion Chamber	γ	1 yr^{-1}, 11.7 yr^{-1}, 2.1 yr^{-1}	(26; 44; 27)
^{239}Pu	β^-	Solid State	α	1 d^{-1}, 13.5 yr^{-1}, 1 yr^{-1}	(18)

3.1 ^{54}Mn

Numerous studies and experiments have been conducted at Purdue University with the intent of exploring external influences of nuclear decay parameters. Many of these studies have involved the radioisotope ^{54}Mn. Figure 3.1 exhibits data taken over a four year period monitoring a 1 μCi sample of ^{54}Mn. This plot also contains a plot of the inverse-square Earth-Sun distance. From the plot it can be seen that measured ^{54}Mn count rate data and that of the Earth-Sun distance appear to track one another. The data indicate a correlation with increased count rate and Earth-Sun distance. This trend has been observed and in numerous experiments as discussed by Jenkins et al.(26).

A lead shielded NaI(Tl) crystal detector was used to record the gross count rate within a region of interest (ROI) centered about the 834.8 keV gamma peak emitted from the daughter ^{54}Cr decay. These data were collected in a controlled environment where temperature, humdity, and supply voltage were monitored. Though gross counts were collected within the ROI, the net counts can be determined by taking into account and correcting for background sources such as ^{40}K as well as other contaminants. Systematic detector effects such as dead time, pulse pileup, and cascade summoning were also taken into account(46). A Pearson correlation coefficient, $\rho_{x,y}$, was calculated to determine the likelihood that observed ^{54}Mn count rate and the inverse-square Earth-Sun distance were correlated. The Pearson coefficient has a value between 1 and -1. A value close to 1 or -1 indicates a strong linear realationship between the two varaibles. The calculated Pearson correlation for these two variables is $\rho = 0.4986$, where the Pearson coefficient of correlation is defined in 3.1.

$$\rho_{x,y} = \frac{\sum(x_i - \bar{x})(y_i - \bar{y})}{\sqrt{\sum(x_i - \bar{x})^2(y_i - \bar{y})^2}} \tag{3.1}$$

The probability,$P_N(\rho_0)$, of obtaining a value of ρ_0 for two uncorrelated variables both of with size N is defined in 3.2. The probability that this correlation coefficient could

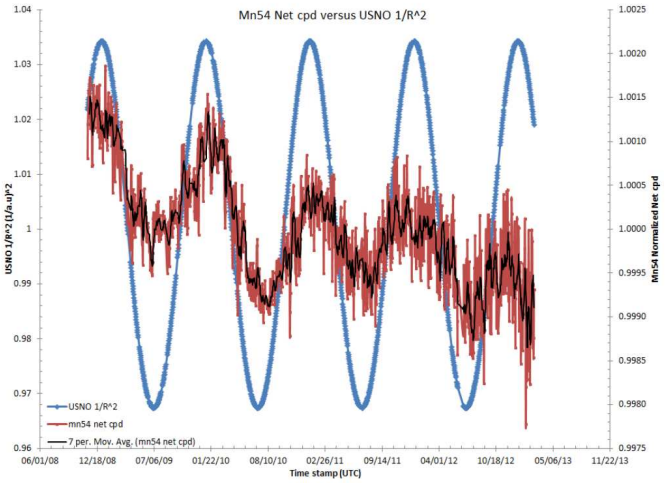

Figure 3.1. Plot of Normalized ^{54}Mn net counts per day and inverse-square Earth-Sun distance ($1/R^2$) versus time illustrating strong correlation of between ^{54}Mn count rate and Earth-Sun distance(46).

arise from uncorrelated data sets is ∼8 x 10^{-89}. Given this extremely low probability, this strongly indicates a relationship between the two datasets.

$$P_N(\rho_0) = \frac{2\Gamma[N-1)/2]}{\sqrt{\pi}\Gamma[(N-2)/2]} \cdot \int_{|\rho_0|}^{1} (1-r^2)^{(N-4)/2} dr \tag{3.2}$$

In 3.2 Γ represents the standard gamma funtion $\Gamma(z)$ where:

$$\Gamma(z) = (z-1)! = \int_0^{\infty} t^{z-1} e^{-t} dt \tag{3.3}$$

3.2 Tritium

A comprehensive review of the half-life of tritium was conducted by NIST in 2000. The recommended value for the half-life of tritium of this review is 4500 ± 8 d, where 8 d corresponds to one standard uncertainty(51). This review does not discuss time-dependent variations observations reported by Shnoll in 1998(18), and Lobashev in

1999(20). There have been additional accounts where periodicities in the decay rate of tritium have been observed since the NIST review(17; 19; 20). Several of these documented observations will be reviewed in the following sections. A discussion of the experimental setup and a sources of systematic error will be addressed.

3.2.1 Shnoll: 1998

Starting in 1955, researchers at M V Lomonosov Moscow State University studying various reaction rates of biological and biophysical processes observed anomalies in the distributions in the reaction rates being measured. These anomalies amount to two to three discrete values in the historgrams of reactions such as the hydrolysis of the muscle proteins: myosin and actomyosin. Further studies over the course of 25 years were conducted in order to determine whether these anomalies were the cause of some trivial effect of the measurement or perhaps systematic error. After this period of study, the nature of the observed discrete states was believed to be of nontrivial, universal nature. By 1983, the focus of the experiments had moved from a biological focus to that of that of a physical one. At this time the radioactivity of numerous radioisotopes were studied. The beta emitters studied include ^{3}H, ^{14}C, ^{32}P, ^{60}Co, and ^{204}Tl. The electron capture reaction of ^{55}Fe to ^{55}Mn was studied as well. However the majority of the data taken were derived from measurements of the alpha decay of ^{239}Pu. The studies were carried out using numerous radiation detectors such as Geiger counters, liquid and solid scintillation counters, as well as solid state detectors. Numerous detector types were used in order to verify that the observed distribution anomalies were not an artifact of a specific measurement technique. Sources of systematic error in the measurement process were studied in order to determine whether such sources were responsible for the observed discrete states in the distribution of the decay rates being examined. These studies consisted of control experiments to address ambient temperature, power surges, amplitude cutoff regime, and other potential measurement artifacts. Great efforts were taken to varify

the repeatability of these observations as well as understand how these observations could have gone unnoticed:

> It ought to be noted that the phemonenon in question does not contradict any 'fundamentals of science'. In particular, the stochastic nature of radioactive decay and its compliance with Poisson statistics are not questioned. It is only that the existing criteria of validity are insensitive to the fine structure of the distributions. For this reason, the conclusion regarding the regularity of discrete distributions especially clearly follows from the detailed similarity of the shapes of histograms obtained independently in different series of measurements. We have observed such similarity of histograms for simultaneous independent measurements of quite different processes in laboratories sometimes separated by hundreds and thousands of miles(18).

Further investigations showed that the shapes of the histograms exhibited periodicites of 24 hours, 27 days, and 365 days. The researchers conclude that their observations "point to the existence of a universal cosmophyiscal (cosmogonic) cause of this phenomenon." Unfortunately, Shnoll et al. do not provide histrograms generated from experiments investigating tritium. Shnoll implies the provided histrograms are representative(18).

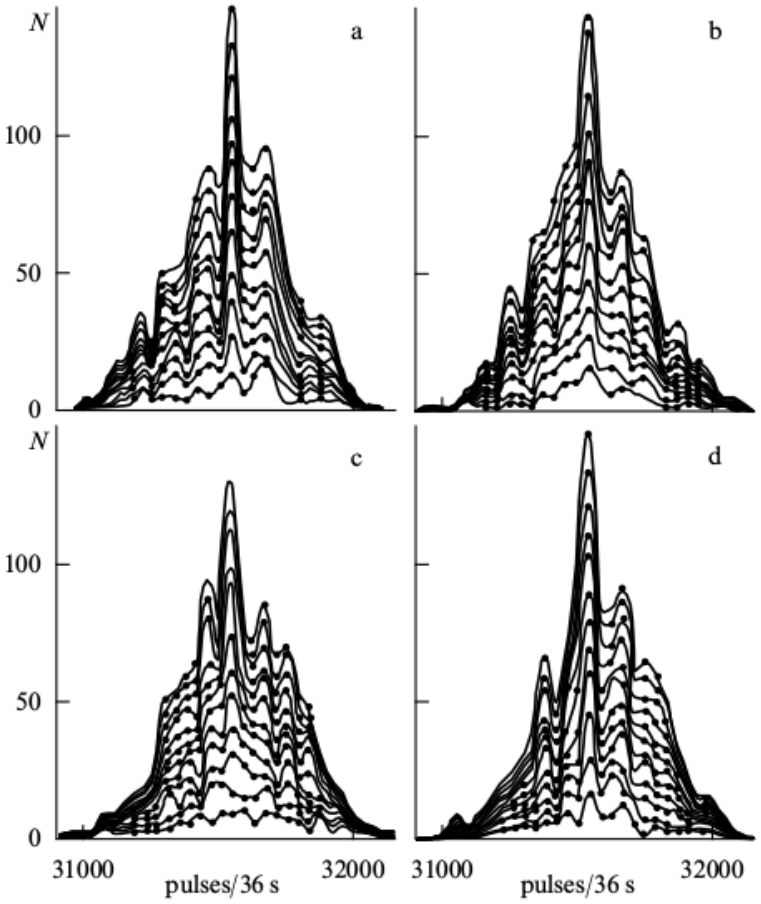

Figure 3.2. Example a histogram generated by Shnoll et al. exhibiting unexpected discrete states and non-randomness in the activity measurements of ^{55}Fe(18).

3.2.2 Lobashev: 1999

Between 1994 and 1998 a series of experiments were conducted at the spectrometer facilities at the Nuclear Research of the Russian Academy of Scineces in Troitsk, Russia to obtain an upper bound on the electron anti-neutrino mass, $m_{\bar{\nu_e}}$. In this experiment an integral magnetic electrostatic spectrometer was used to perform electron energy spectroscopy near the tritium beta decay endpoint energy, 18.00 KeV to18.77 KeV. The spectrometer is designed to create a "magnetic bottle" in order to adiabatically guide the betas to the $Si(Li)$ solid state counter. Energy spectroscopy was performed by varying the spectrometer stopping potential in steps. The direction of the of the high voltage source scannning for the stopping was reversed each cycle (1-2h) in the voltage range of 18.00 to 18.77 kV (20).

An anomalous energy step was observed 5-15 eV below the tritium decay end point energy. This energy step or "bump" was varied periodically with a frequency of .5 yr^{-1}(20).

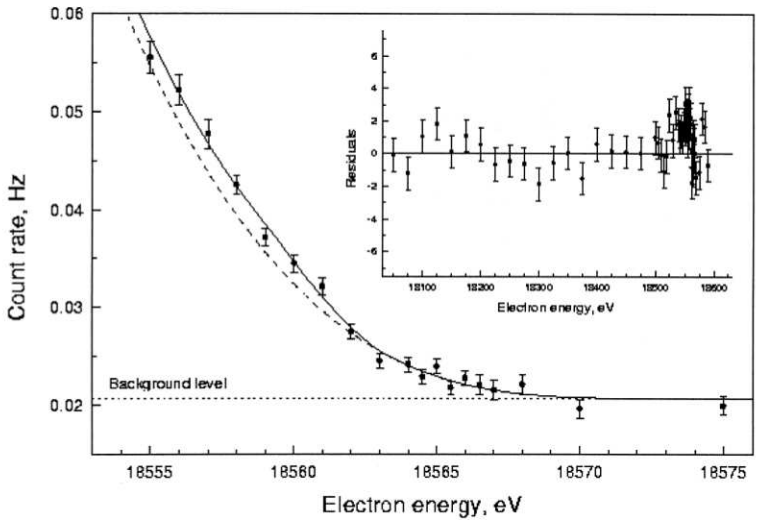

Figure 3.3. Observed step in the tritium beta spectrum near the beta end point energy

Great care was taken to address sources of systematic error. Deadtime, pulse pileup, drift in source intensity affecting detector spectrum loss, and tritium decay occuring within the spectrometer. Additional sources of systematic error such as the observed asymmetry in the spectrometer response to voltage scanning direction and some "plasma-like effects in the spectrometer" also contribute to the overall systematic error but require further investigation. The authors, however, do not believe the observed anomaly can be explained solely by the presense of systematic error.

The authors note that the 0.5 yr^{-1}periodicity of the energy step is perhaps consistent the earth moving through a "cloud" of cosmological neutrinos, and that the energy step near the beta endpoint energy is due to unknown capture mechanism of cosmological neutrinos by tritium atoms. This capture is then accompanied with the emission of monochromatic electrons. Despite the speculative nature of this explanation, the observed energy step may provide evidence of an unknown neutrino capture mechanism (20). Finally, one interesting aspect of the discussion provided

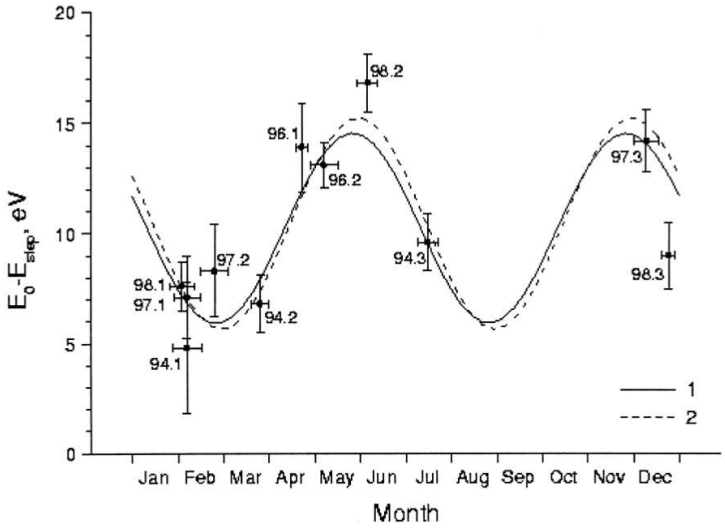

Figure 3.4. Periodic variation of the observed tritium decay end point energy in the Troitsk neutrino mass experiment

by the authors is that the absence of continous measurement allows for the fitting of

more complicated periodic funcitons to the data set. This raises the question of the overall merit of these fits in the absence of data, and therefore makes any conclusions and inferences suspect. This concern elucidates the value for experiment where the activity of the radioisotpe of interest is monitored continously.

3.2.3 Falkenberg: 2001

Starting in the Fall of 1980 to the spring of 1982, Eckhard Falkenberg used "a strip of phosphorescent material containing tritium [that] was placed in front of an array of photo diodes" to study the longterm behaviour of ^{3}H decay. The intent of the experiment was to explore the notion of Nikola Tesla's that radioactive decay was induced by small particles(45). The currents from the photo diodes array was summed, amplified, low-pass filtered, and displayed with 3.5 digits of resolution. This experiment ran for a total of 553 days where 73 measurements taken at approximately a rate of one measurement per week. The experimental setup was designed and characterized in order to address systematic sources of error associated with the current measurement. Steps were taken to address both environmental and electrical sources of systematic error. The diode array and the source were placed in a light and air tight container the temperature of which was controlled by PID temperature controller. The temperature of the setup as held at 23.0 °C with a long-term variation of ± 0.08°C. The entire apparatus was placed in basement which "almost" made the experiment independent of seasonal changes. Falkenberg claims that the overall noise and long term drift contribution is approximately $\pm$ 0.01% of the overall measurement. It his analysis Falkenberg used 12.35 years for the half-life of tritium.

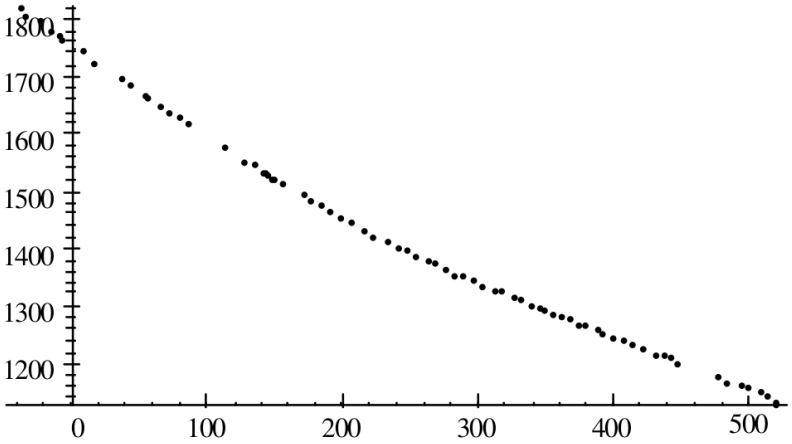

Figure 3.5. Raw experimental data of the decay rate of ^{3}H taken by Falkenberg

In addition to the exponential decay of the tritium, Falkenberg took into account the degradation of the phosphorescent material using:

$$A_o(t) = be^{-\lambda t}e^{-(1-e^{-ct})}, \tag{3.4}$$

where λ is the half-life of tritium and b and c are fit parameters with c reflecting the phosphorescent degradation effects. Falkenberg observed an approximate peak

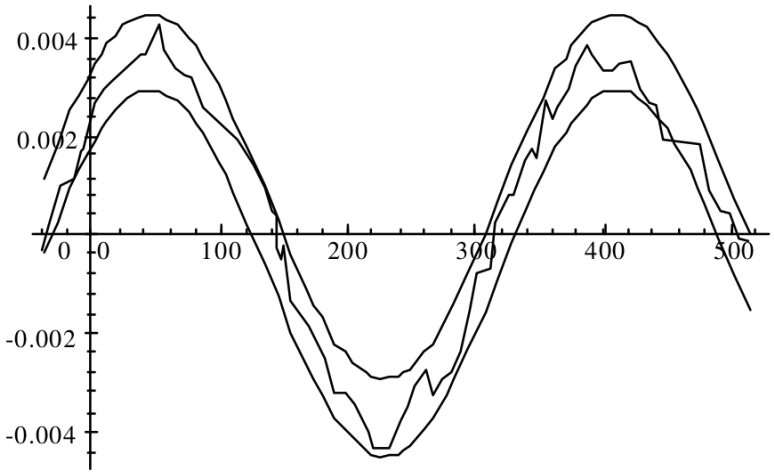

Figure 3.6. ^{3}H decay rate data detrended by Falkenberg illustrating seasonal dependence

amplitude with an approximate period of 365 days. Falkenberg speculates that if the sun was the only source of neutrinos, then one would expect a peak amplitude of $\pm 3.3\%$ due to the variation in solar neutrino flux induced by the ocillatory earth-sun distance. This experiment highlights the need to address potential sources of systematic error, which is critical for any experiment to be conducted over an extended period of time.

3.2.4 Veprev: 2012

Tritium beta decay was studied by the Karpov Institute of Physical Chemistry in Moscow, Russia. The source used was a "$\sim$1 uCi activity produced by VNIMP

(Russia) was the radionuclide solution in the toluene scintillator (ZhS-8) located in the quartz flask of 28mm diameter and 65nm height." The measurements were carried out at the Beta-2 facility which consists of three photomultipliers arranged at an angle of 120° to one another in a horizontal plane. The photocathodes were mounted in holes of cylindrical fluorplastic reflector in which the sample was placed. Lead bricks were used to reduced background as well the use of multiple correlation processing in order to reduce parasitic effects. This approach used both signal amplitude and time correlation of the pulse as means to reduce background. The Beta-2 analyzer consists of two channels for measuring both ^{3}H and ^{14}C activities. The second channel was used to measure the high energy portion of the tritium spectrum which counted pulses with a multichannel PCI-ADC built into the monitoring PC running Spectraline software. This setup was used to study the time dependence of tritum over the course of days, weeks, and months. Measurement were performed over two separate periods in 2008 one measured in August through September and the other conducted from October to December of the same year(19).

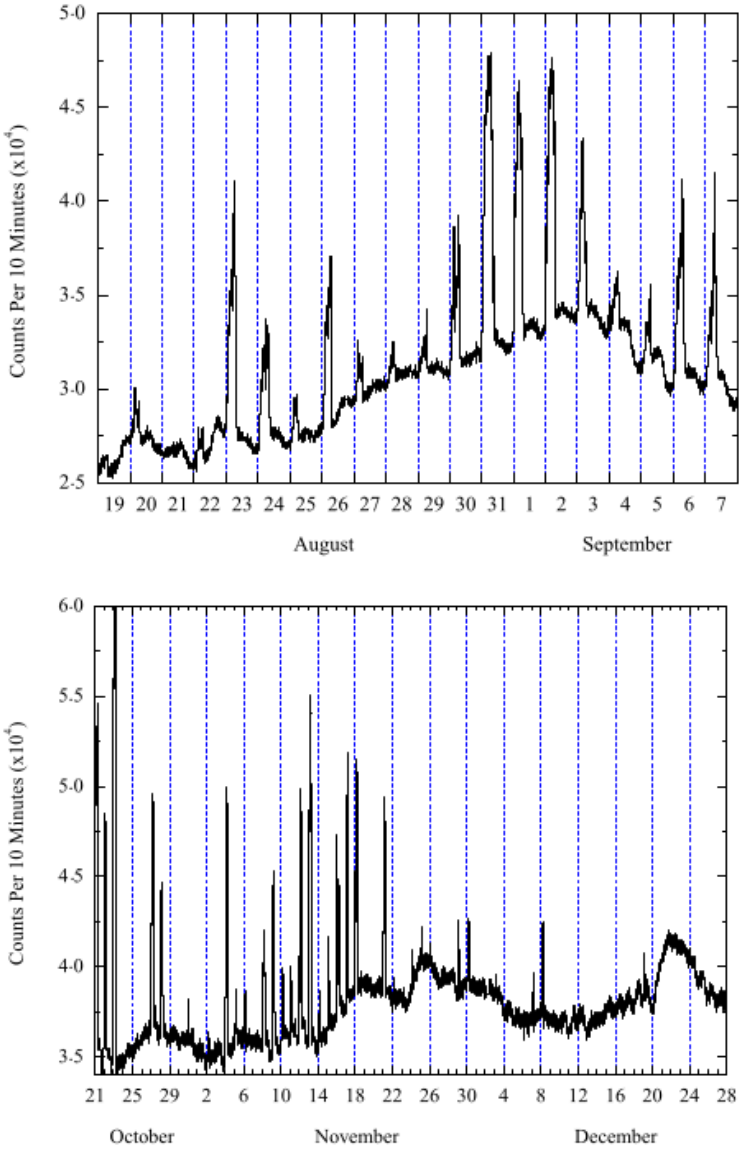

Figure 3.7. ^{3}H decay rate data exhibiting a daily periodicity in the measured count rate.

A strong day-night dependence as well as 27 day periodicity was observed in the counting rates. The fractional change varied from day to day but a max change of 60% was observed between day and night counting rates. A 22% fractional change with a 25 day period was observed during the August-September timeframe and a 11% fractional change with approximately a 27 day period was observed during the October-December timeframe.

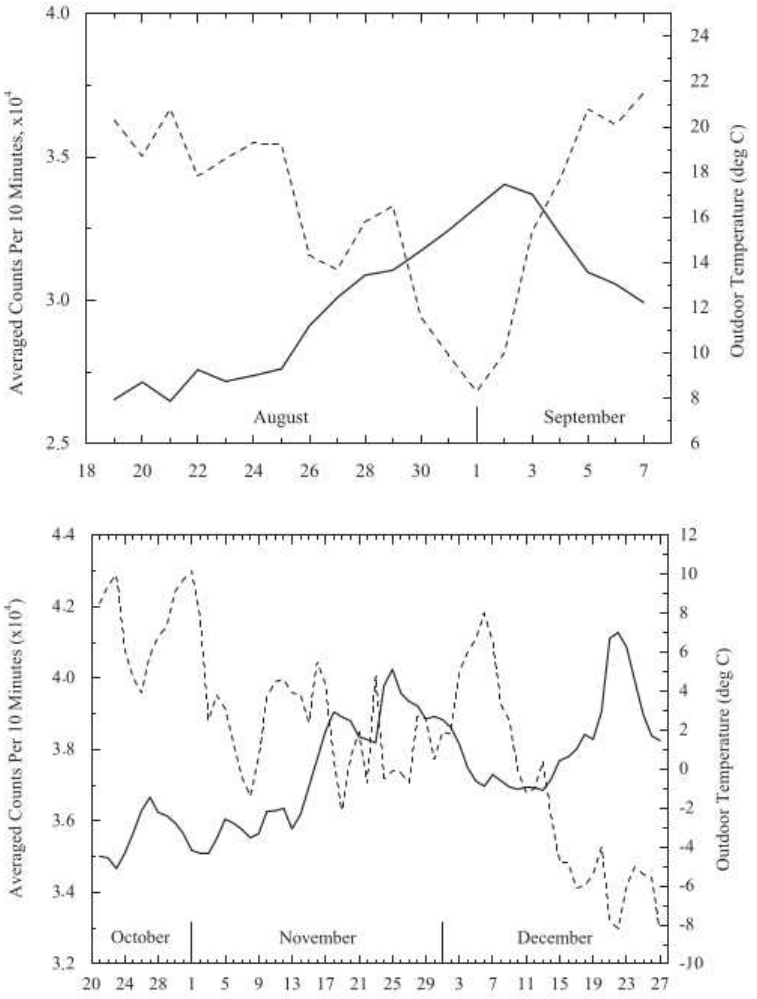

Figure 3.8. ^{3}H decay rate data detrended by Falkenberg illustrating seasonal dependence

A short discussion of seasonal temperature effects on the experimental setup was provided. The outdoor temperature appears to be anticorrelated to average counts

rates. The authors point out that the counting rate minimum and temperature maximum and vice-versa do not coincide, however no discussion is presented regarding delay or phase. The possible influence of solar neutrinos is mentioned given the 27 day periodicity observed in the data, and various solar system behaviors observed to have a similiar periodicity.

4. Γ-CELL ROOM ^{54}Mn EXPERIMENT

4.1 Experimental Setup

A preliminary experiment utilizing the the electron-antineutrino flux generated by the decay of two Co-60 sources at NSWC Crane was performed in the spring of 2016. Figure 4.1 shows the room layout where the experiment was conducted. The experiment consisted of moving a pair of lead shielded Bicron 2 x 2-inch NaI(Tl) crystal detectors and a 5 microrcurie Mn-54 source between two locations within the NSWC Crane irradiator room. The room contains two large Co-60 sources with the ratio of source strengths being a factor of 5. The Co-60 generated neutrino flux at the γ-cell position is roughly 2-3$\times$ 10^{10} $\bar{\nu}_e/cm^2s$ compared to the solar neutrino flux of 7$\times$ 10^{10} $\bar{\nu}_e/cm^2s$ which varies by approximately 7% from perihelion to aphelion. The Co-60 generated neutrino flux at the door location is roughly 1-2$\times$ 10^8 $\bar{\nu}_e/cm^2s$.

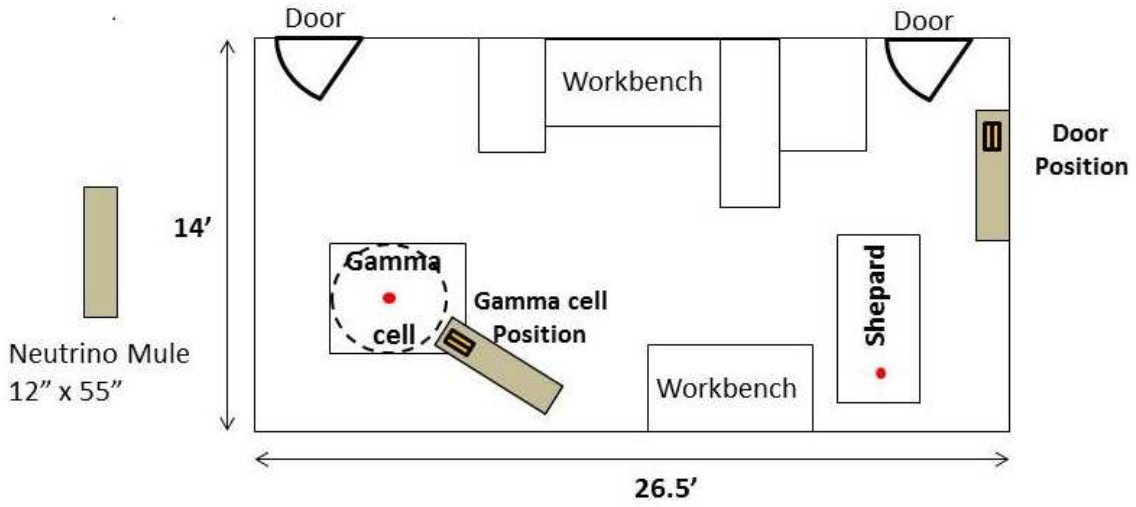

Figure 4.1. Layout of Irradiator Room

The intent of the experiment was to determine if the electron capture rate of ^{54}Mn can be directly perturbed by varying the neutrino flux exposure. In the event neutrinos can perturb the electron capture rate of ^{54}Mn, a step in the measured count rate of the 834.8 keV gamma associated with the reaction would be observed given numerous assumptions regarding the experimental setup. These assumptions include but are not limited to the size of the effect, the sensitivity of the experimental setup, and the ability to account for and minimize sources of systematic error. Figure 4.2 shows the mobile experimental setup consisting of the wooden dolly referred to as the "Neutrino Mule," the lead shielding cave containing a pair NaI(Tl) detectors with Ortec PMT bases with preamplifiers, and the control laptop computer which runs the Maestro32 MCA software version 7.01 for conducting gamma ray energy spectroscopy. The

Figure 4.2. Neutrino Mule at door position (low neutrino flux) with computer running the Ortec Maestro

second location, the γ-cell irradiator position, can be seen in figure 4.3. Markings were placed on the floor at both locations in order to aid in reproducibility of mule orientation and position.

Figure 4.3. Neutrino Mule at γ-cell irradiator position (high neutrino flux) with lead shielding cave

A critical aspect to the success of any experiment is the ability to thoroughly characterize and take into account sources of error. This experiment relies heavily upon the sensitivity and accuracy of counting ^{54}Mn decays via the detection of the 834.8 keV gamma from de-excitation of ^{54}Cr. A representative spectrum from a 1800 seconds capture run can be seen in figure 4.4. The main peak centered at channel 600 is the 834.8 keV gamma peak associated with the ^{54}Cr de-excitation. To the left of this peak can be seen the Compton scattering continuum with smaller peak riding upon it. The peaks correspond to the backscatter and characteristic X-ray peaks created primarily by the materials surrounding the NaI(Tl) detector, which in this setup is predominately lead. An excellent treatment of the myriad of radiation effects taking place within the detector and resulting spectrum can be found in Knoll (47). An important contribution to spectrum is that of the background radiation. Taking into account the background contribution within the region of interest (ROI) of the 834.8 keV peak is needed in order to increase accuracy and sensitivity of the overall

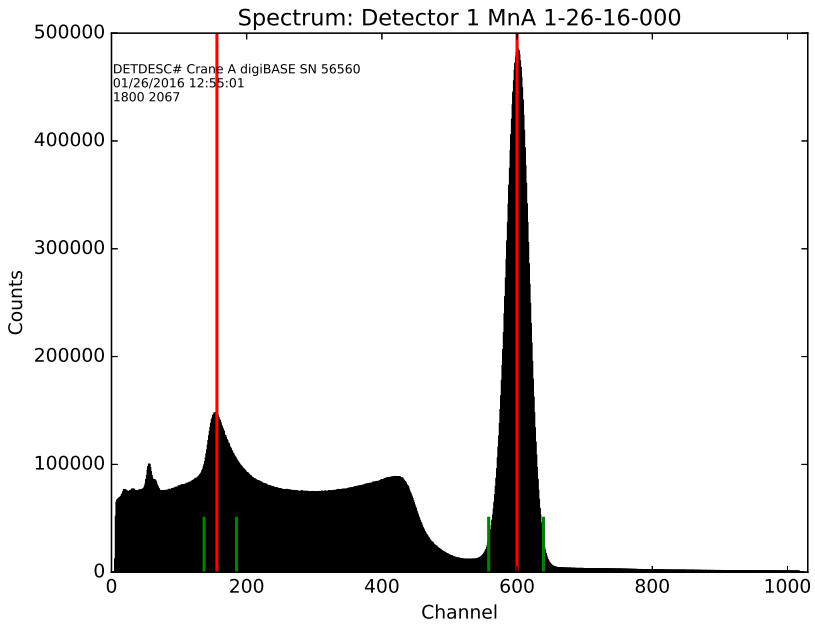

Figure 4.4. Typical gamma ray spectrum from a 1800 seconds run monitoring the 5 microcuire ^{54}Mn source.

experiment. A background characterization study was performed at both the door and gamma-cell positions. This study is discusssed in the following section.

4.2 Background Characterization

The background contribution within the ROI acts as an interference as well as source of error. The ROI in this case is defined as channel 560 to 640, which is marked by green vertical lines in figure 4.4. The gross counts for this ROI ranged from 15.6×10^6 to 19.5×10^6 for the two NaI(Tl) detectors used in this experiment. The ability to maintain this ROI in a consistent, stable manner in order to measure the counts within is necessary for the reduction of systematic error. Environmental conditions such as temperature can affect the electronics associated with the ORTEC PMT base, preamplifier, and any other electron is associated with the detector system. These environmental effects will present as shifts in detector operation parameters such as detector gain, ADC response, and the applied high voltage. The MAESTRO-32 MCA

software by ORTEC attempts to account for variation in the detector electronics response over time and environmental effects by means of a gain stabilizer feature within the MAESTRO software. The feature works by having the operator choose a spectrum peak of interest, in the case of this experiment the 834.8 keV peak, and set the corresponding spectrum channel. Channel 600 was set as the 834.8 keV for this analysis. Once the channel is set, the software with automatically make coarse and fine adjustments of the detector gain in order to keep the peak of interest at the assigned channel. This feature aids in maintaining the ROI in a consistent, stable manner(48).

Representative background spectra for both the door and gamma-cell position can be seen in figures 4.5 and 4.6 respectively. There are a few things to note with regards to these background spectra. The first is that the background is approximately 15 times greater at the gamma cell position than at the door position. Second, the background spectra are absent any peaks near the ROI. The peak present at around channel 50 provides minimal benefit given it is relatively far removed from the ROI.

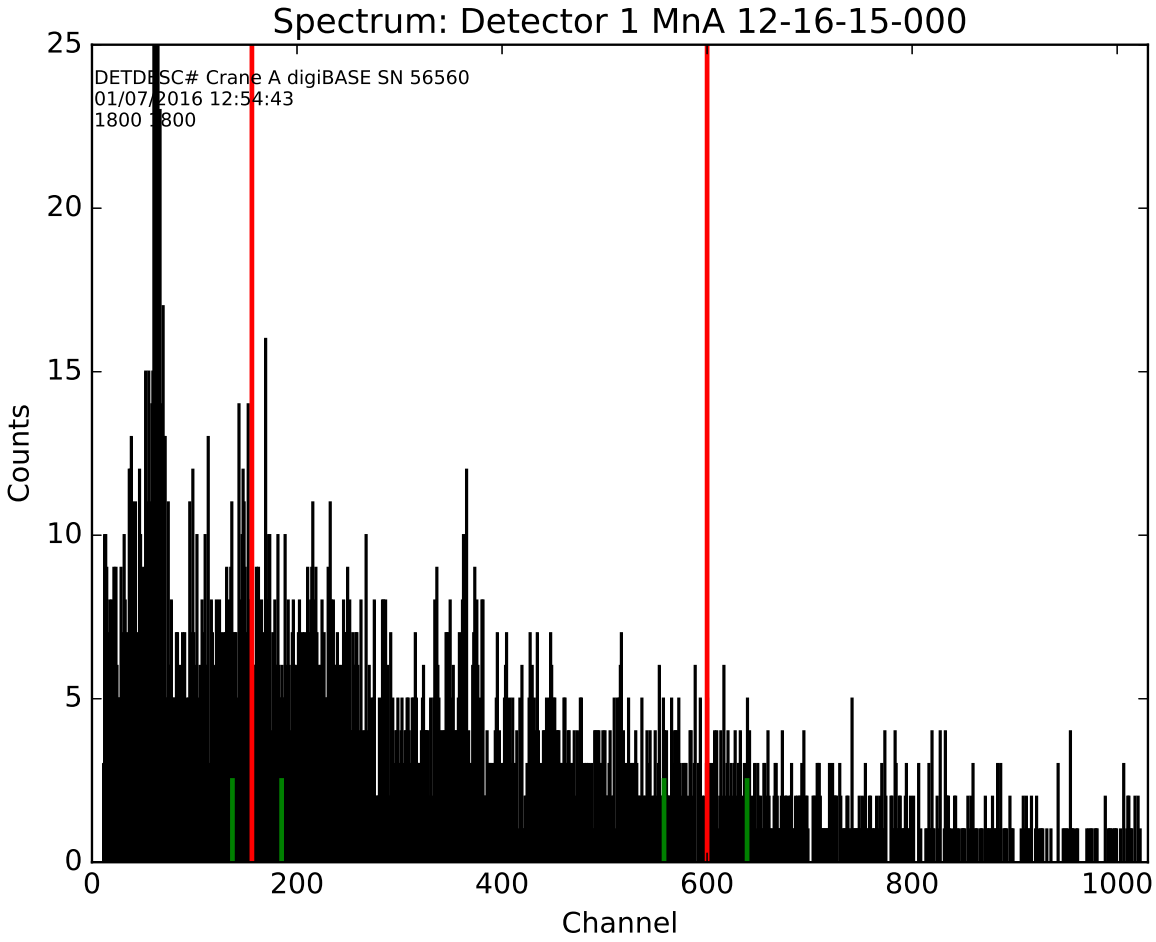

Figure 4.5. Typical gamma ray spectrum from a 1800 seconds run monitoring the background at the irradiator room door position.

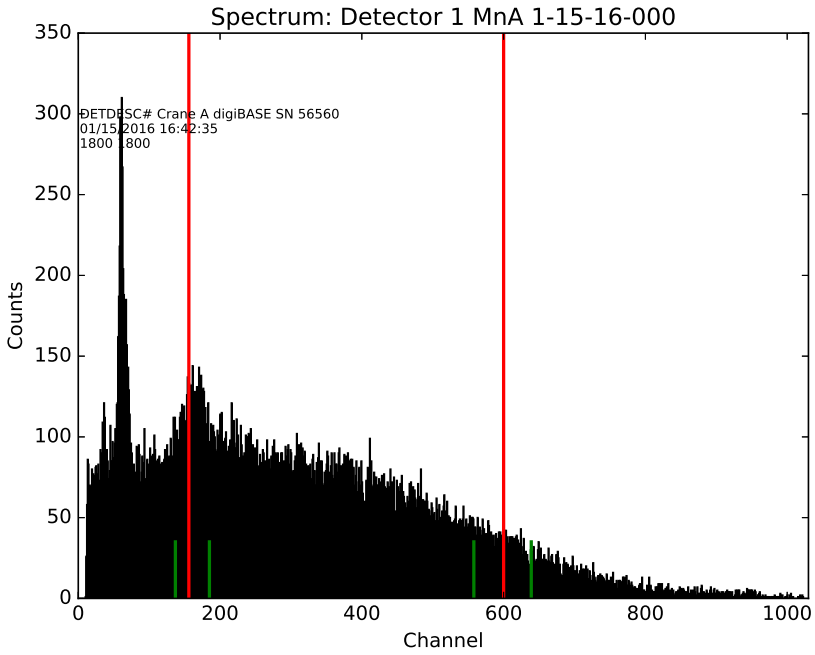

Figure 4.6. Typical gamma ray spectrum from a 1800 seconds run monitoring the background at the gamma-cell position.

The absence of any distinct peaks near the ROI eliminates the use of gain stabilization for background studies carried out over an extended period of time. Background is expected and often assumed to be constant over time. In order to confirm this assumption for this setup, an understanding of detector drift over time was required. The drift study consisted of conducting an initial calibration of both detectors using the 5 microcurie ^{54}Mn source and 834.8 keV characteristic peak. The source was then removed and the two detectors were allowed to run continous for approximately 9 days. The collection period was broken into approximately 475 collection runs of 1800 seconds. Throughout this period the ^{54}Mn source was placed in between the detectors and spectrum channel associated with characteristic peak was recorded. The 834.8 keV peak drift over the 9 day period for both detectors can be seen in figure 4.7. The two detectors did not experience drift at the same rate, but both exhibited an

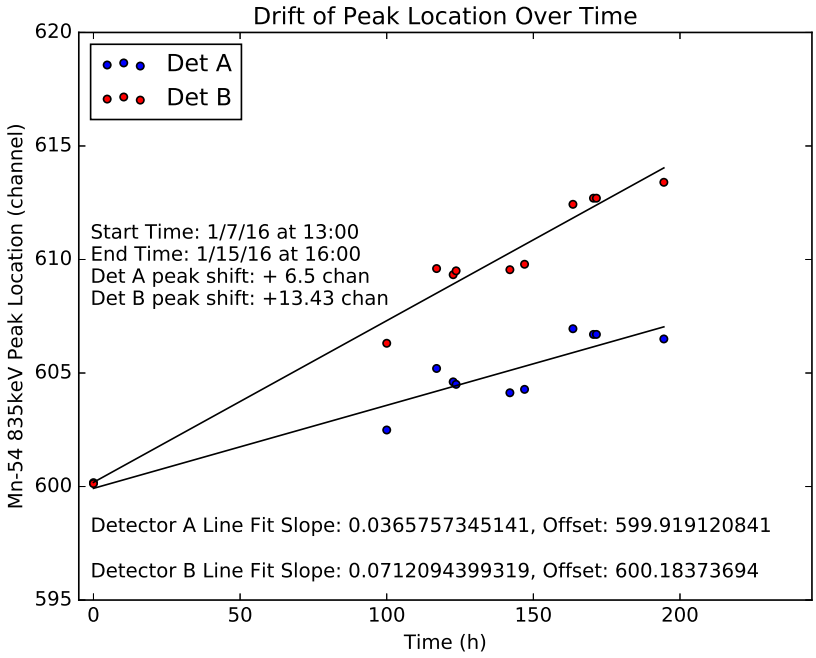

Figure 4.7. Drift of Mn-54 Peak over a total of 8 days

overall linear behavior with respect to time. The fit parameters from the drift study were then used to calibrate background data taken over a week long a period at the gamma cell postion. Calibrated and uncalibrated data taken for both detectors can

be seen in figures 4.8 and 4.9. The linear dirft can be seen in the uncalibrated data for both detectors, as well as an overall flat response in the corresponding calibrated data. The conclusion of this study resulted in the values found in table 4.1 of ex-

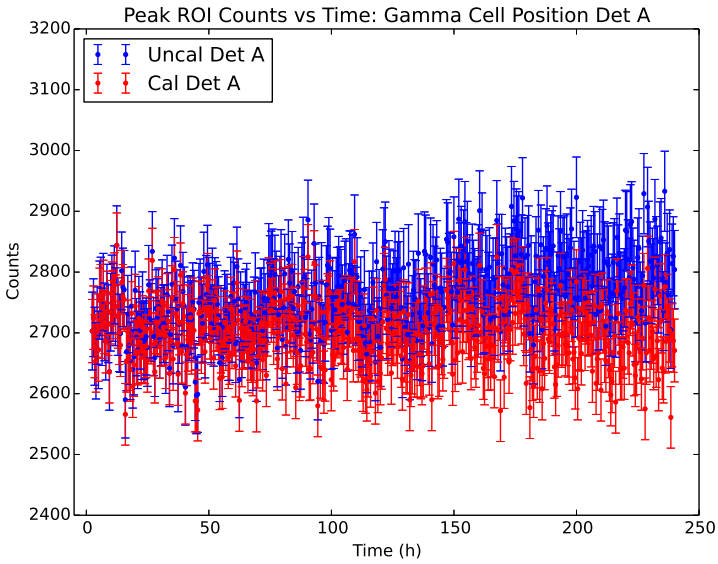

Figure 4.8. Detector A corrected background counts using linear fit parameters from drift experimenunt.

pected background count contributions to the ROI for both detectors. The typical peak signal counts within the ROI and statistical error are presented as well to provide a reference of scale. The two detectors were assigned the arbitrary designations of "Detector A" and "Detector B."

Table 4.1.
ROI Signal and Background Counts: Det A - Det B

Counts $\pm\sqrt{Counts}$	Detector A	Detector B
Background Door	183 ± 10	153 ± 12
Background Gamma	2776 ± 53	2701 ± 52
834.8 keV Signal	19.535 x 10^6 ± 4 x 10^3	15.587 x 10^6 ± 4 x 10^3

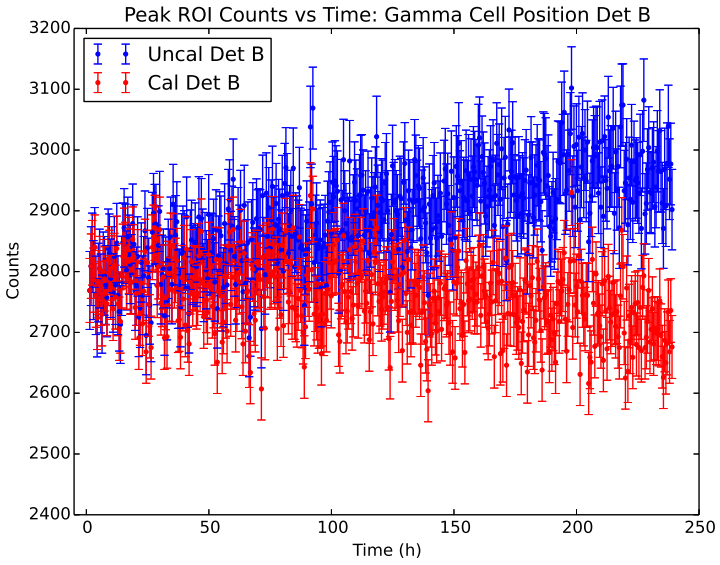

Figure 4.9. Detector B corrected background counts using linear fit parameters from drift experimenunt.

4.3 Transition Experiment

In 2016 three experimental trials were conducted with each trail lasting approximately 24 days. During each trial the neutrino mule moved to either the door or gamma cell position and allowed to collect data for 2 to 3 days. At the end of this data collection period the mule was then carefully moved to the opposite location for 2-3 days. This process was repeated until a thousand 1800 second collection runs were captured. The first trial was initiated on January 26th, the second on February 25th, and the third on April 11, 2016. The dead time for detector A(B) at beginning of the experimental trials was approximately 14.0% (12.3%) and had reduced to 11.7% (9.7%) by the end of the third trial. The two detectors used for the experiment can be seen in figure 4.10. The detectors were held together via hose clamps in order to keep the detector-source orientations as rigid as possible. The ^{54}Mn source was placed in between the two detectors on top of a nickel notched plate which aided once again in maintaining stable detector-source orientations. Though care was given to

Figure 4.10. NaI(Tl) detector pair orientation loacted within the lead shielding cave atop of the neutrino mule.

make the source location as symmetric as possible with respect to both detectors, it is likely the small asymmetries in the detector orientationsthat account for the observed differences in dead times. Temperature, pressure, and relative humidity were moni-

tored during the experimental trials using a Thermo Recorder TR-73U environmental monitor unit.

4.4 Transition Experiment Results

4.4.1 Trial 1

A second trial was initiated on the 26th of January 2016 and completed on the 19th of February 2016. The results of the first transition experiment trial for both detector A and detector B can be seen in figure 4.11 and figure 4.12 respectively. These figures contain two data sets which include the normalized ROI counts and the sum of the spectrum counts on the high energy side of the ROI. The sum counts of high energy side of the ROI serve as a clear indicator of the mule location and the tranisitions between locations. As mentioned before, the gamma-cell location's background is approximately 15 times greater than the door location. This background is dominated by the large amount of ^{60}Co present in the gamma-cell. Given that the ROI is centered about 834.8 keV and the beta decay of ^{60}Co has two characteristic gammas at 1.17MeV and 1.33MeV, the high energy back (HEB) region right of the ROI should be strongly modulated by mule position. The observed data reflects this fact. The exponential behavior of the ROI data sets are detrended using a 297 days for detector A data and 300 days for detector B. These values are roughly in the neighborhood of the accepted value of 312.12 days(49). The reason for this discrepancy is due to the error associated with the dead time correction made by Maestro-32 software. The error associated with the dead time compensation varies over time and is discuss in detail by Nistor(30). The background ROI counts found in table 4.1 are subtracted from the ROI for detector and mule location. A twenty five point average of the two data sets is plotted in order to observe overall data set trends. The detector A data appears to indicate modulation of the ROI counts as a function of mule position and therefore potentially anti-nuetrino flux. The "near" and "far" labels for the various regions in figure 4.11 correspond to the gamma-cell and door positions respectively.

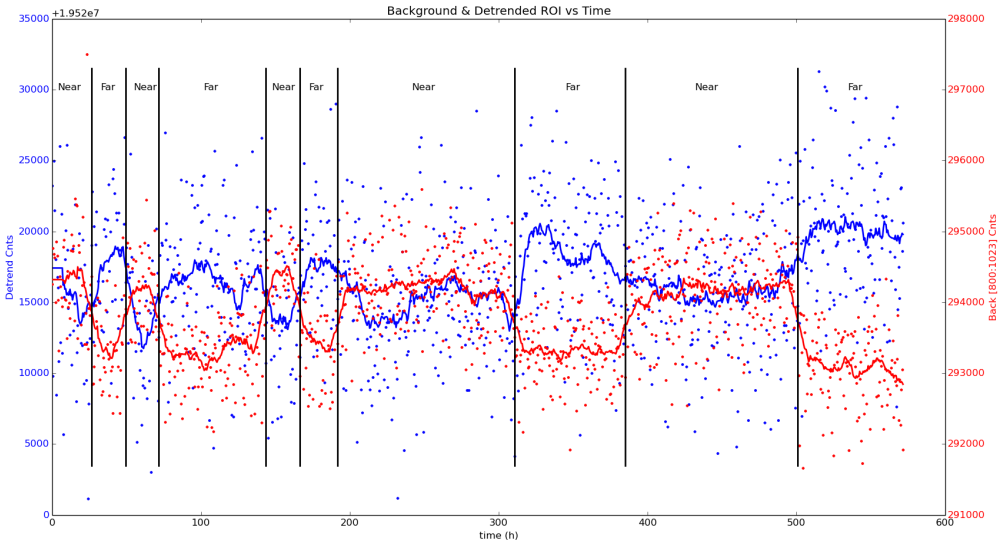

Figure 4.11. Trial 1 transition data from detector A with normalized high energy background and ROI counts.

If this modulation was indeed an indication of some mechanism affecting the electron capture rate of ^{54}Mn, it appears that the close proximity of the ^{54}Mn source to the large ^{60}Co source reduces the observed count rate. This effect is opposite that of other experiments where time dependence in nuclear decay parameters have been reported (26; 31; 46). Unfortunately, this same modulation is absent in detector B dataset. There also appears to be additional structure to both data sets which could indicate environmental effects.

4.4.2 Trial 2

A second trial was initiated on the 25th of February 2016 and completed on March 20th 2016. The results of the second transition experiment trial for both detector A and detector B can be seen in figure 4.13 and figure 4.14 respectively. In the second

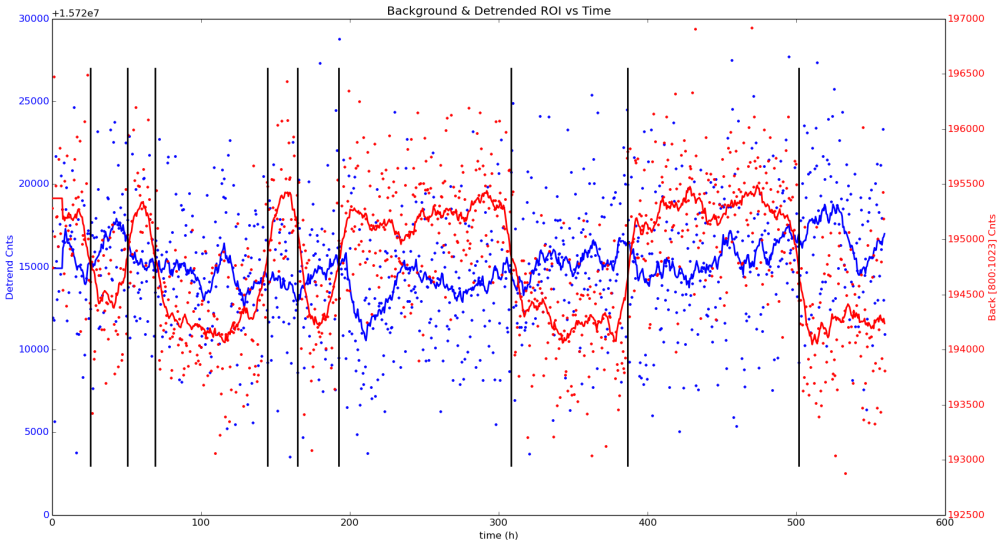

Figure 4.12. Trial 1 transition data from detector B with normalized high energy background and ROI counts

trial a slight modulation of the ROI counts can be seen in the detector A data set and its behavior is again opposite that of previous ^{54}Mn reported data(46).

4.4.3 Trial 3

A third trial was initiated on the 11th of April 2016 and completed on May 4th 2016. The results of the third transition experiment trial for both detector A and detector B can be seen in figure 4.15 and figure 4.16 respectively. The results from detector A for trial three is consistent with results from the previous two trials. However, with regards to detector B a discontinuity in the observed data appears approximately halfway through the trial. This is likely due to a shift in the the NaITl 2" x 2" scintillator crystal caused by a mechanical shock to the system. This could have happened by bumping the front of the neutrino mule into the gamma-cell.

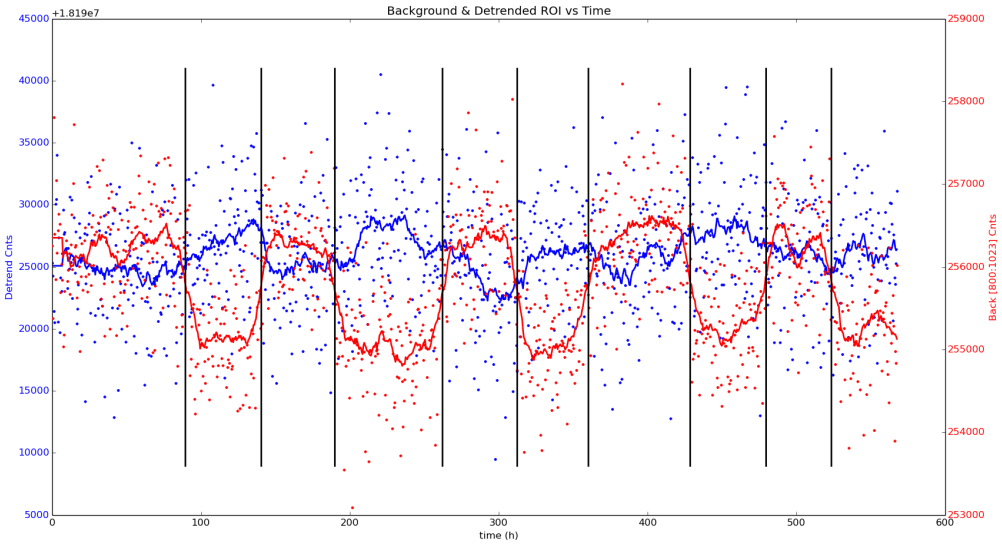

Figure 4.13. Trial 2 transition data from detector A with normalized high energy background and ROI counts.

Given the lack of consistency between the two detectors and the presence of this discontinuity futher analysis of the data has not been conducted.

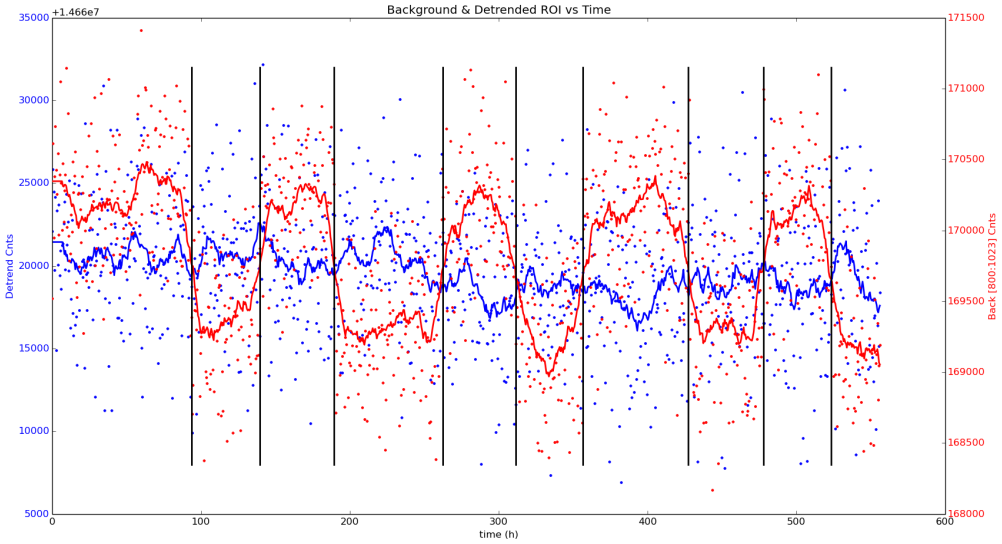

Figure 4.14. Trial 2 transition data from detector B with normalized high energy background and ROI counts.

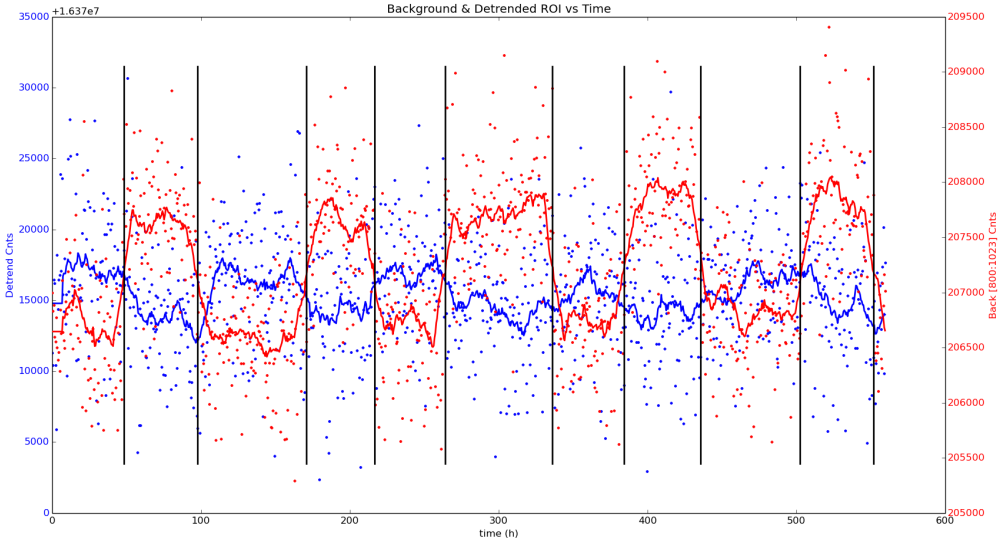

Figure 4.15. Trial 3 transition data from detector A with normalized high energy background and ROI counts.

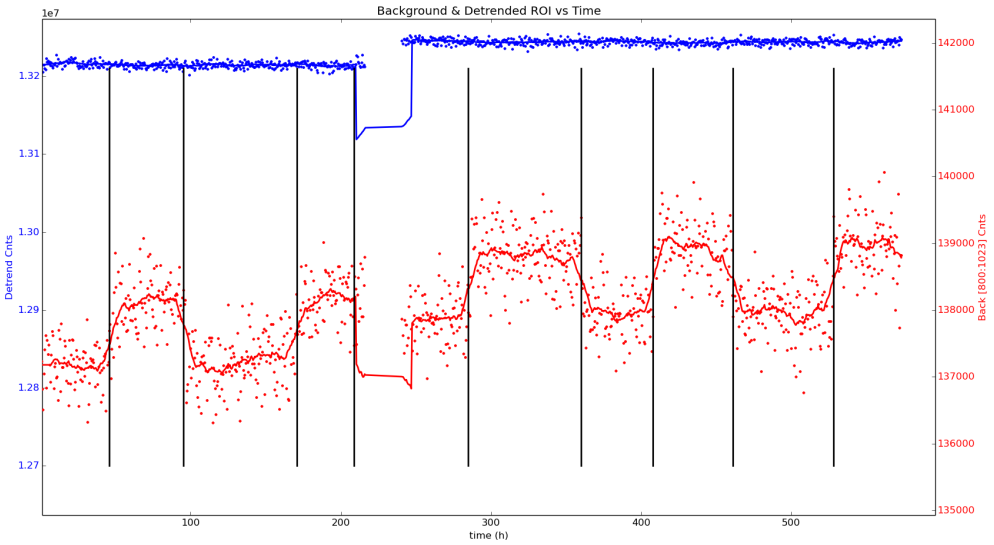

Figure 4.16. Trial 3 transition data from detector B with normalized high energy background and ROI counts.

4.5 Discussion of Results and Sources of Error

The results from the transition experiment trials are inconclusive with regards to observing a position dependence on the observed decay rate of the ^{54}Mn source. As seen in Table. 4.1, the expected signal counts range from approximately 15 to 20 million counts. The associated statistical error is of the order of 4000 counts. This equates to an approximate fractional statistical error of $2 \cdot 10^{-4}$. This value maybe sufficient to reliably detect an effect of the order 10^{-3} but unlikely for smaller effects. This is assuming that the total contribution from sources of systematic error are of the same order of magnitude or smaller. The following sections discuss some of the known sources of systematic error with in the transition experiment setup.

4.5.1 Environmental Effects

The ambient environment was not controlled for the transition experiments trials. Figure 4.17 illustrates the variation in ambient temperature during first trail of the transition experiment to range from 20 to 23$^{\circ}C$. The coefficient of thermal expansion for NaI is 47.3×10^{-6} per degree Celsius. As the crystal expands the solid angle subtended from the source expands resulting in an increased count rate. The solid angle is proportional to the cross-sectional area of detector. A three degree increase of temperature would amount to an approximate fractional change of 2.7×10^{-3} which is likely larger than the targeted effect attempted to be measured. The effect of temperature on the setup can have a significant impact the observed count rates and most be controlled in future experiments.

Figures 4.18 and 4.19 illustrate the variation of relative humidity and barometric pressure during the first trial. The relative humidity ranged from 20 to 70% over the course of the experiment. The barometric pressure ranged from 970 to 1070 hPa over the course of the experiment. The possible effects of humidity and barometric pressure are not as clearly understood as those associated with temperature. Regardless of

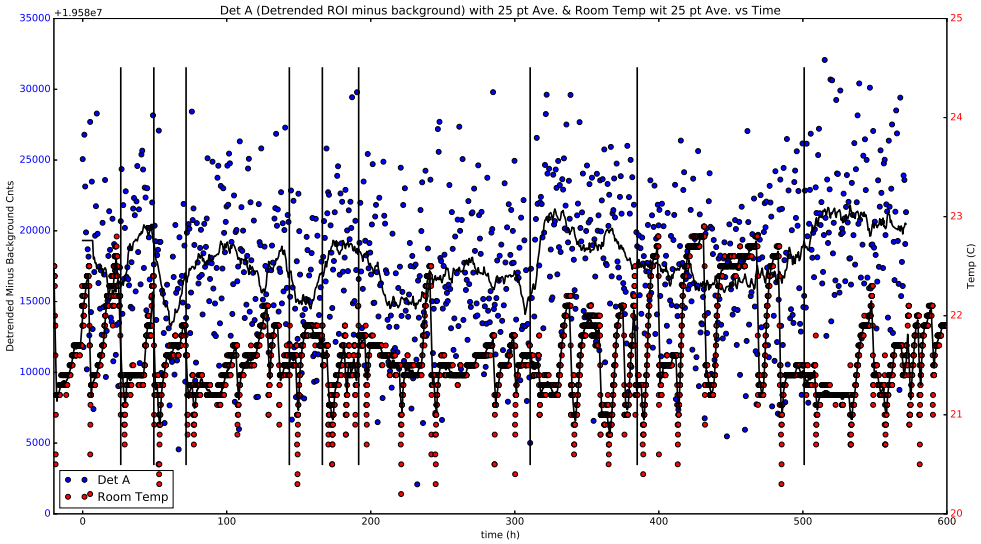

Figure 4.17. Trial 1 transition data from detector A with ambient temperature monitoring data.

the potential effects future experiments should maximize the amount of control of ambient experimental environment.

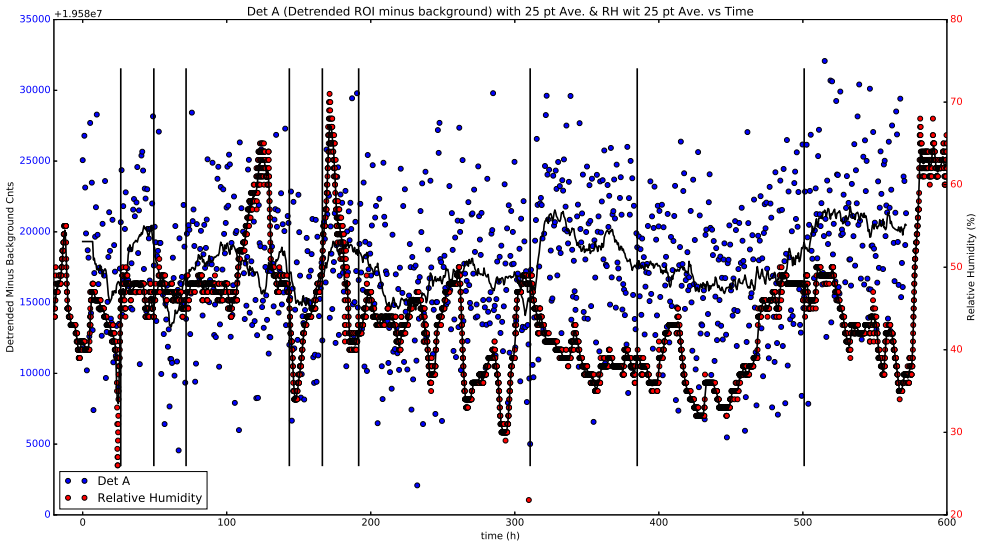

Figure 4.18. Trial 1 transition data from detector A with ambient relative humidity monitoring data.

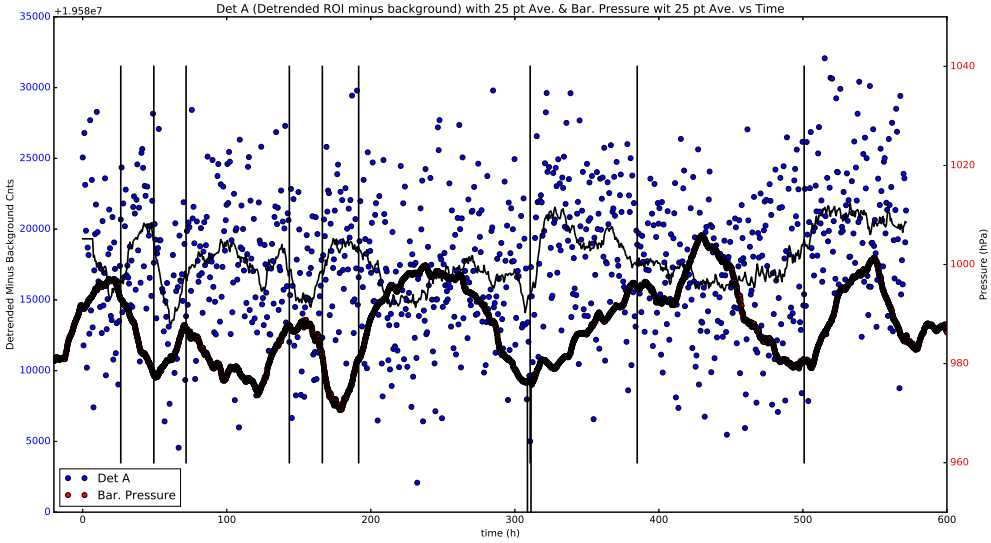

Figure 4.19. Trial 1 transition data from detector A with ambient barometric pressure monitoring data.

4.5.2 Mechanical Shock and Vibration

The observed discontinuity in the ROI and background counts of detector B in trial 3 strongly indicate the need to protect the experimental setup from mechanical shock and vibration. This is a challenging requirement given that the experiment consists of moving 1700 lbs of lead upon a wooden mule back and forth across an uneven floor of approximately 25 feet.

4.5.3 Repeatability of Mule Placement

Figure 4.20 is plot of ROI background counts as function of small lateral perturbations of approximately 0.25" from the target location. These data indicate that the variation in the mule postion could induce a fractional change of 2 x 10^{-4}. The estimate for this effect is less than that of other sources of systematic error previously mentioned but should be addressed in future experiments.

4.5.4 Dead Time Correction

A thorough dead time analysis for this setup was not conducted but could be applied. Approaches to compensate, and adjust for, systematic effects of deadtime are discussed by Nistor(30). Other possible effects such as Self Induced Decay (SID) are also address by Nistor. These analysis has significant bearing if future detector-based counting experiments are to be pursued further.

4.5.5 Conclusion and Path Forward

Given the numerous sources of systematic error present in the current setup, a more detailed analysis of each source is needed along with setup improvements to minimize systematic error. The experimental setup needs significant refinement if future transition experiments are to be performed. Ambient environmental control, shock and vibration protection, as well as a repeatable process to accurately place the

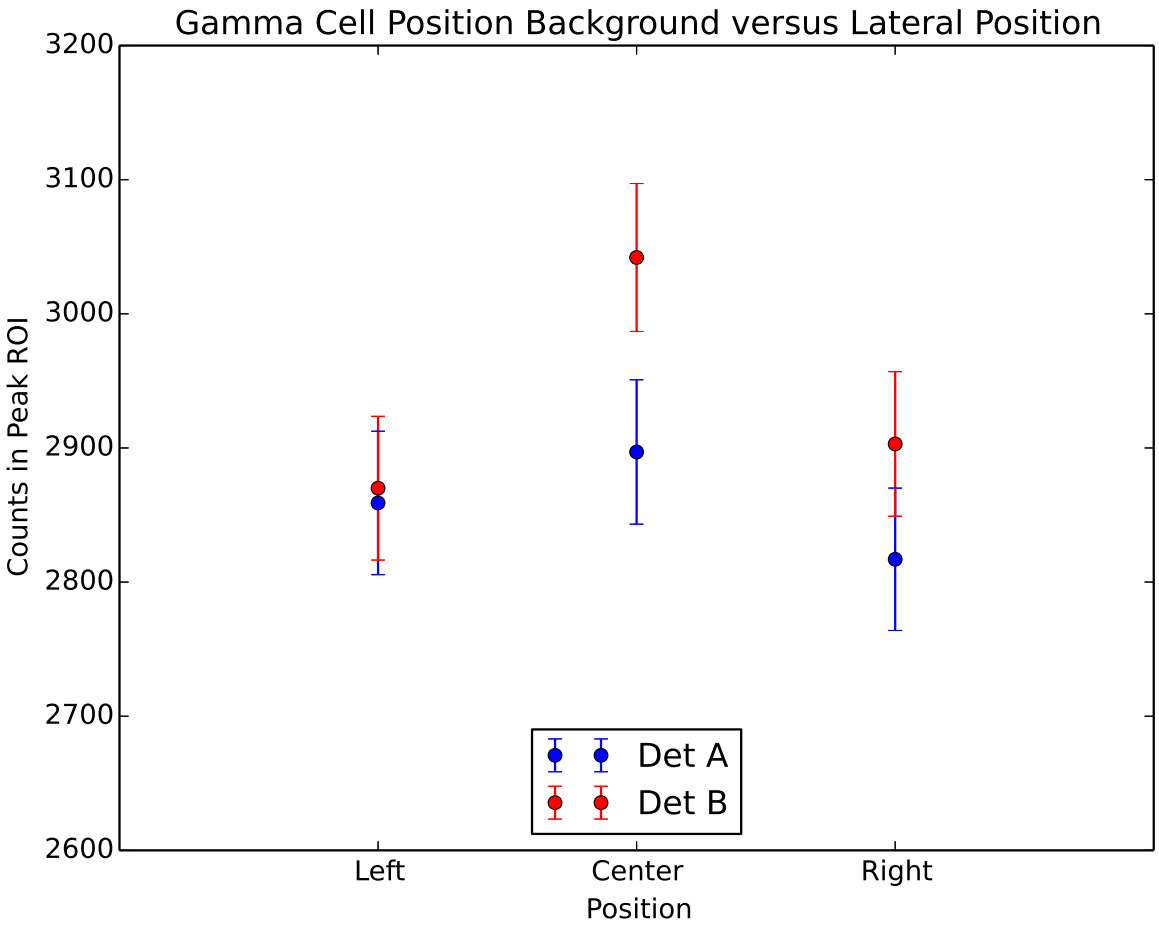

Figure 4.20. Detectors A and B ROI background count contribution as a function of laterial mule variation at gamma cell position.

mule in the target location is required. The neutrino mule is constructed out of wood with the intent to make a rigid robust frame to support 2000 lbs of lead. Over the course of the experiment the rigidity of the mule weakened and the amount of 'play' in the mule frame became very noticeable. Future experiments will require a new mule design incorporating a more robust approach perhaps utilizing Bosch extruded aluminum framing.

5. TRITIUM DIRECT CONVERSION BETAVOLTAICS: A NEW METHODOLOGY FOR DECAY PARAMTER MONITORING

Tritium is a heavy isotope of hydrogen consisting of one proton and two neutrons that decays with a half-life of (4500 ± 8) days (51). In tritium decay, a neutron in the tritium nucleus decays via the weak interaction, producing ^{3}He, an electron, and an electron antineutrino. While trace amounts of tritium occur naturally due to cosmic ray interactions with the atmosphere, large scale production is accomplished by neutron irradiation of ^{6}Li. Tritium has a wide variety of uses, ranging from glow-in-the-dark exit signs at movie theaters to nuclear weapons. Tritium is also used in betavoltaic batteries, and this work explores the possibility that these devices can be used to determine the half-life of tritium.

Since 1977, there have been four generic approaches to measure the half-life of tritium: calorimetry (52), ^{3}He collection (53), bremsstrahlung (54) and beta counting (55). Conventional counting-based half-life experiments utilize thallium-doped sodium iodide, NaI(Tl), scintillation detectors that convert energy from incident radiation into light in the visible spectrum, which is then detected with a photomultiplier tube. These counting detectors track specific energy peaks in the spectra and are heavily susceptible to dead-time (which is related to downtime after each counting event), pileup (when two events close in time are not resolved and thus the sum of their energies is recorded), and Compton background which results in asymmetric peaks. In contrast, the betavoltaic current is a macroscopic effect due to large numbers of interactions taking place within the diode structure, which minimizes the systematic effects associated with conventional counting techniques.

The potentially most significant advance that could be realized by using betavoltaics to measure radioactive half-lives is that intense sources can be characterized without concern for rate-related effects such as dead-time and pile-up. Given that betavoltaics are not limited by the challenges imposed upon conventional counting based methods, use of betavoltaic methods may offer opportunities to develop similar approaches to rapidly measure, verify, and continuously monitor half-lives of other radioisotopes. Betavoltaics are small, compact current sources with a footprint of approximately 5 cm^2. In this chapter, I explore using a betavoltaic to monitor and measure the half-life of tritium; propose a methodology; perform an actual experiment; and present those results.

Periodic variations in the decay of Tritium have been observed independently in at least four prior experiments using three different radiation detection methods: solid state (Si), liquid scintillator, and photodiodes (17; 18; 19; 20). Given these observations, and the recognition that tritium is the simplest radioactive isotope, it is an ideal candidate for further explorations into the existence of time-varying nuclear decay parameters. As a means to explore new methods of measuring the half-lives of radioisotopes, and to explore time varying decay parameters, the current generated by a tritium-based betavoltaic battery was monitored continuously during multiple experimental trials. The intent of these experiments was to identify sources of noise, environmental effects, as well as instrumental effects that must be addressed in order to make reliable continuous electrical measurements over extended periods of time, i.e. several years. The model used to represent the behavior of the betavoltaics will be discussed and examined. In addition, the numerous environmental and electrical parameters associated with the experimental will be discussed as well as the associated mitigations.

5.1 Betavoltaic Cells

Betavoltaics are readily available and accessible sources of tritium. Betavoltaic cells are composed a semiconductor based diode (p-n junction) and a radioisotope. As the radioisotope decays, ionzing radiation is emitted which in turn creates electron-hole pairs within the p-n junction's depletion region where the associated electric field separates and sweeps out these pairs generating an electrical current(22; 23). The

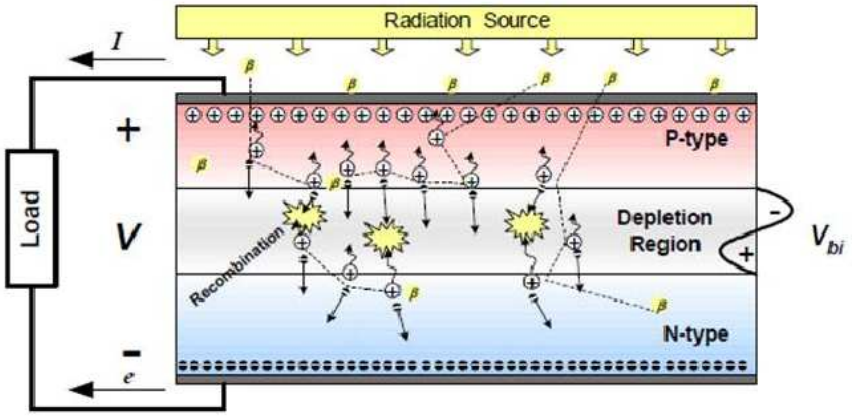

Figure 5.1. Diagram of how the kinetic energy of daughter particles produced in radioactive decay is converted into electricity (22).

betavoltaic's electrical current is to first-order directly proportional to the activity of the radioisotopes present in the device. The current measured from these devices is a macroscopic effect due to the very large number of interactions taking place within the diode devices. One potential advantage of this approach is that large sources can be characterized without systematic error arising from deadtime and pulse pileup effects that occur in counting based experiments, and are excerbated when measuring large sources with high count rates(47). The ultimate intent of this approach is a long term precision monitoring of a beta-voltaic current in order to observe any time-dependence in the beta decay of tritium. The ideal experimental setup is one that is both environmentally stable and allows for the monitoring of these betavoltaics indefinitely.

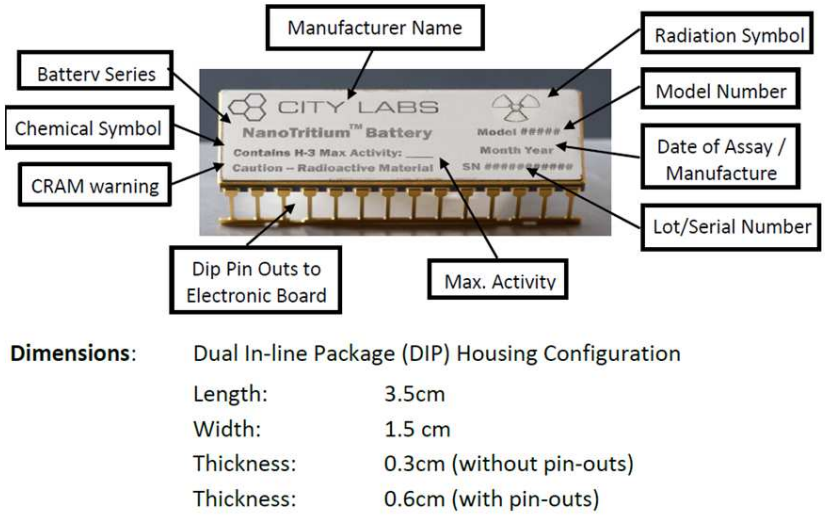

Figure 5.2. Tritium based betavoltaic manufactured by City Labs

5.2 Modeling Betavoltaic Cells

The following section will provide an overview of the p-n junction physics of operation. This overview will serve as the basis for the discussion and understanding of betavoltaic operation, electrical test, and data analysis.

5.2.1 The Ideal Diode Equation and Deviations

Before discussing the behavior of a betavoltaic, it is important to review the basic operation of a p-n junction diode. The unique characteristic of a typical p-n junction is its rectifying behavior, meaning the conduction of electrical current is dependent upon the relative bias of the p-type, hole-rich semiconductor material to the n-type, electron-rich semiconductor material. This effect is due to the potential difference that is generated via the dissimilar carrier concentrations (dopants) in the two materials. Holes diffuse from the p-type material into the n-type material, and at the same time electrons diffuse from the n-type material to the p-type. This effect constitutes a diffusion current. As the diffusion of these carries continues, charge begins to build

up on opposites sides of the junction. This accumulated charge creates a field which causes carriers to be swept across the junction in the opposite direction of the diffusion current. This effect constitutes a drift current. Charge builds up until these currents cancel each other out and a static equilibrium is achieved resulting in an electric field and the associated potential drop across the junction. The movement of these carriers across the junction results in a region that straddles the junction interface that is depleted of carriers, and is known as the depletion region. This built-in potential is often referred to as V_{bi}. The potential drop, V_{bi}, takes place entirely with in the depletion region. Therefore the associated electric field is confined to this region as well. The field within the depletion region is critical for charge collection within betavoltaic devices.

In steady-state thermal equilibrium at zero bias, no current flows. When a forward applied bias V_{app} is place across the junction, i.e. the p-type material is placed at a higher voltage with respect to the n-type, this bias has the effect of canceling out all or a portion of the built in potential and thus reducing the potential barrier for conduction across the junction. In the reverse bias scenario where the p-type material is placed at a lower potential with respect to the n-type, this bias adds to the potential barrier and inhibits conduction across the barrier. The general rectifying behavior of a p-n junction diode can be seen in Fig. 5.3. These deviations are due to carrier generation and recombination within the depletion region. The mathematical models for forward and reverse bias operation can also be seen in the Fig. 5.3. The second terms in both models are first order deviations from the ideal diode Eq. (23)

$$I = I_{\mathrm{rs}} \left\{ \exp\left[\frac{eV_{\mathrm{app}}}{nk_{\mathrm{B}}T} \right] - 1 \right\}. \tag{5.1}$$

Here I_{rs} is the reverse saturation current, e is the magnitude of the electron's charge, V_{app} is the applied voltage, n is the diode's ideality factor (which measures how closely the diode is accurately described by the ideal diode equation), k_{B} is the Boltzmann constant, and T is absolute temperature in Kelvin. A detailed description of the derivation of the ideal diode equaiton and the associated deviations can be found in volume II of the Modular Series On Solid State Devices(23).

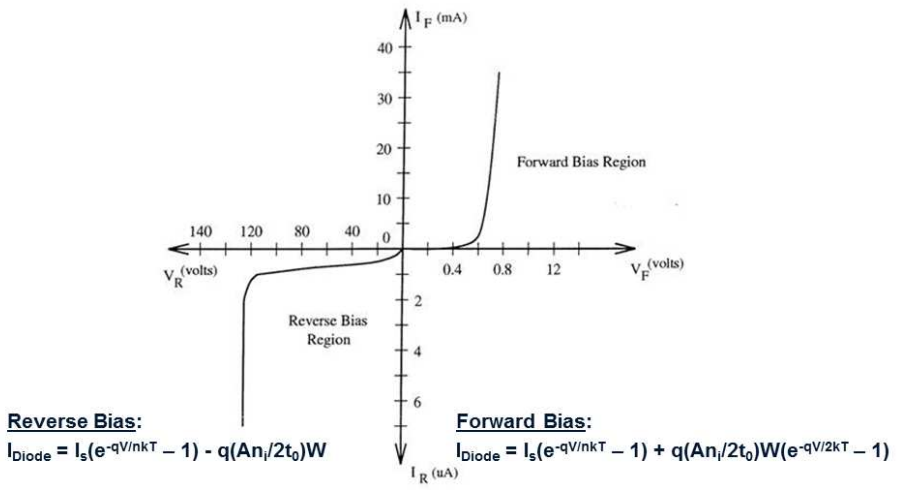

Figure 5.3. General diode behavior as a function of voltage with associated mathematical models for forward and reverse bias.

5.2.2 Betavoltaic Model

Betavoltaics are typically modeled as a current source in parallel with a diode and a shunt resistor with a series resistor as shown in Figure 5.4. The radiation induced

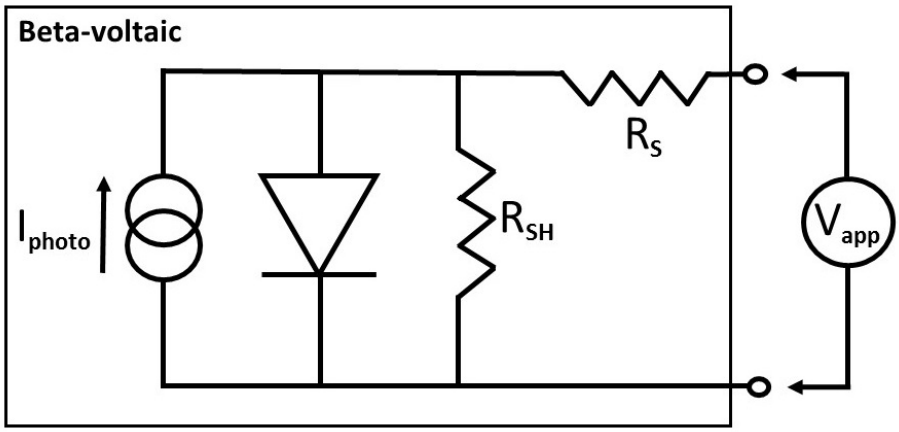

Figure 5.4. Schematic for a betavoltaic battery. Here R_{SH} and R_{S} denote the shunt and series resistors, respectively.

drift current, I_{rad}, flows in the opposite direction of the forward bias diffusion current, where the overall device current is (56)

$$I = I_{\text{rs}} \left\{ \exp \left[\frac{e(V_{\text{app}} - IR_{\text{S}})}{nk_{\text{B}}T} \right] - 1 \right\} + \frac{V_{\text{app}} - IR_{\text{S}}}{R_{\text{SH}}} - I_{\text{rad}}. \tag{5.2}$$

Again I_{rs} is the reverse saturation current, e is the magnitude of the electron's charge, V_{app} is the applied voltage, n is the diode's ideality factor, k_{B} is the Boltzmann constant, and T is absolute temperature in Kelvin. R_{S} and R_{SH} are the series and shunt resistance respectively. R_{S}, which is typically small (on the order of ohms), depends on the bulk material properties of the semiconductor and on the contact resistance of the electrical contacts to the semiconductor device. R_{SH} is usually large (on the order of hundreds of megaohms) and depends on the quality of the diode junction with regards to maufacturing defects(81; 82; 80). The measured betavoltaic current described by Equation 5.2 can be thought of being composed of two components: I_{dark} and I_{rad} as seen in equation 5.3.

$$I_{\text{BV}} = I_{\text{dark}} - I_{\text{rad}} \tag{5.3}$$

The betavoltaic's electrical current is dominated by I_{rad} and is directly proportional to the activity of the tritium present in the device when operated near or at zero volts as seen in equation 5.3. The net effect of I_{rad} is to shift the entire I-V curve down the y-axis, as seen in Figure 5.5, by the value I_{sc}, the short circuit current which is the value of I_{rad} at zero volts. The radioisotope-induced current in the betavoltaic, I_{rad}, is governed by (57),

$$I_{\text{rad}} = eA_{pn}G_{ss}(W_t + L_p + L_n), \tag{5.4}$$

where A_{pn} is the cross-sectional area of the p-n junction, W_t is the depletion region width of the of p-n junction, and L_p and L_n are corresponding diffusion lengths in the p and n region of the diode. $G_{ss} = g\dot{\gamma}_{ss}$ is the steady state electron-hole pair generation rate in pairs per cubic centimeters per second, where g is the conversion factor for electron-hole pairs per cubic centimeter per rad (Si), and $\dot{\gamma}_{ss}$ the steady

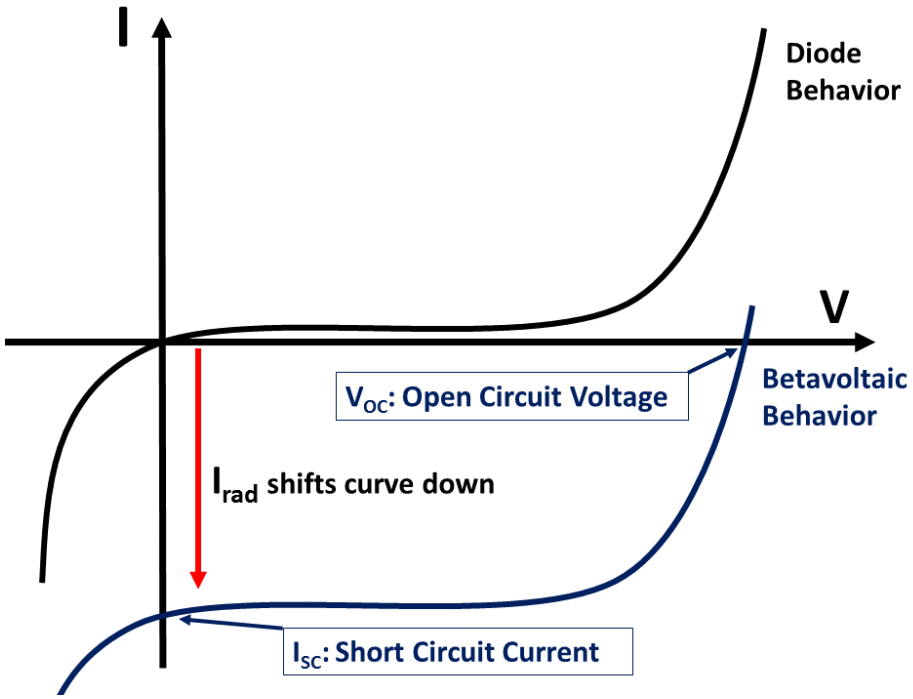

Figure 5.5. The effect I_{rad} has on the observed I-V sweep of a betavoltaic device.

state dose rate measured in rad (Si) per second. All of the terms except for G_{ss} are constants to first-order, and therefore I_{rad} can be redefined as

$$I_{\text{rad}} = eR_{\text{e-p}}E_{\text{convert}}\dot{A}_0 e^{-\lambda t}, \tag{5.5}$$

where $\dot{A}_0$ is the initial activity of the betavoltaic, $R_{\text{e-p}}$ is the average number of electron-hole pairs produced per decay, λ is the decay constant equal to $\ln 2/t_{1/2}$ where $t_{1/2}$ is the decay the half-life of the radioisotope present in the betavoltaic, and E_{convert} is the conversion efficiency factor. Unless otherwise specified, in the context of this work $t_{1/2}$ refers to the half-life of tritium with an accepted value of (4500 ± 8) days. Using 7.5% for the conversion efficiency, and 1000 for the average number of electron-hole pairs generated per 5.7 keV beta (the average β energy for tritium), the calculated approximate current is 50 nA for a betavoltaic cell loaded with 115 millicuries of tritium. The betavoltaic used in this experiment had an initial current of approximately 50 nA which is consistent with a 7.5% conversion efficiency. These

values are based on previous work conducted at Purdue University on representative devices(22). A figure of merit used to characterize betavoltaic performance and design is the maximum betavoltaic current,$I_{\max}$, defined as

$$I_{\max} = eR_{\text{e-p}}\dot{A}_0 \tag{5.6}$$

Table 5.1 summarizes calculations of I_{sc} and ,$I_{\max}$ for various semiconductor materials using a activity of 105 millicuries and an efficiency of 7.5%. The 105 millicuries value was chosen based on the information provided by City Labs that the acitivity of the devices used in this work had an activity of 115 millicuries on 1/18/2017. It is important to note that GaAs and InGaP materials bound the observed short circuit current from the betavoltaic devices used in the effort. In addition to this fact, City Labs has patents where they discuss the use of these materials in the fabricating betavoltaic devices with 7.5% efficiency (91; 92).

Table 5.1.
Maximum short circuit current calculated for various materials.

Material	Si	GaAs	InGaP	4H SiC	GaN	Diamond
Band gap Energy (eV)	1.1	1.43	2.26	3.26	3.45	5.45
e-h gen. Energy (eV)	3.6	4.23	6.3	5.05	10.0	13
$R_{\text{e-p}}$	1583	1352	905	1128	570	438
$I_{\max}$ (nA)	981	838	617	699	353	272
Efficiency (%)	7.5	7.5	7.5	7.5	7.5	7.5
I_{sc} (nA)	74	63	21	52	27	20

All of the factors which multiply the exponential in Eq. (5.6) can be treated as a constant, and hence that the expression of I_{rad} reduces to,

$$I_{\text{rad}} = I_0 e^{-\lambda t} \tag{5.7}$$

I_{rad} is the current of interest with regards to measuring and monitoring nuclear decay parameters. All other contributions to the measured current can be considered sources of unwanted noise. In the next section an approach to isolating I_{rad} is discussed.

5.2.3 Isolating I_{rad}

In order to accurately determine the half-life of tritium by measuring the current of a tritium based betavoltaic, one must account for various sources of error associated with the current measurement. The dominant contribution to the observed betavoltaic current is the tritium decay at low bias, < 1 V. However, it can be seen from Fig. 5.4 that there are other contributions to the measured current under an applied bias, V_{app}. These depend on manufacturing quality as well as on the device physics of the semiconductor diode, and the sum of these contributions is denoted as I_{dark}. I_{dark} represents a source of error when measuring I_{rad}, and it is assumed that the measured current is the sum of I_{dark} and I_{rad} as seen in Eq. (5.3). In order to account for this source of error, a reference diode (without tritium) from the same wafer lot of our betavoltaic was monitored in parallel and an assumption was made that this reference diode captures the I_{dark} contribution to the betavoltaic current. I_{rad} can then be determined by measuring both the betavoltaic and reference diode in parallel, and then subtracting the measured reference diode current from the measured betavoltaic current. An additional benefit of this approach is that environmental effects associated with I_{dark} such as temperature, pressure, and voltage are taken into account and are mitigated. Up until this point an implicit assumption in the models presented is that the betavoltaic does not degrade over time. In order to take into account betavoltaic degradtion an additional term, ζ_{degrad}, can be added to I_{BV} and can be seen in Eq. 5.8.

$$I_{\text{BV}} = I_{\text{dark}} - I_{\text{rad}} + \zeta_{\text{degrad.}} \tag{5.8}$$

The likely manifestation of ζ_{degrad} is the introduction of radiation induced defects resulting in the reduction of the junction shunt resistance and hence an increase

in I_{dark}. Banerjee et al. demonstrated by irradiating silicon photovoltaic cells with electrons of various energies that shunt resistance degrades due to electron irradiation. The 1 MeV electron irradiation lowered the shunt resistance value causing an increase in I_{rs}, the reverse saturation current, above a temperature threshold of 250 °C. This effect reduces the open circuit voltage and overall device performance(83; 84). In the context of measuring nuclear decay parameters, this degradation is a source of noise in the form of excess dark current. However, given that the electron energy used by Banerjee et al. is 175 times greater than that of the mean beta energy for tritium decay, ζ_{degrad} will be assumed to be negligible for this work.

In conjunction with measuring the current from a betavoltaic cell and a reference diode in parallel, periodic I-V sweeps can be performed on both devices. These I-V sweeps can then be used to track the evolution of critical device parameters over time. The key parameter in this context is the shunt resistance, which can be estimated by measuring the slope of the I-V sweep near zero volts. Fig. 5.6 captures the degradation and I_{rad} isolation approach. For the proposed method illustrated in

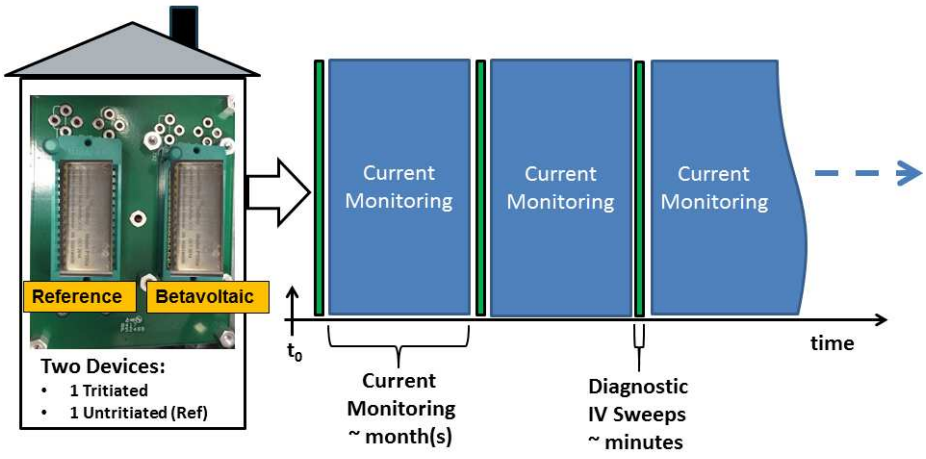

Figure 5.6. Proposed process for isolating I_{rad} and monitoring betavoltaic degradation via periodic I-V sweeps.

figure 5.6 to be effective, great care must be taken to ensure that the reference diode is representative of the betavoltaic device being monitored. No two semiconductor

junctions are identical, so any differences between the reference diode and the underlying diode of the betavoltaic need to be characterized and taken into account. One challenge to conducting periodic I-V sweeps is that of cable capacitance. In order to take accurate current measurements over an extended period of time, stability of the test setup is critical. Triaxial cables were implemented in this setup in order to implement remote four wire sense. However, these cables provide a source of shunt capacitance that affects the current measurement being performed by the physical measurement unit (PMU), the Keithley 2634B. The charging or discharging of this shunt capicatance substracts or adds current to the measured current value. I-V sweeps bias the device at varies voltages which can be higher than the monitoring bias used during the continous current measuring period. These elevated voltages can charge the shunt capacitanace, which will discharge at the lower monitoring voltage and skew measurement results. This skew will persist until the shunt capacitance is discharged and the setup stabilizes. Data indicate that days maybe required in order for the setup to stablize due to various parasitic capacitance effects such as cable charging. I-V sweeps inject instability into the current measurement process. The initial experiments conducted in this work did not implement periodic I-V sweeps. I-V sweeps were only conducted at the begining of current monitoring periods.

5.3 Betavoltaic Experimental Setup

The following section describes the overall experimental approach to mitigate and monitor enviromental and electrical influences on the experimental setup.

5.3.1 Setup Overview

Stability of the betavoltaic setup to environmental and electrical effects is critical to noise reduction. Multiple steps were taken to achieve as stable operating conditions as possible given resource constraints. The setup was designed to isolate, stablize, and monitor environmental conditions. Electrical parameters such as line voltage,

line frequency, and applied bias to the reference and betavoltaic were all monitored in real-time. The schematic of the isolation and monitoring approach can be seen in Figure 5.7.

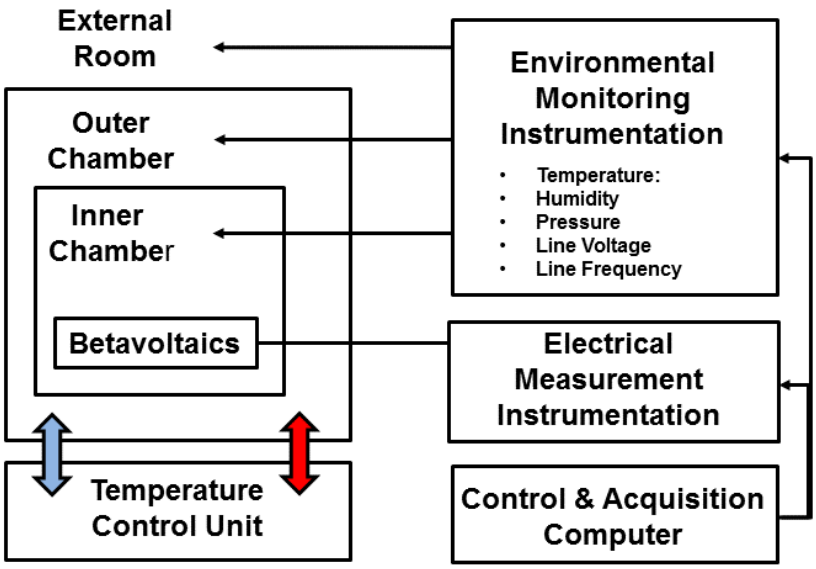

Figure 5.7. Betavoltaic Test and Environmental Monitoring Approach

5.3.2 Temperature, Humidity, and Pressure

Environmental conditions such as temperature, pressure, and humidity can be sources of systematic error. The extended duration of these experiments exacerbates such effects, requiring environmental stability over long periods of time. Therefore significant thought must be given on how to achieve the best possible environmental stability. Fig. 5.7 is a layout of the experimental setup for measuring the tritium decay induced electrical current from a City Labs betavoltaic cell and monitoring the environment. The outer chamber is an extruded polystyrene rigid foam isolated temperature controlled enclosure. The internal temperature is stabilized by using a Peltier thermoelectric solid-state air conditioner in conjunction with a proportional-integral-derivative (PID) controller. The inner chamber is an aluminum box which

contains the betavoltaic battery, the reference diode, and environmental monitoring electronics for logging the temperature, pressure, and relative humidity.

In situ Enviromental Monitoring of Test Chamber

The electronics used to measure the ambient environment inside the test chamber can be seen in Fig. 5.8. The monitoring system is composed of a bus pirate and a BME280. The bus pirate is commercial generic interface board that supports several communication protocols such as I2C, SPI, JTAG, and USB. The bus pirate is used as a USB bridge between the control computer and the BME280 enviromental monitor utilizing the I2C protocol. BME280 range and accuracy specifications for monitoring

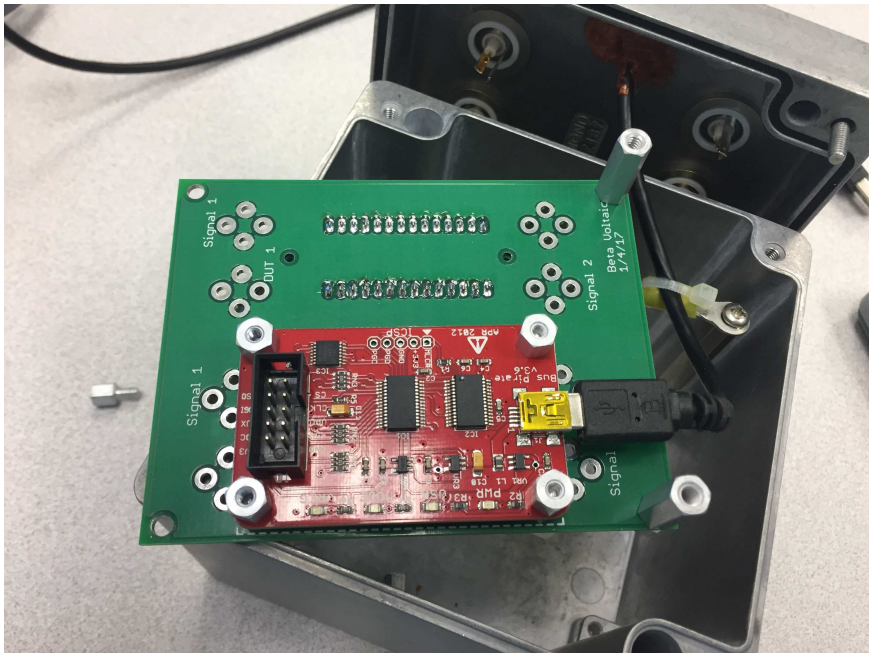

Figure 5.8. BUS Pirate and BME280 Temperature, Pressure, and Humidity monitor

temperature, humidity, and pressure can be found in Fig. 5.9. Sealed one liter glass bottles filled with water were placed around the inner chamber to increase the test

Key features

- Package — 2.5 mm x 2.5 mm x 0.93 mm metal lid LGA
- Digital interface — I²C (up to 3.4 MHz) and SPI (3 and 4 wire, up to 10 MHz)
- Supply voltage — V_{DD} main supply voltage range: 1.71 V to 3.6 V; V_{DDIO} interface voltage range: 1.2 V to 3.6 V
- Current consumption — 1.8 µA @ 1 Hz humidity and temperature; 2.8 µA @ 1 Hz pressure and temperature; 3.6 µA @ 1 Hz humidity, pressure and temperature; 0.1 µA in sleep mode
- Operating range — -40...+85 °C, 0...100 % rel. humidity, 300...1100 hPa
- Humidity sensor and pressure sensor can be independently enabled / disabled
- Register and performance compatible to Bosch Sensortec BMP280 digital pressure sensor
- RoHS compliant, halogen-free, MSL1

Key parameters for humidity sensor[1]

- Response time ($\tau_{63\%}$) — 1 s
- Accuracy tolerance — ±3 % relative humidity
- Hysteresis — ±1% relative humidity

Key parameters for pressure sensor

- RMS Noise — 0.2 Pa, equiv. to 1.7 cm
- Offset temperature coefficient — ±1.5 Pa/K, equiv. to ±12.6 cm at 1 °C temperature change

Figure 5.9. BME280 environmental monitoring specifications

setup's thermal inertia and reduce inner chamber temperature variation, due to room temperature fluctuations.

Humidity and Surface Contamination

One source of potential noise, in the form of parasitic leakage paths and currents, is due to a combination of moisture and surface contamination. Surface contamination in the form of solder flux, body oils, and salts can provide ionic contamination when combined with ambient moisture. This can reduce insulator resistance and form leakage paths which interfere with the accuracy and repeatability of electrical measurements. These paths are likely to form between conductors held at different potentials (59). An illustration of these paths can be seen in Fig. 5.10. Several small desiccant pouches were placed in the inner chamber in order to reduce the relative humidity and prevent condensation from forming. The desiccant pouches used in this experiment can be seen in Figure 5.11.

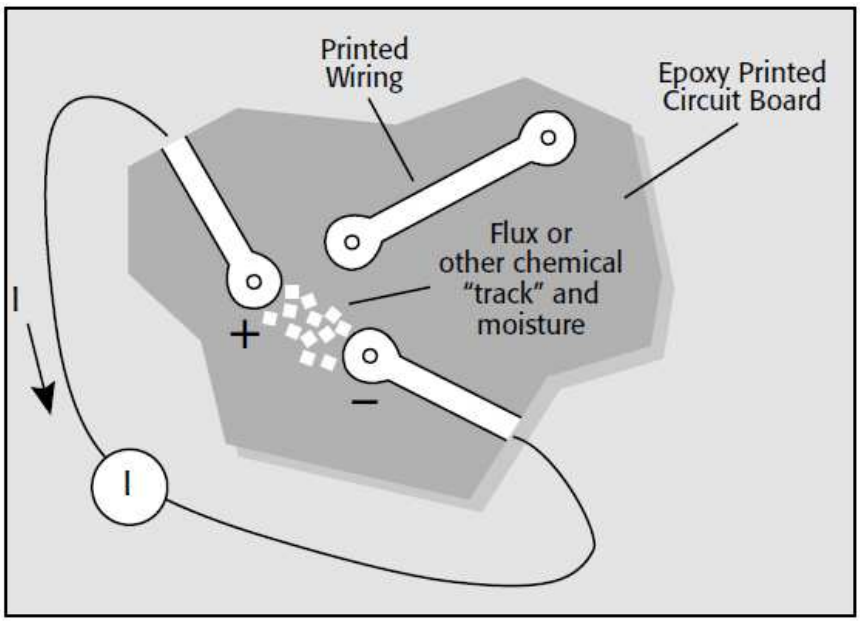

Figure 5.10. Electrochemical parasitics generated via the combination of moisture, surface contaminants, and electric potentials (59).

5.3.3 Electromagnetic Interference

In the course of building this experimental setup, a source of electromagnetic interference (EMI) was identfied. This source of EMI was the power to the TECA 3400, Peltier thermoelectric solid-state air conditioner unit. In Fig. 5.12 EMI generated from the TECA unit can be seen in the output of the BME280 temperature senor as well as a thermocouple used to measure ambient room temperature. The EMI is seen as oscillating noise present in these signals. The source of the EMI is likely due to power electronics and relays needed to convert the 120VAC at 60 Hz to 5-32VDC. Fig. 5.12 illustrates the removal of this EMI noise when power is removed from the TECA unit confirming the source of the EMI. Steps were also taken to mitigate this source of electromagnetic interference by wrapping the power cabling to the TECA unit with EMI shielding, and by maximizing the distance between these power cables and the triaxial measurement cabling. EMI shielding techniques such as single point ground for the elimination of ground loops, wrapping electrical interconnects with

Figure 5.11. DESI PAK desiccant packages placed in the aluminum contained with the betavoltaic test device and reference diode into to mitigate parasitic leakage paths excerbated by humidity.

EMI shielding material, and placing the betavoltaics in an aluminum container which acts as a Faraday cage, were implemented in the setup. Fig. 5.13 is an image of the aluminum container which will contain the betavoltaic battery, reference diode, and environmental monitoring electronics for logging the temperature, pressure, and relative humidity. It is a two piece container consisting of a lid and the main body.

5.3.4 Mechanical Shock and Vibration

The impact of mechanical shock and vibration were also considered in the design of the setup. The table on which the setup was built sits upon mechanical shock dampening rubber gaskets, as does all of the electrical equipment. Mechanical shock

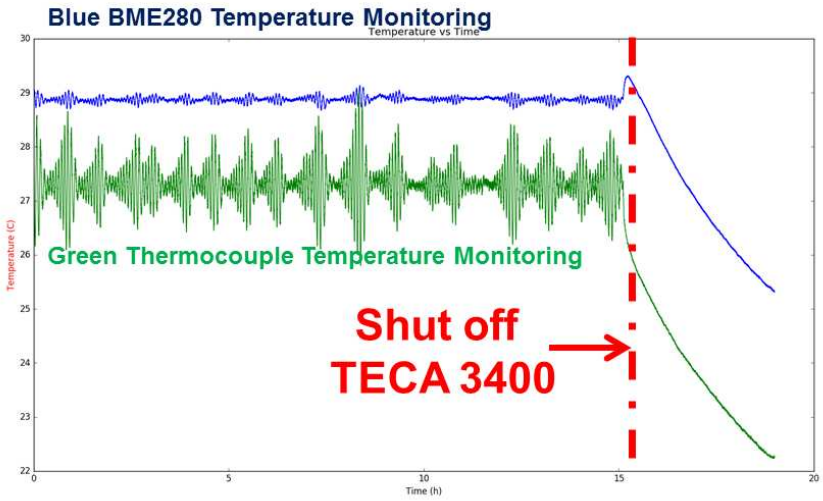

Figure 5.12. Observed electromagnetic interference in the outputs of a thermocouple and BME280 temperature monitoring intergrated circuit due to the TECA 3400 temperature control unit. The blue trace is the BME temperature read out, and the green trace is the thermocouple readout.

and vibration can provide noise sources when measuring currents < 1 μA due to triboelectric and piezoelectric effects (59). Any vibration, movement, mechanical shock, and/or flexing of the setup cabling can induce electrical noise. The triboelectric charge generation mechanism is illustrated in Figure 5.14 and is caused by frictional motion of surfaces in contact with one another. This motion causes charge to be freed from the material and accumulate. This accumulated charge can result in electrostatic discharge (ESD) which can damage electrical devices and equipement. In order to mitigate chances of ESD damage to the reference and betavoltaic devices, proper ESD precautions were taken when handling these devices. This precaution included wearing an ESD smock and an ESD wrist strap tied to ground through a 1 megaohm resistor, as well as standing on an ESD floor mat which aid in preventing the build up of charge. The test bench on which the setup is built and where devices are handled, sits upon an ESD mat. An air ionizer was used in addition with aformentioned mitigations anytime the test articles were handled. The piezoelectric charge generation

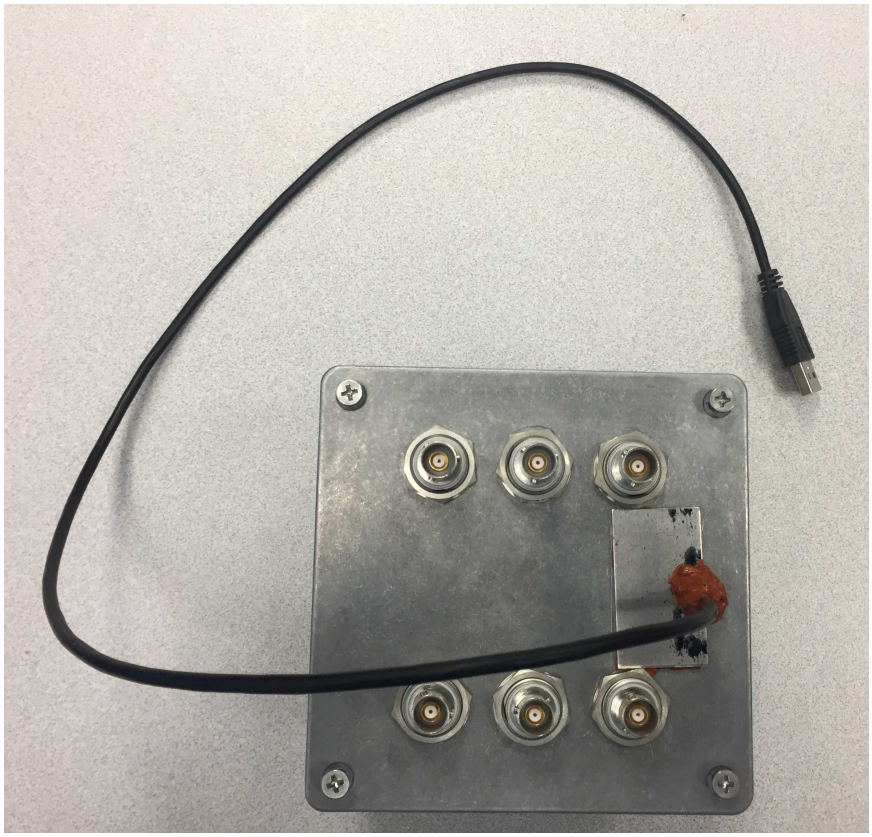

Figure 5.13. Betavoltaic test enclosure in which the betavoltaic and reference diode currents are measured and the local environment is monitored.

mechanism is illustrated in Fig. 5.14, and is due to mechanical stress generating free charge in a given material. This can contribute to noise as well as a source of ESD. The rubber ESD mat upon which the setup sits provides some vibration dampening. Additional vibration and shock dampening rubber sheets were placed under all of the electrical instrumentation and cabling.

5.3.5 Electrical Configuration

A Keithley 2634b was chosen as the a electrical measurement instrument for this experiment and can be seen in Fig. 5.16. This unit was selected due to its precision voltage and current sourcing and measurement capability. Sourcing and measurement

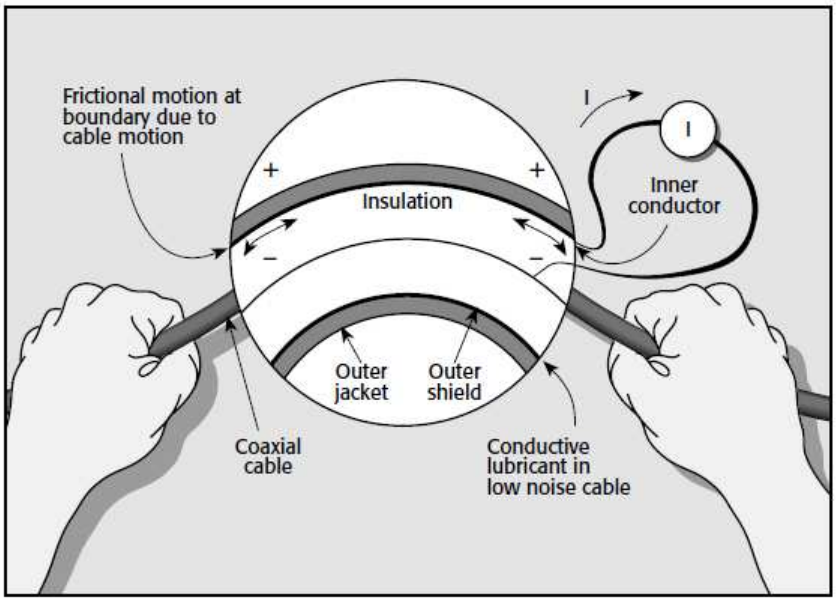

Figure 5.14. Charge generation process in electrical cables due to the triboelectric effect (59)

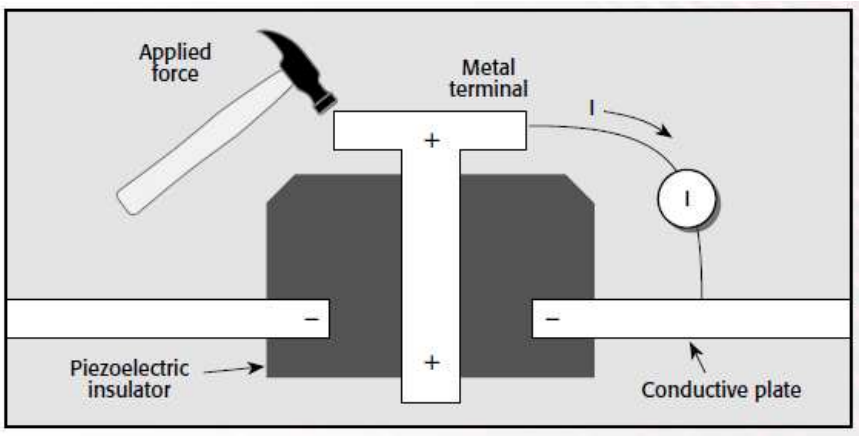

Figure 5.15. Charge generation process in electrical systems due to the piezoelectric effect (59)

on the 2634b is programmable, which allows for custom automated I-V sweeps. In addition to programming custom electrical tests, the 2634b has an onboard processor. This capability allows for more complex test sequences such as those described in the previous section regarding I_{rad} isolation. The Keithley 2634b is controlled remotely

via GPIB, a standard communications protocol, by a desktop computer running Windows 7.

A Keithley 2634b source meter measured an initial current of 50 nA with an accuracy of ± 80 pA. This accuracy is derived from the manufacturer's reported operating environmental specification of 23°C ± 5°C and < 70% relative humidity over the 100 nA current measurement range, which is 0.06% of the reading + 40pA. The resolution can be further improved by taking multiple measurements and averaging. In order to reduce this by two orders of magnitude, 10^4 measurements must be taken and averaged. This equates to four measurements per day with sub-picoampere sensitivity at a sampling rate of one measurement every two seconds. The decay rate of tritium with a half-life of 4500 days will decrease by a factor of approximtely $1.5 \cdot 10^{-4}$ in the course of one day, which amounts to 7.7 pA per day with a starting current of 50 nA.

The 2634b has two channels, denoted as A and B, with the ability to source and measure both current and voltage. We used channel A to measure the betavoltaic current and channel B to measure the reference diode current. A benefit of this approach is that a common noise sources affecting the Keithley 2634b such as V_{line}, alternating voltage supplied to the Keithley, and environmental conditions (such as temperature and humidity) are taken into account and can be removed (by subtraction of the two measured current responses). Provided the two diodes do not differ in essential properties. In addition, the betavoltaic and reference diode voltages are sourced using four-wire sense to mitigate cable losses. This four-wire sense scheme can be seen in Fig. 5.17. In four-wire sense, two leads force voltage and current, while the other two leads measure the voltage applied to the device under test (DUT) allowing the source measurement unit to verify that the desired voltage is being applied. This technique allows for compensation of any voltage drop or parasitic resistances between the source measurement unit (Keithley 2634b) and the DUTs, the betavoltaic and the reference diode. Four-wire sense is typically employed in high current situations where there is a significant voltage drop due to lead resistance, and precise voltage control is required. We further benefit from the use of triaxial cable, which consists of

Figure 5.16. Keithley 2634B Source Measurement Unit (SMU)

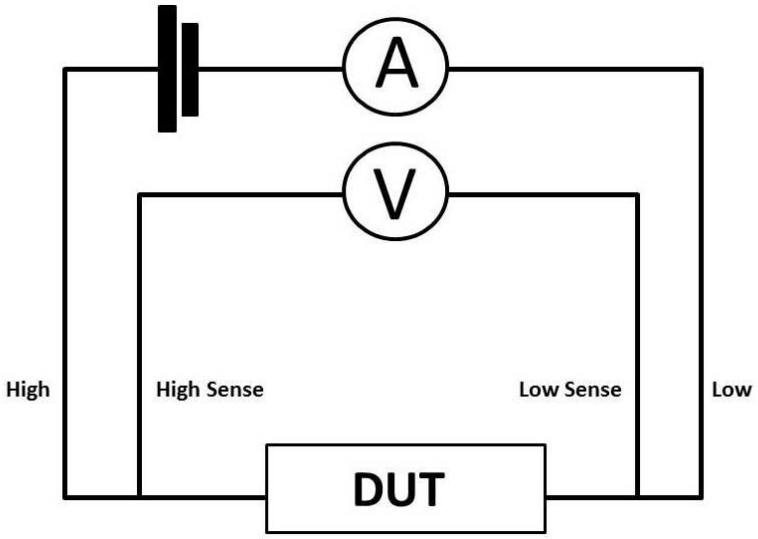

Figure 5.17. 4 Wire Sense Schematic, where DUT denotes the device under test.

a center conductor, a guard, and an outer shield. The combination of triaxial cables and four-wire sense provide improved noise suppression. A schematic of the electrical interface to the betavoltaic and reference diode can be seen in Fig. 5.18. Triaxial cable with its guard and outer shield provide a Faraday cage-like shielding for the signal cables interfacing to the betavoltaic printed circuit board (PCB) seen in Fig. 5.19. The beta-voltaic PCB has two dual inline package (DIP) sockets for 28 pin betavoltaic devices.

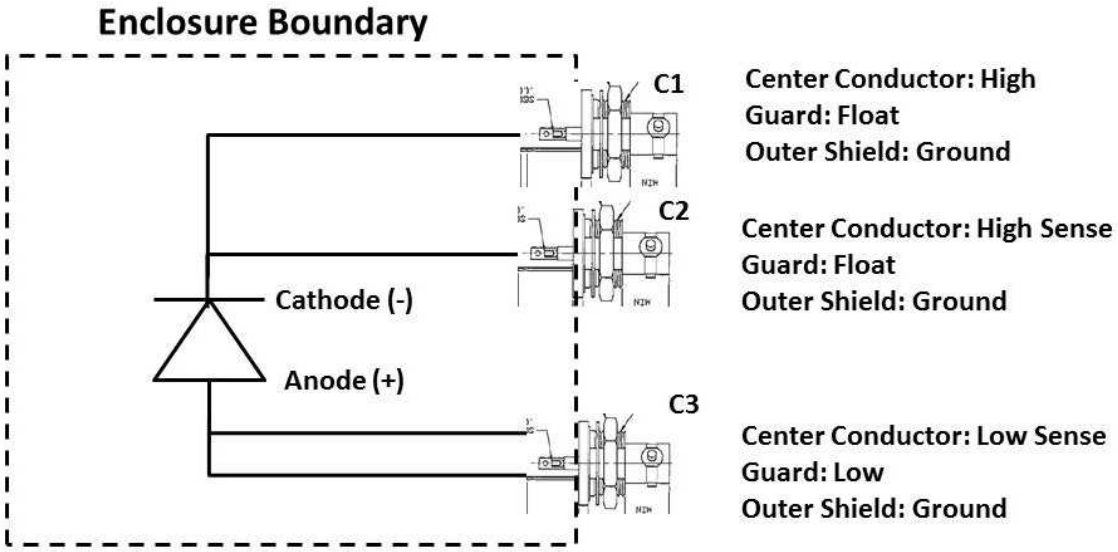

Figure 5.18. Electrical Schematic of Betavoltaic Measurement

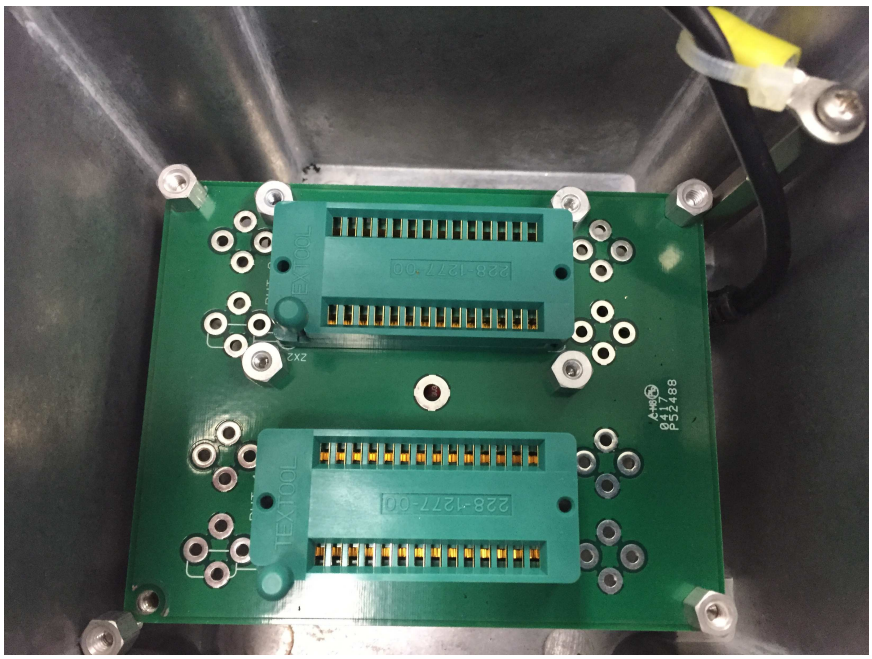

Figure 5.19. Betavoltaic PCB

5.3.6 Electrical Parameter Monitoring

In addition to monitoring temperature, pressure, and humidity within the aluminum container where the betavoltaic and reference diode are located, temperature was monitored in the outer chamber as well as in the external room. The outer chamber temperature was monitored using a Keithley 2110, which has a thermocouple interface on the front panel. The Keithley 2110 can be seen in Fig. 5.20. The 2110 in addition to the thermocouple interface used in this setup, provides another SMU channel for electrical measurement if required in the future. The external room temperature, AC line voltage, and AC line frequency are monitored in real time by a 34970a SMU, which can be seen in Figure 5.21. All AC power provided to the setup is sourced from an uninterruptible power supply (UPS). The UPS is connected to external power via a wall socket, and serves three purposes. First, it provides a single ground reference in order to prevent ground loops, which can adversely effect instrument functionality and measurement accuracy. Second, the UPS provides some filtering of the incoming wall power. Finally, it provides backup power for approximately two to three hours in the event of a building power outage.

5.3.7 Finalized Setup

The finalized experimental setup can be seen in Fig. 5.22. Measurements of the reference diode and betavoltaic voltage and current are taken aproximately every 700 ms. Measurements of the humidity, temperature (inner chamber, outer chamber, and room), pressure, AC line voltage, and AC line frequency are taken approximately every 7 seconds. All measurements are time stamped and logged in text files stored on the control desktop computer. Two text files are generated per day: an enviromental monitoring data file and an electrical measurement data-file. The file names are composed of three values: date of file creation, time of file creation, and a file designator. The electrial measurement files are designated by "a" for analog. The environmental measurement file is designated by "BME" in reference to the BME280

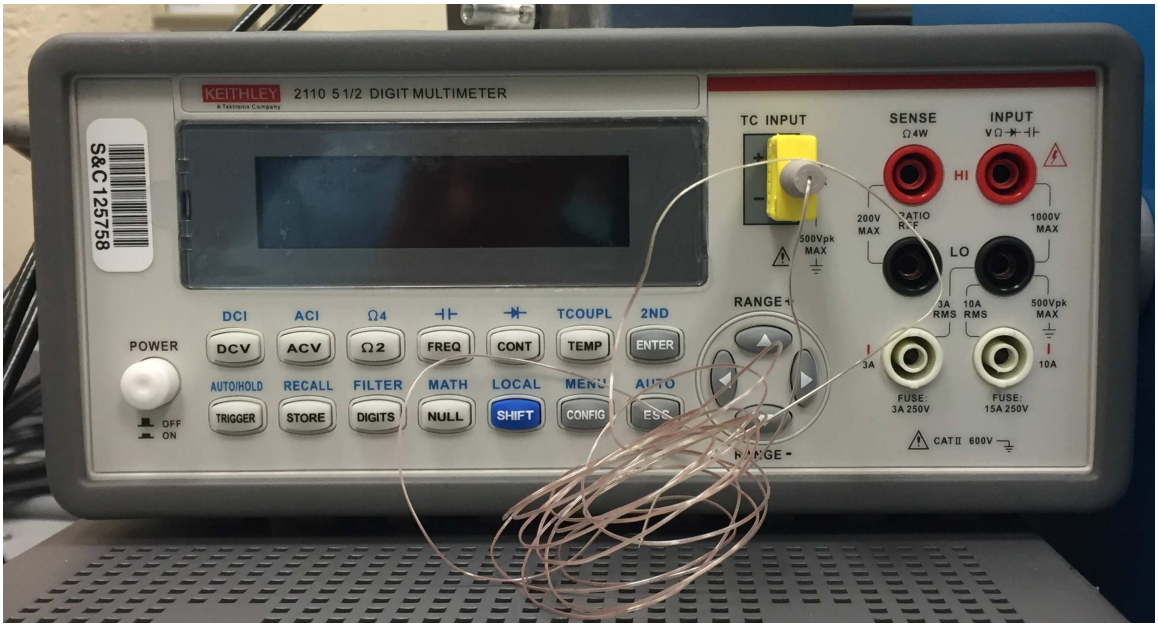

Figure 5.20. Keithley 2210 physical measurement unit used for continous monitoring of outer chamber temperature.

environmental monitor. Representative data, mean values, standard deviations, and ranges for the environmental monitoring data can be seen in Fig. 5.23. The ranges referenced in Fig. 5.23 are approximately six standard deviations, three above and three below the measured mean. The data are normalized and offset in order to place all of the data on one graph. The intent of the graph is to capture and convey the typical observed variation in the various experimental parameters over time. Data from the room temperature monitor are not shown.

5.4 Procured Betavoltaic Devices and Reference Diodes

A total of four devices were procured from City Labs Inc., two betavoltaics and two representative reference diodes. The reference diodes came from the same wafer as the diodes that were used in the fabrication of the received betavoltaics. The

Figure 5.21. 34970a physical measurement unit used for continous monitoring of ambient room temperature, AC line voltage, and AC line voltage frequency.

following section reviews these data and the decisions that were made in choosing which devices to be used in the betavoltaic current monitoring experiment.

5.4.1 CityLabs I-V Sweep Data

City Labs was very accommodating in providing additional electrical performance data as well as untritiated samples in support of this effort. City Labs does not typically provide untritiated samples due to the proprietary nature of their betavoltaic

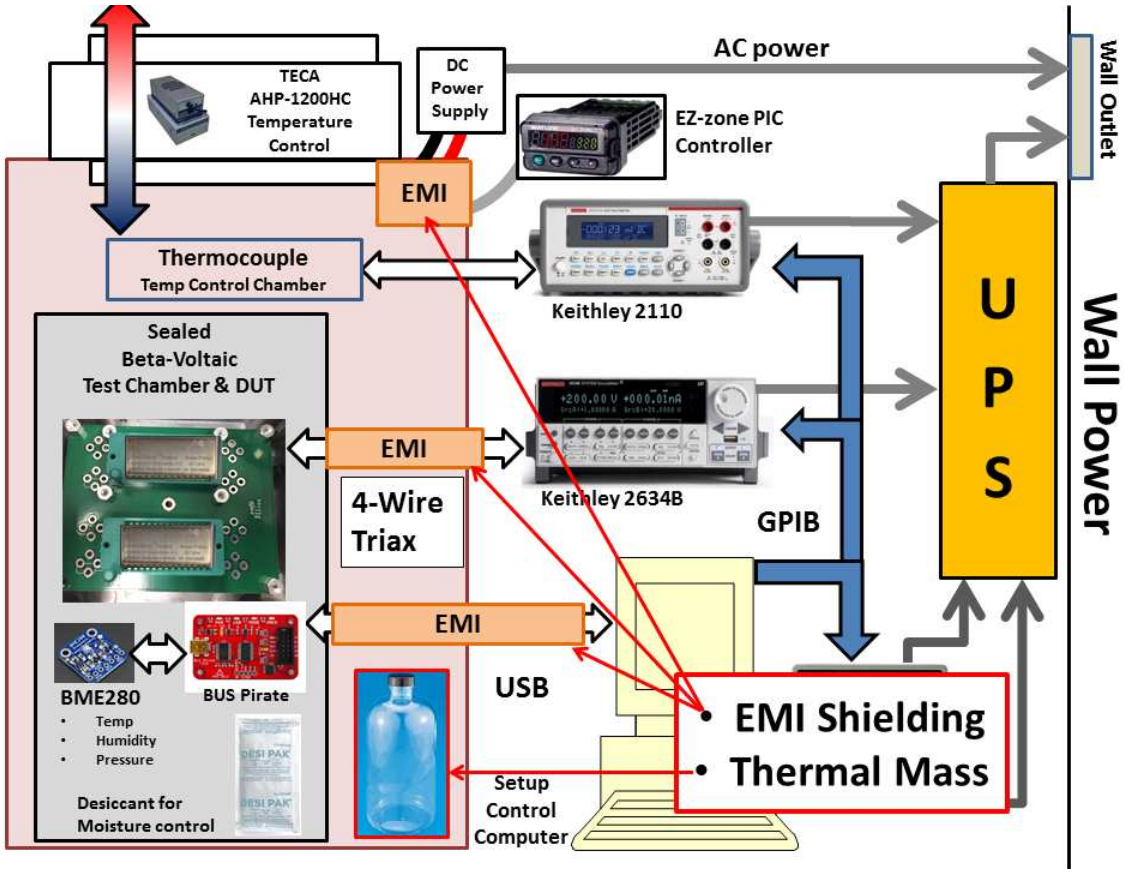

Figure 5.22. Finalized experimental configuration with continous environmental and electrical parameter monitoring.

design and fabrication process. City labs provided I-V sweeps of the betavoltaics devices prior to and after tritiation.

Betavoltaic Data

Figures 5.24 and 5.25 are the I-V curves provided for two active beatvoltaic devices, SN18 and SN20. The figures list several key parameters for each device. These parameters are I_{sc}, short circuit current, V_{oc}, open circuit voltage, V_{mp}, voltage at maximum power, I_{mp}, current at maximum power, the calculated maximum power,

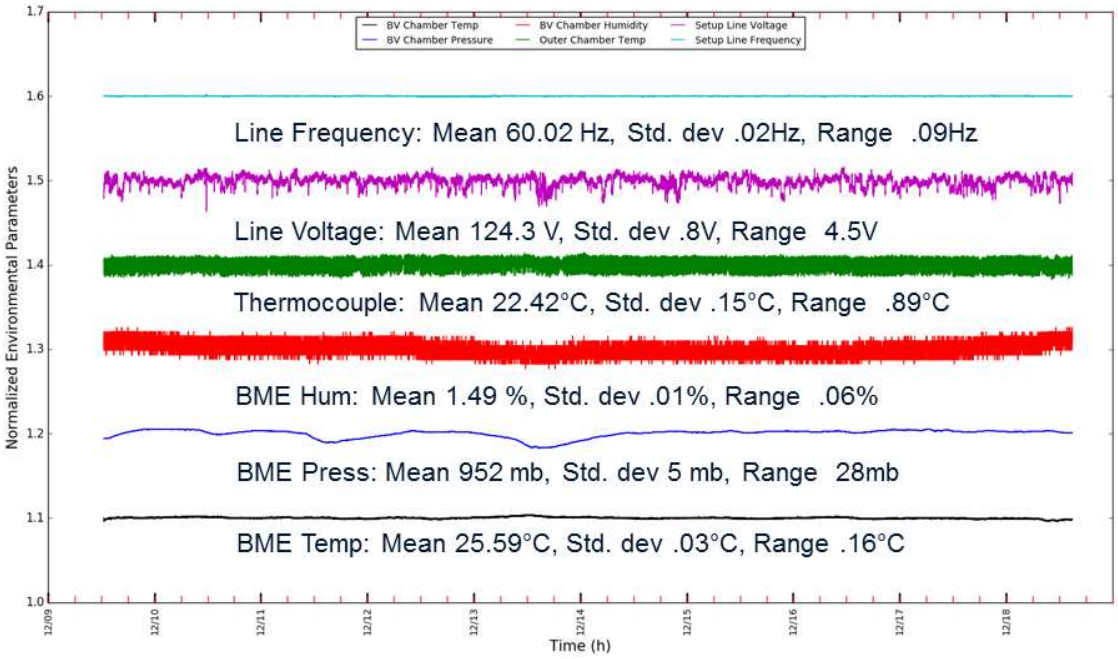

Figure 5.23. Representative environmental and electrical parametric monitoring data.

and the fill factor. Fill factor (FF) is a figure of merit for photovoltaic and betavoltaic performance, and is defined as

$$FF = \frac{P_{\max}}{I_{\text{sc}} V_{\text{oc}}}. \tag{5.9}$$

The higher the fill factor value, the higher the quality of the device, the more square-like the I-V curve, the better it performs. For the purposes of this experiment there are two critical parameters of interest, I_{sc} and R_{SH}. It is important to note that the I-V curves are rotated about the x-axis due to plotting the negative of the measured current. The actual sign for I_{sc} is negative. For this work, -I versus V will be plotted as opposed to I versus V in order to be consistent with the City Labs data format. Ideally for this experiment the higher the I_{sc} the more likely we can assume that it is directly proportional to the decay rate of the radioisotope present in the betavoltaic. The greater the value of I_{sc}, the greater the signal to noise ratio of I_{rad} to I_{dark}.

Battery Serial Number	1020140018	Max Power	2.21E-05 mW
Battery Measurement Date	Tue, Jan 17, 2017 5:11 PM	Vmp	5.15E-01 V
Activity Level	115.07 mCi as	Imp	4.28E-05 mW
	1/18/2017	Isc	5.55E-08 A
		Voc	6.57E-01 V
		Fill Factor	60.5 %

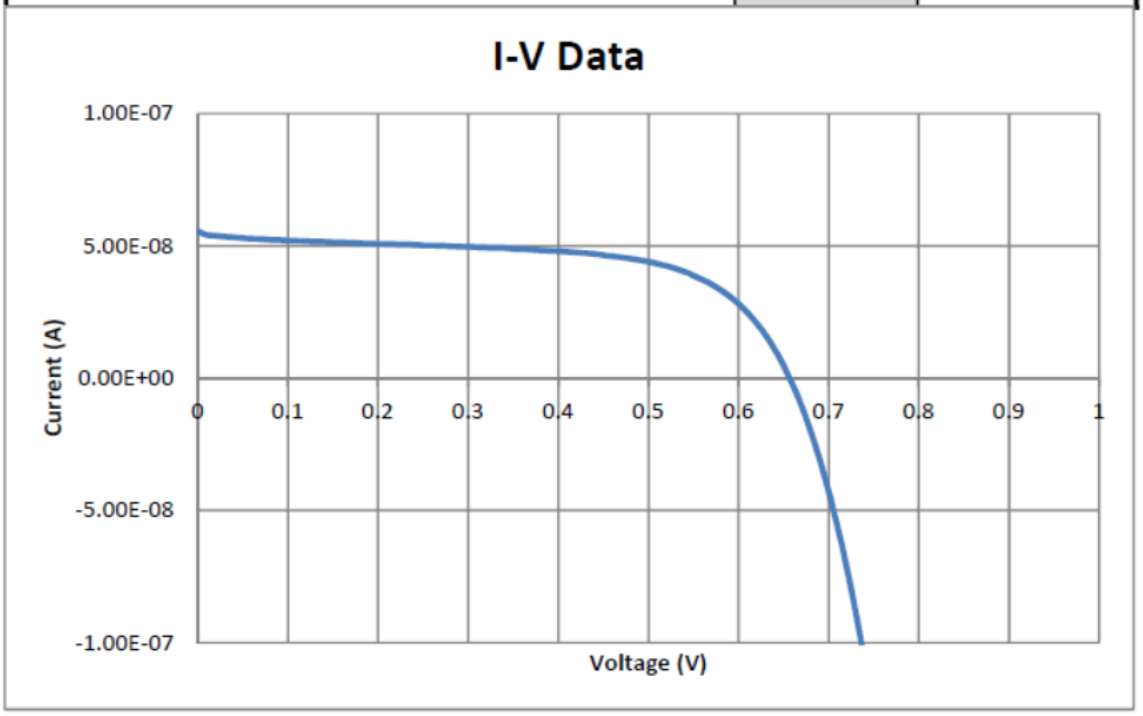

Figure 5.24. CityLabs I-V Curve data for serial number 18 that was provided to Purdue University upon receipt of the devices.

For these reasons, SN18 was chosen to be used in this experiment over SN20 due to the larger short circuit current of 55.5 nA opposed to 36.7 nA respectively. R_{SH} is indirectly represented within the fill factor value. The higher R_{SH}, the more square the I-V curve and the higher the quality of the junction as previously stated. It can be clearly seen from Eq. 5.2 that the higher the value of R_{SH} the smaller the contribution of the second term proportional to R_{SH}^{-1} is to the overall measured current.

Battery Serial Number	1020140020	Max Power	1.53E-05 mW
Battery Measurement Date	Tue, Jan 17, 2017 5:13 PM	Vmp	5.35E-01 V
Activity Level	115.07 mCi as of 1/18/2017	Imp	2.87E-05 mW
		Isc	3.67E-08 A
		Voc	7.02E-01 V
		Fill Factor	59.53 %

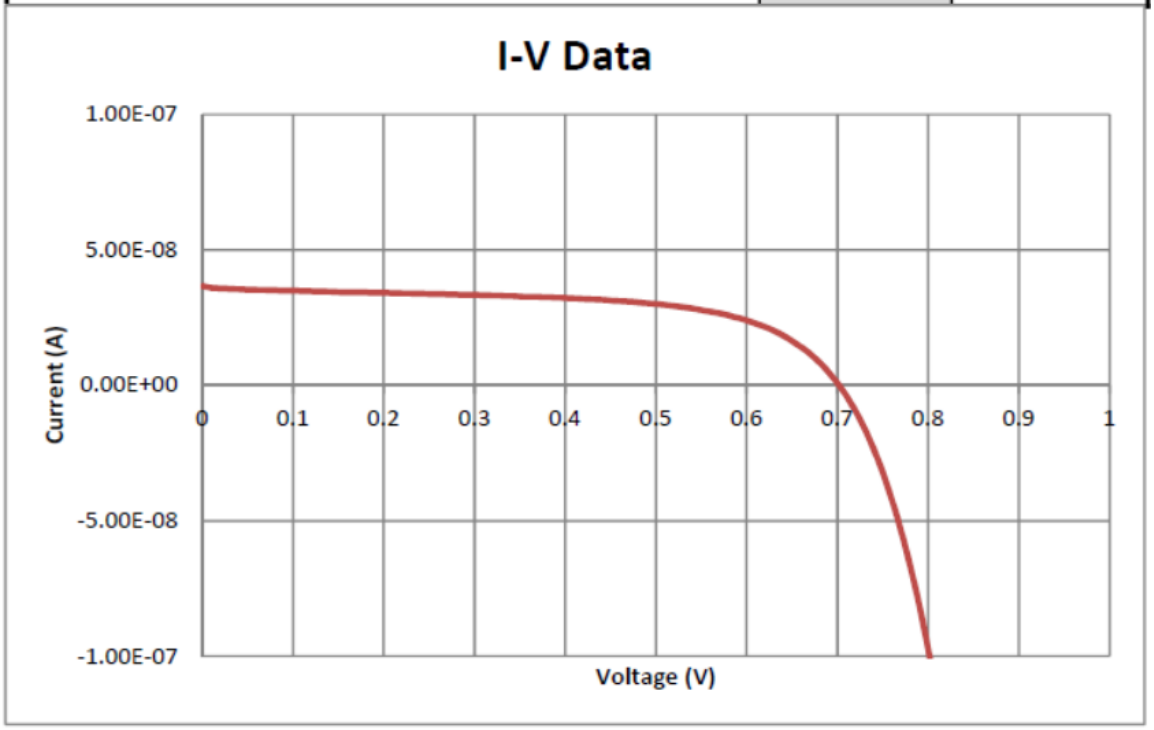

Figure 5.25. CityLabs I-V Curve data for serial number 20 that was provided to Purdue University upon receipt of the devices.

Reference Diode Data

As previously mentioned, reference diodes from the same wafer lot as that of the two betavoltaics were provided in addition to I-V curves of the betavoltaics prior to tritiation. I-V sweeps of the two reference diodes taken by Purdue University, and the I-V curves taken by City Labs of the two betavoltaics prior to tritiation, can be seen in Fig. 5.26. It can be clearly seen from Fig. 5.26 that Reference B and serial number 18 have the most closely related I-V curves in the plot. This fact served

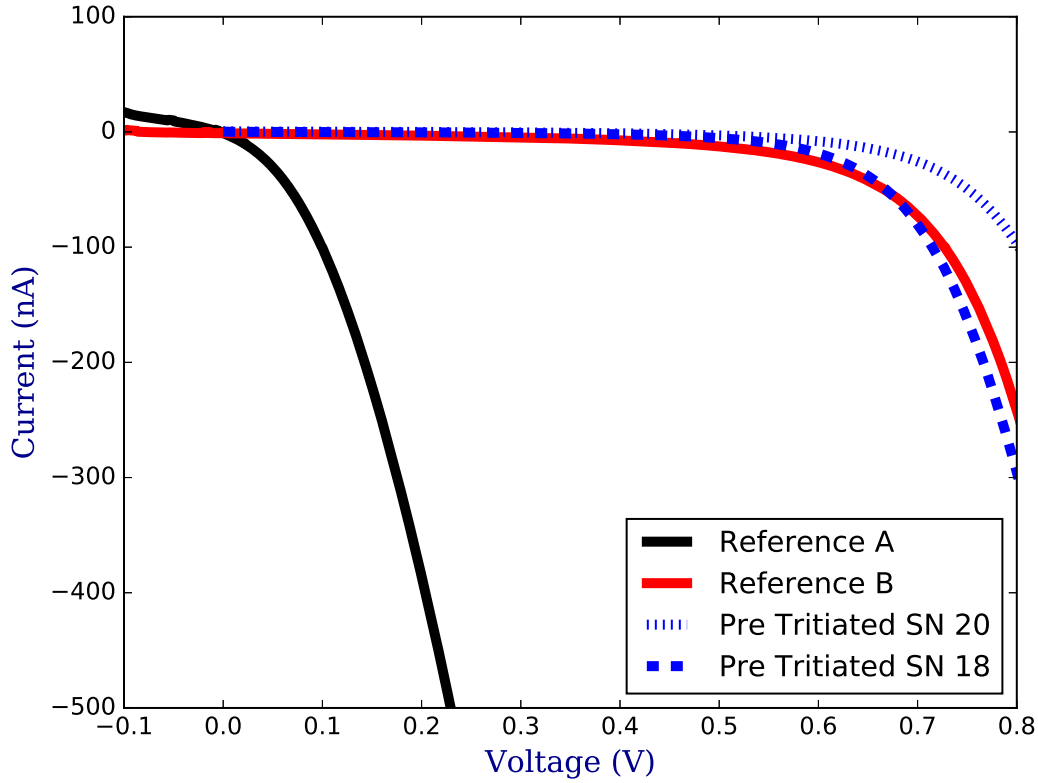

Figure 5.26. I-V sweeps of Reference A and B with I-V sweeps of SN18 and SN20 prior to being tritiated

as the basis for deciding to use reference B in the betavoltaic current monitoring experiment. Fig. 5.27 plots this same data from 0 to 0.1 volts, and illustrates the offsets between the curves. These offsets can be due to some combination of the following factors: environmental conditions at the time of measurement, the different equipement and setup used for the measurements, and physical differences within the devices themselves.

As an example of the effects of these factors on the electrical measurement process, Fig. 5.28 is a plot of two I-V curves of the same device, reference B, taken aproximately 8 months apart with the same electrical equipement. The one differ-

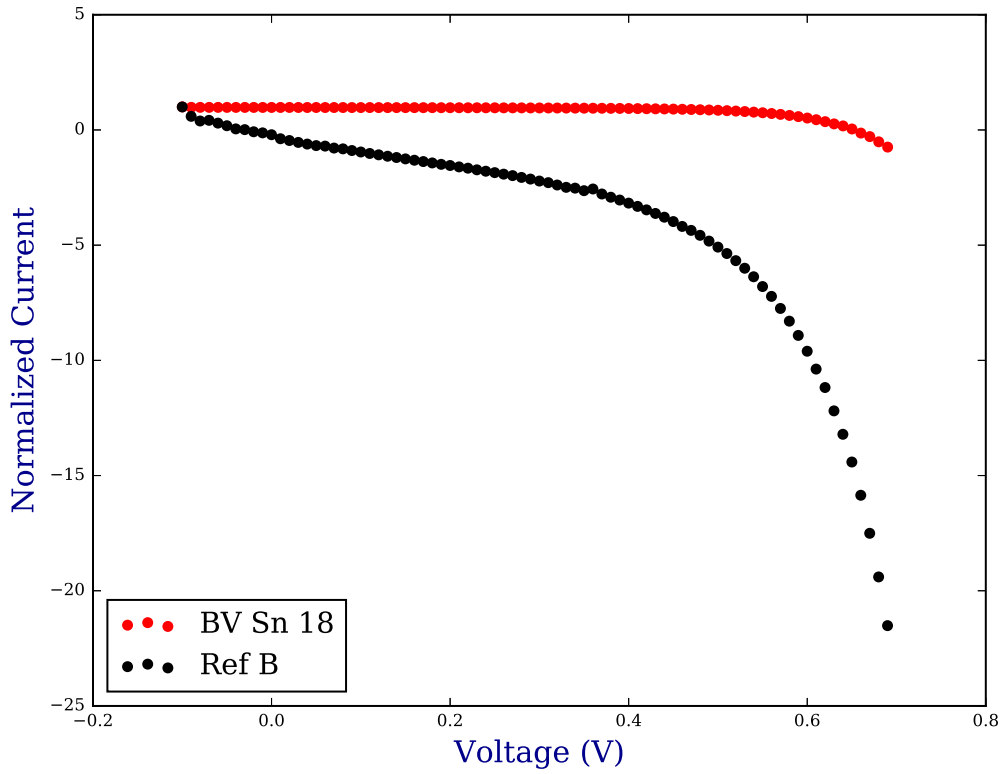

Figure 5.27. I-V sweeps of Reference A and B with I-V sweeps of SN18 and SN20 prior to being tritiated

ence between the two electrical test configurations is the length of triaxial cable used in the measurement. The 12/17 I-V curve used 15' cables with ambient temperature of 25.5°C, whereas the later measurement taken in 7/18 used 10' cables at an ambient temperature 27.5°C. The reduction in cable length would affect the amount of shunt capacitance affecting the measurement. This serves as one example of equipment variation responsible for measurement variation. Temperature control is a critical parameter in taking repeatable electrical measurements. The 2°C increase in temperature and the difference in cable length are likely responsible for the steeper I-V curve of the second measurement, seen in Fig. 5.28. Higher measured current values

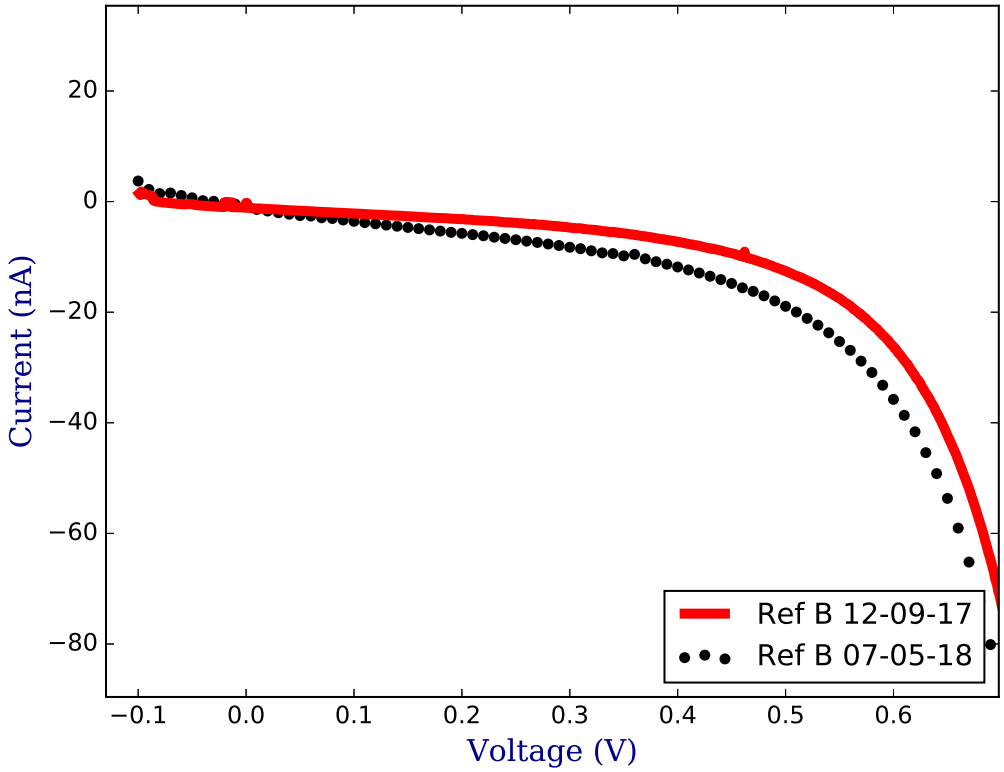

Figure 5.28. I-V sweeps of reference B taken 8 months apart.

in the second measurement are consistent with increased carrier concentration in the semiconducting devices at higher temperature(24).

I-V Curve Comparison

The intent of this experiment was to monitor a betavoltaic device and a reference diode in parallel with the intent of subtracting the measured reference current from the measured betavoltaic. By doing this the I_{dark} contribution could be eliminated from Eq. 5.8, and I_{rad} could be isolated as dicussed in the previously. This approach breaks down in the event the reference diode is not representative of the diode used in

the fabrication of the betavoltaic. Fig. 5.29 plots I-V curves for both the betavoltiac chosen for this experiment, serial number 18, and the selected reference diode, reference B. The curves exhibit the expected behavior, and are consistent with Fig. 5.5 except that the signs are reversed. Upon closer inspection, Fig. 5.30 illustrates the

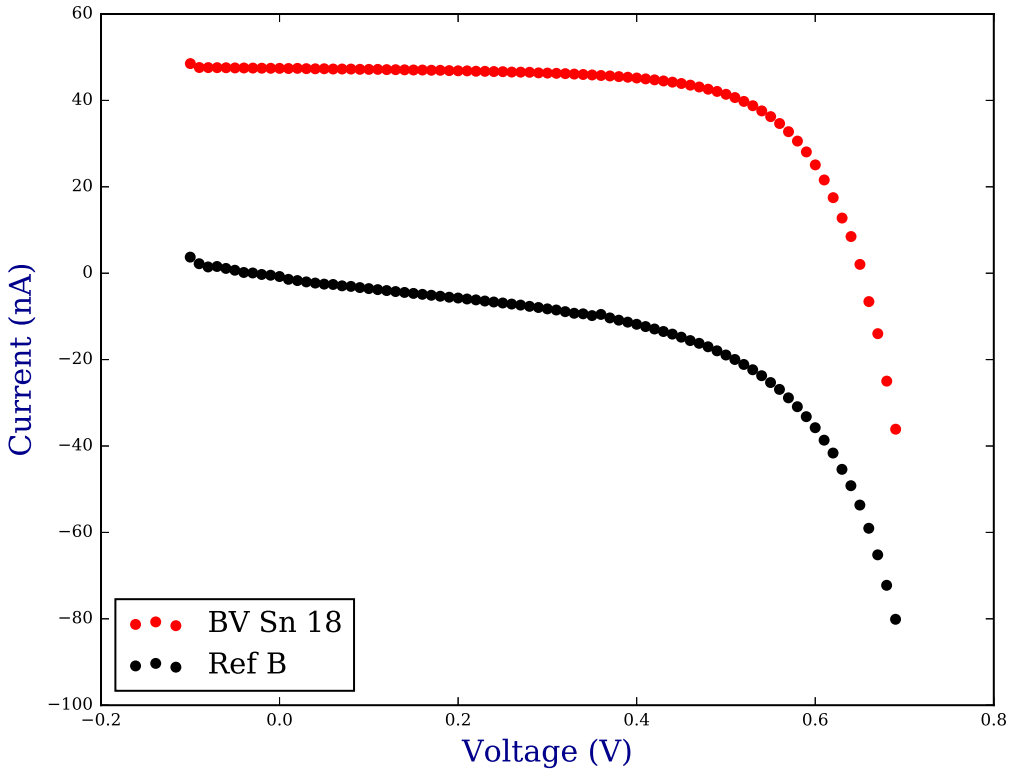

Figure 5.29. I-V sweeps of the serial number 18 and reference B plotted togther for comparison.

differences in the over shapes of the two curves. In this plot the measured betavoltaic current is offset by 48.5 nA which is the approximate value for I_{rad}. This offset aids in clearly distinguishing the difference in the overall shapes of the two curves. Subtracting 48.5 nA from the measured betavoltaic current is an approximate method for removing I_{rad} and isolating the I_{dark} of the selected betavoltaic. The offset I-V curve

is far move flat in nature in the range of 0.1 to 0.4 volts in comparison to reference B. The difference in slope of these two I-V curves within this range is likely to due to the overall quality of the devices. R_{SH} can be inferred from the slope of this I-V sweep about zero volts. A summary of R_{SH} measurements will be discussed in the following section. Upon inspection of these I-V curves, it appears that the assumption that reference B is representative of the betavoltaic device used in these experiments may be inaccurate, or only a rough approximation.

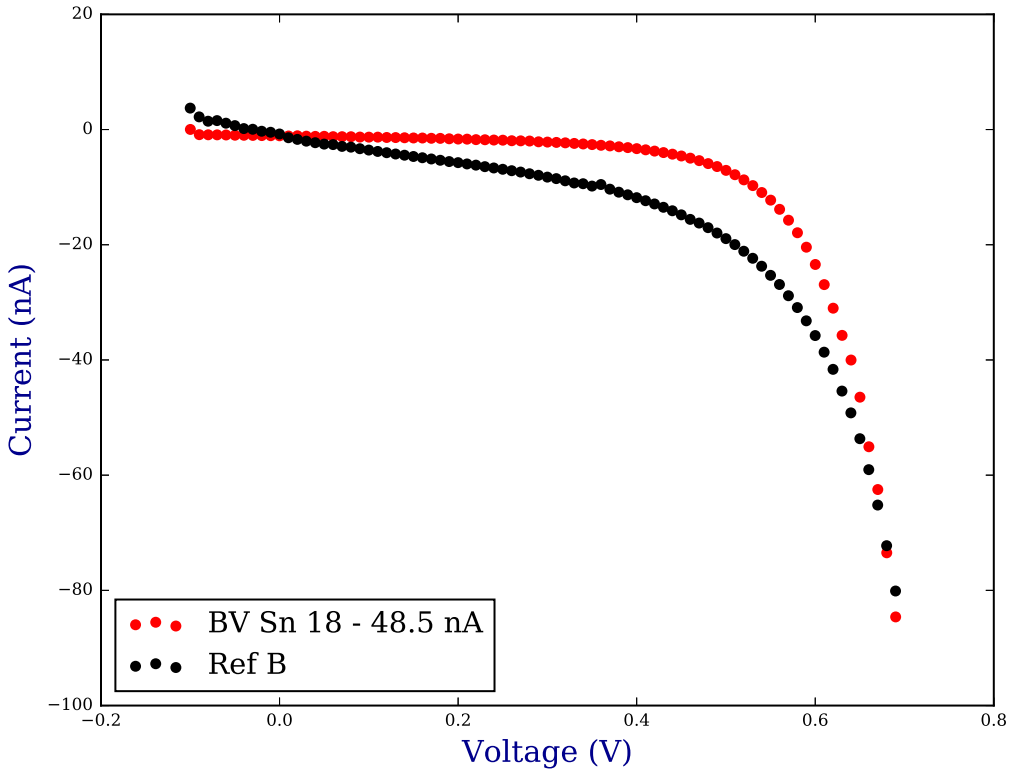

Figure 5.30. I-V sweeps of the serial number 18 and reference B plotted togther for comparison, where the measured betavoltaic value is offset by 48.5 nA.

Shunt Resistance

The shunt resistance, R_{SH}, is a critical parameter for accessing betavoltaic quality. It can be inferred from Eq. 5.2 that R_{SH} can be determined by calculating the slope of the I-V curve at zero volts, and can be defined as

$$R_{\mathrm{SH}} = (\frac{dV}{dI})_{(V=0.0V)} \tag{5.10}$$

Numerous I-V curves have been measured for both the betavoltiac and reference diodes over the course of the last year. A linear fit to the I-V curve data within the range of -0.1 to 0.1 V was used to calculate R_{SH} by taking the inverse of the fit slope parameter. This was also done for the range 0 to 0.1 volts since City Labs provided data did not extend below 0 volts. Table 5.2 summarizes these calculations. There are several takeaways from the data. The measurement of the reference diode shunt resistance is less variable (in absolute terms) than that of the betavoltaic device. This variability in both is likely due to a suboptimal curve sweep routine used to control the Keithly PMU. Parameters such as settling time are critical to precision repeatable volts sweeps. Settling time is the amount of time delay prior to taking a current measurment after the sourced voltage has been incremented. Most electronic equipement does not respond instantaneously and therefore requires time to stablize once an electrical parameter has been altered. However, this does not explain why the betavoltaic shunt resistance is more variable than of that of reference diode. One can speculate that it may be be due the fact that the betavoltaic curve is far more flat in the region of interest than that of reference diode, and the calculation of the slope is more sensitive to a variation in the data.

The voltage range and the number of data points used in the fit affect the calculated value. This is to be expected. Despite the variation, the data are sufficient to conclude that the betavoltiac shunt resistance is approximately 3 to 10 times larger than that of the reference diode. It can be inferred from these data that the diode used in

Table 5.2.
Shunt resistance calculations for serial number 18 and reference B devices.

Device	Date	Voltage Range (V)	Source	$R_{\mathrm{SH}}(M\Omega)$
Reference B	12-09-17	-.1 to .1	Purdue	73
Reference B	12-09-17	0 to .1	Purdue	93
Reference B	06-22-18	-.1 to .1	Purdue	45
Reference B	06-22-18	0 to .1	Purdue	60
Reference B	06-26-18	-.1 to .1	Purdue	61
Reference B	06-26-18	0 to .1	Purdue	55
Reference B	07-05-18	-.1 to .1	Purdue	50
Reference B	07-05-18	0 to .1	Purdue	44
BV SN 18 Pre H3	10-08-14	0 to .1	City Labs	330
BV SN 18	07-05-18	-.1 to .1	Purdue	445
BV SN 18	07-05-18	0 to .1	Purdue	400

the fabrication of serial number 18 is of higher quality than that of reference B. The measured current of reference B at a given voltage can be considered an upper bound on the dark current contribution to the measured current of the serial number 18 at the same voltage bias. This actual value of serial number 18's dark current contribution could be as much as 10 times smaller than that of reference B. This is consistent with the observed I-V curve "flatness" of serial number 18 in comparison to that of reference B's I-V curve.

In order to understand the behaviour of shunt resistance as a function of temperature, data were provided by another research group at Purdue University who had conducted IV sweeps on betavoltaics over temperature(22). Fig. 5.31 is consistent with standard diode behaviour with the exception of the vertical offset due to I_{rad} Fig. 5.32 illustrates the temperature dependence of R_{SH}. These results are consistent with previous work by Banerjee et al. and the known behavior of semiconductor resistivity,

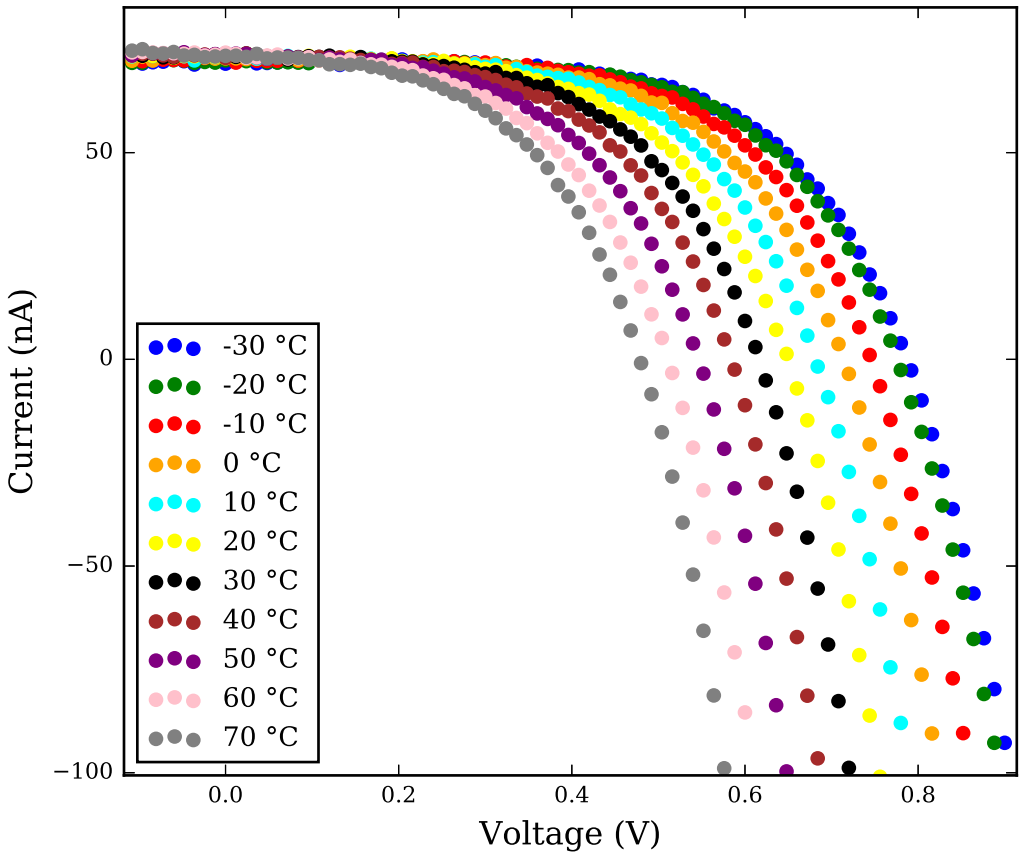

Figure 5.31. Betavoltaic IV curves taken over a temperature range of −30°C to 70°C

which decreases with increased temperature due to increased carrier concentration by thermal emission (83). Given the data presented in Fig. 5.32, a linear fit was applied to the data in order to determine R_{SH} as a function of temperature. The fit and the associated parameters are

$$R_{\mathrm{SH}} = (0.42 \pm 0.02 - 0.0055 \pm 0.0007 \times T) \times 10^{9}. \tag{5.11}$$

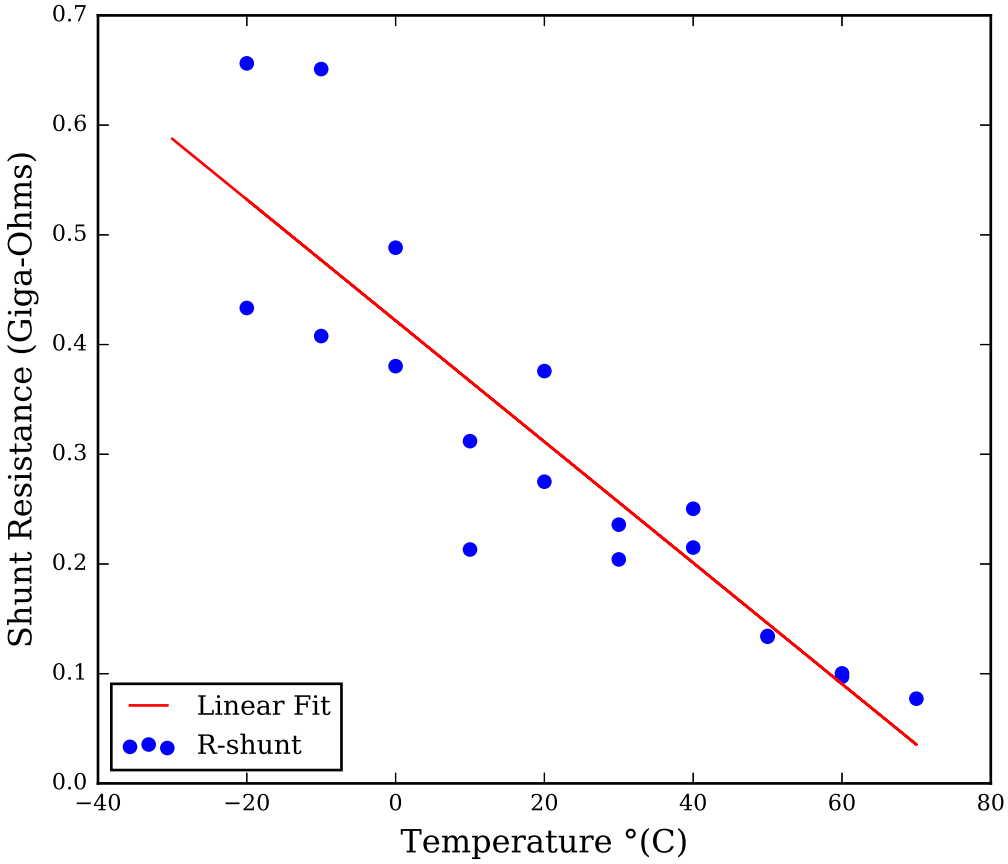

Figure 5.32. Calculated shunt resistance plotted versus temperature. The red line is a linear least-squares fit to the data.

5.5 Analysis of Betavoltaic Current Contributions

It is important to revisit the betavoltaic model in order to quanitify the values of the various model parameters. This approach will allow for approximations and simplification of the overall model described by Eq. 5.12 below.

$$I = I_{\mathrm{rs}} \left\{ \exp\left[\frac{e(V_{\mathrm{app}} - IR_{\mathrm{S}})}{nk_{\mathrm{B}}T} \right] - 1 \right\} + \frac{V_{\mathrm{app}} - IR_{\mathrm{S}}}{R_{\mathrm{SH}}} - I_{\mathrm{rad}}. \tag{5.12}$$

R_{S} has not been directly measured for these devices, however typical values for R_{S} are less than 1 ohm. Assuming R_{S} is of the order of 1 ohm, then it can be dropped

from Eq. 5.12 given that the variation (one standard deviation) in the applied voltage is approximately 1E-5 volts and that the IR_{S} is of the order of 5E-8 volts given a measured current of 50 nA. Making this approximation the model is reduced to

$$I = I_{\mathrm{rs}} \left\{ \exp\left[\frac{eV_{\mathrm{app}}}{nk_{\mathrm{B}}T} \right] - 1 \right\} + \frac{V_{\mathrm{app}}}{R_{\mathrm{SH}}} - I_{\mathrm{rad}}. \tag{5.13}$$

The measurement current is approximately 50 nA and is dominatd by the I_{rad} term at voltages near zero given that I_{dark}, the first two terms in Eq. 5.13, is zero at zero volts. For this reason bias voltages in the range of -0.1V to 0.1 V were chosen for current monitoring purposes. Given an accepted half-life of 4500 days for tritium, the expected daily reduction of the current is approximately 0.015%. This amounts to roughly 8 pA per day. The 8 pA per day value will serve as metric for quantifying current contributions and converting them to units of time in the Context of the Accepted Half-life Value or (CAHV). The $\frac{V_{\mathrm{app}}}{R_{\mathrm{SH}}}$ term in Eq. 5.13 for a bias of $0.1V$ and a shunt resitance value of 300 $M\Omega$, is $\frac{V_{\mathrm{app}}}{R_{\mathrm{SH}}}$ equal to 333 pA corresponding to approximately 42 days of decay.

The measured reference B diode current at $-0.1V$ is approximately -0.9 nA and serves as an upper bound for the betavoltaic I_{dark} contribution. In a previous section it was estimated that this value is anywhere from 3 to 10 times greater than the actual value for I_{dark} for betavoltaic serial number 18. Assuming a conservative factor of 3, this amounts to approximately 38 days of decay in the CAHV. I_{dark} has both temperature and voltage dependence. Great effort was taken to control both temperature and bias voltage for this experiment. The temperature variation for this experiment has a standard deviation of approximatley 0.1%. The fractional change in I_{dark} due to a 3σ change in temperature is approximately 0.002% or 3.6×10^{-3} pA or 39 ms in the CAHV. The bias voltage variation for this experiments has a standard deviation of approximatley 0.005%. Using this fact, the fractional change in I_{dark} due to a 3σ deviation in bias voltage is approximately 0.001% or 1.8×10^{-3} pA or 20 ms in the CAHV. This analysis strongly indicates that I_{dark} can be considered a constant, and its contribution is less than 1% of the measured betavoltaic current.

5.6 Results

5.6.1 Error Analysis

Before discussing the experimental results of subsequent analyses, it is important to review how both statistical and systematic error was estimated. The following datasets consisted of binned raw data for half hour intervals. Here x_j^{bin}, is the calculated binned betavoltaic value for the j^{th} bin of raw data defined as

$$x_j^{bin} = \bar{x}_j = \frac{1}{N_j} \sum_{i=1}^{N_j} x_i^{raw} \tag{5.14}$$

where N_j is the number of data points in the j^{th} bin. Given equation 5.14, the statistical error for each x_j^{bin} is defined as

$$\sigma^{Stat.} = \sigma x_{\text{j, Stat.}}^{bin} = \frac{\sigma_{\bar{x}_j}}{\sqrt{N_j}} \tag{5.15}$$

This estimation for the statistical errror assumes that the raw data to be binned is normally distributed within the half hour interval. The fractional change due to the exponential decay is 0.015% per day, which equates to 0.0003% every half hour. This small fractional change is unlikely to skew the raw data within the bin. A representative histogram of the raw betavoltaic current measurements within a bin can be seen in Fig. 5.33. The histogram of the raw data indicates that the raw data are normally distributed. This approach is an estimate for the statistical errror and likely captures a portion of the systematic error in the measurement.

The Keithley instrumental error for an individual k^{th} measurement x_k^{raw} is

$$\sigma x_k^{raw} = .06\% \times x_k^{raw} + 40 \text{ pA}. \tag{5.16}$$

The systematic error was estimated by propagating the Keithley individual measurement error through the binning of the betavoltaic data for each binned data point. This was done by adding the individual measurement errors in quadature.

$$\sigma^{Syst.} = \sigma x_{\text{j, Syst.}}^{bin} = \frac{\sqrt{\sum_{i=1}^{N_j} (\sigma x_i^{raw})^2}}{N_j} \tag{5.17}$$

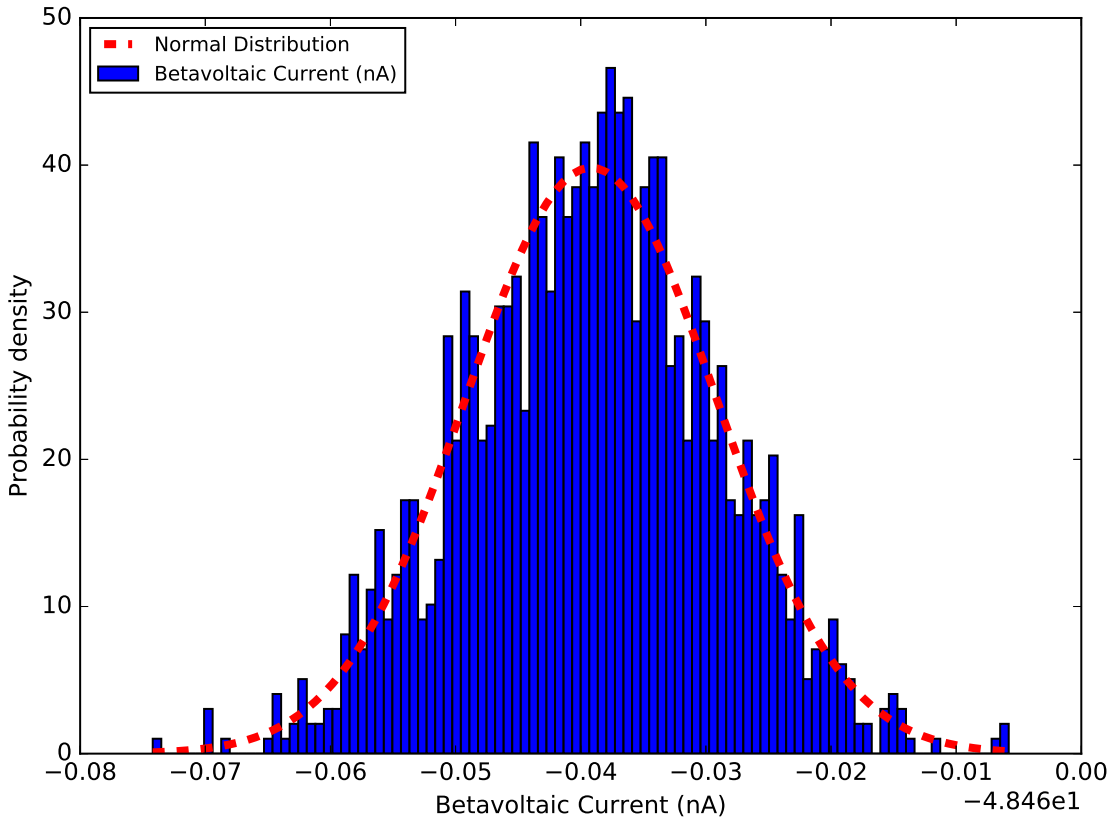

Figure 5.33. Representative histogram of raw betavoltaic current data within a half hour bin

It is important to note that Eq. 5.16 is the stated measurement accuracy of the Keithley 2634b. This error is interperted as an absolute error for a calibrated device for a given measurement, it does not appear from the specification to address overall device stability over time. This is important because stability over time is more critical to this experiment than that of absolute accuracy. It is the rate of change of the current from which the half-life is derived, not the absolute value. Given that this error estimate does not address stability over time, it is possible that this approach may overestimate the systematic error within a given measurement.

In the sections to follow the datasets consisting of binned data were fit to numerous models using a non-linear least squares fit curve fitting function found in the optimize module of Scipy (60; 61). This function returns both the fit parameters as well as the covariance matrix (error matrix), which provides the associated error for each fit parameter. The statistical error, $\sigma^{Stat.}$ for each binned datum point was then used as the error value when executing the curve fit function in the optimize module of Scipy. The square root of the corresponding covariance matrix element for the λ parameter was converted to days and is reported as an estimate for the statistical half-life error for each fit. This same process was used for calculating the systematic error by substituting $\sigma^{Syst.}$ for $\sigma^{Stat.}$.

5.6.2 Experiment 1: Jasper, IN Collection Interval: 1-21-2018 to 3-6-2018

For this experiment, a small forward voltage of 0.1 V was applied to the betavoltaic. This value was chosen in order to operate the device in a stable condition. The applied voltage and current of both channels were recorded approximately every 0.7 seconds.

Environmentals: Experiment 1

Electrical data for both the betavoltaic and the reference diode as well as ambient environmental conditions were captured continuously for a period of 45 days at a rate of 1.4 Hz and 0.14 Hz respectively. The mean and one root-mean-square (RMS) standard deviation for the measured environmental parameters are given in Table 5.3. A Pearson correlation between each parameter and betavoltaic current was calculated, and is presented in the table.

Table 5.3.
Electrical and environmental parameters and their associated RMS variations over the 45 day data collection for Experiment 1.

Parameter	Unit	$\bar{x}$	σ	Pearson Coeff.
BV Voltage	(V)	0.10	1.3×10^{-5}	-0.401
Ref. Diode Current	(nA)	-0.814	0.005	0.757
BME Temperature	(°C)	23.79	0.04	0.717
BME Pressure	(Pa)	957	7	0.080
BME Rel. Humidity	(%)	2.06	0.09	-0.951
AC Line Voltage	(VAC)	124.1	0.80	-0.097
AC Line Frequency	(Hz)	60.02	0.01	0.033

Data Analysis: Experiment 1

The betavoltaic data collected during this experiment are shown in Fig. 5.34, which has the raw betavoltaic current measurements, a 0.5 hour binned average, and the projected betavoltaic current using the accepted half-life of 4500 days, both currents starting from the initial measured I_{rad}. The binned data were used for fitting purposes and half-life determinations.

Table 5.4.
Observed and projected current summary for Experiment 1

Data	Initial (nA)	Final (nA)	Delta (pA)	Percent of Initial (%)	0.1 V/R_{SH} (pA)
Observed	-49.554	-49.191	-363	0.73	333
Projected	-49.554	-49.211	-341	0.69	333

Several fits were explored in order to identify dominant factors associated with the betavoltiac model presented in previous sections of this work. These fits were used

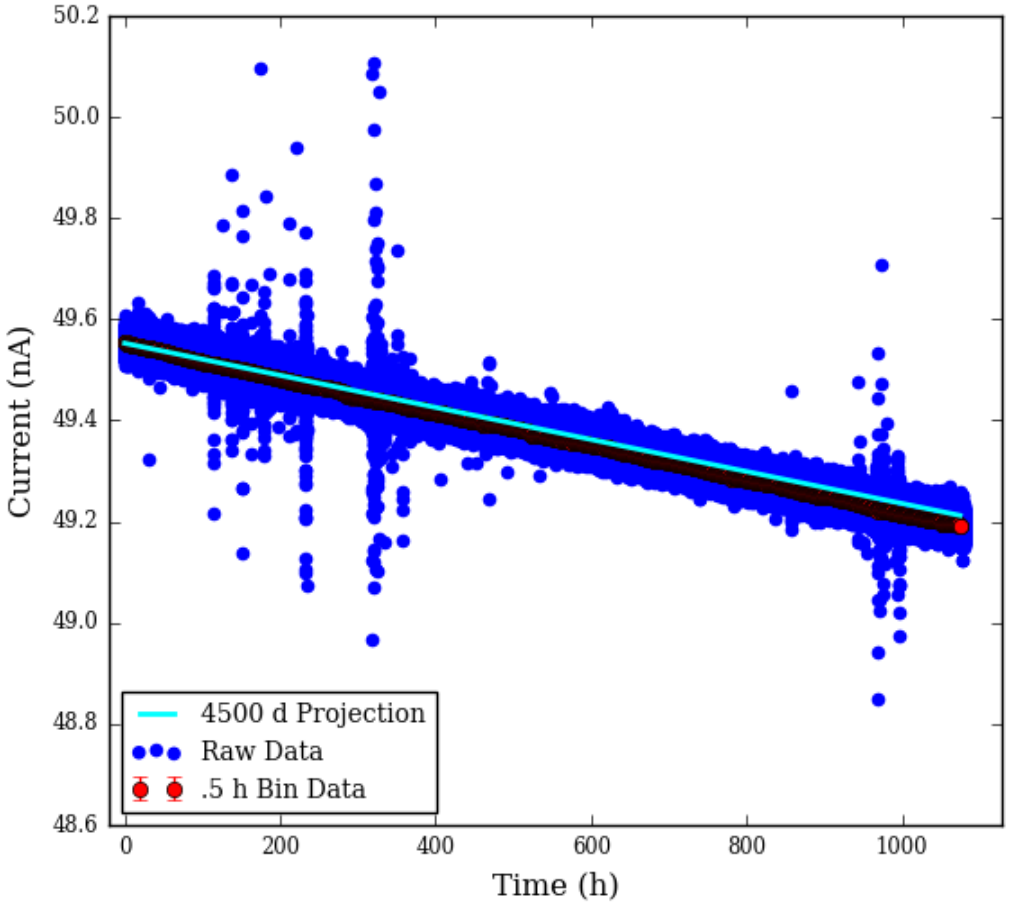

Figure 5.34. Measured BV Current, binned BV current, and projected BV current using the accepted tritium half-life for Experiment 1

to model the measured betavoltaic current from serial number 18. Current measurements were also taken on reference B, however these data are not utilized in the data fitting process. For all subsequent experiments, the reference diode data are used to bound betavoltaic fit parameters.

$$Fit0 = C_0 \exp[-\lambda t] \tag{5.18}$$

Fit0 models the measured betavoltaic current as a simple exponential function dominated by I_{rad}. This fit assumes I_{dark} is negligible and can be ignored. Given that the I_{dark} contribution to the measured betavoltaic current is estimated to be in the range of 0.09 to 0.3 nA, less than 1 % of the overall measured current, this appears to be a reasonable assumption.

$$Fit1 = C_0 \exp[-\lambda t] + C_1(\exp[\frac{e(V)}{k_{\mathrm{B}}T}] - 1) + \frac{V}{0.3} \tag{5.19}$$

Fit1 is Fit0 plus I_{dark}. Including I_{dark} incorporates both temperature and bias voltage. A value of 300 $M\Omega$ is used for the betavoltaic R_{SH}.

$$Fit2 = C_0 \exp[-\lambda t] + C_1(\exp[\frac{e(V)}{k_{\mathrm{B}}T}] - 1) + \frac{V}{(0.4218 - 0.0055 \times T)} \tag{5.20}$$

Fit2 attempts to take into account the temperature dependence of R_{SH}, and leverages the linear fit presented in the previous section on shunt resistance.

$$Fit3 = C_0 \exp[-\lambda t] + C_1(\exp[\frac{e(V)}{k_{\mathrm{B}}T}] - 1) + \frac{V}{0.3} + C_2 \times h \tag{5.21}$$

Fit3 attempts to compensate for lost current due to parasite current paths due to humidity and ionic contamination on the surface of the betavoltaic device. C_2 can be described as humidity compensation coefficient which has units of nA per % RH. A value of 300 $M\Omega$ is used for the betavoltaic R_{SH} in Fit3.

$$Fit4 = -49.8830 \exp[-\lambda t] + C_1(\exp[\frac{e(V)}{k_{\mathrm{B}}T}] - 1) + \frac{V}{0.3} - 0.01 \times h \tag{5.22}$$

Fit4 sets the humidity compensation coefficient to -0.01, as well as sets the intial value of I_{rad} to -49.8830 nA.

$$Fit5 = C_0 \exp[-\lambda t] + C_1(\exp[\frac{e(V)}{k_{\mathrm{B}}T}] - 1) + \frac{V}{(0.4218 - 0.0055 \times T)} + C_2 \times h \tag{5.23}$$

Fit5 is Fit3 with the exception of incorporating the temperature dependence of R_{SH}.

The data fits used a non-linear least squares curve fitting function as previously mentioned.

Table 5.5.
Parameter bounds were used in the fitting of Experiment 1 data. These bounds leverage the measurements taken on the reference diode, which serve as an upper bound on I_{dark} contribution to the measured betavoltaic current of serial number 18.

Fit	C_0 (nA)	λ	C_1 (nA)	C_2 (nA/%RH)
Fit0	NA	N/A	N/A	N/A
Fit1	-51 to -46	0 to ∞	0 to 1	N/A
Fit2	-51 to -46	0 to ∞	0 to 1	N/A
Fit3	-51 to -46	0 to ∞	0 to 1	-1 to 1
Fit4	-49.8830*	0 to ∞	0 to 1	-0.01*
Fit5	-51 to -46	0 to ∞	0 to 1	-1 to 1

Table 5.6.
Fit parameters results and tritium half-life determinations for Experiment 1. Statistical and systematic error values for the half-life are reported. The reported $\chi^2_{D.F.}$ value was calculated with the estimated value for statistical error.

Fit	C_0 (nA)	C_1 (nA)	C_2 (nA/%RH)	$t_{1/2}$ (d)	$\sigma^{Stat.}t_{1/2}$ (d)	$\sigma^{Syst.}t_{1/2}$ (d)	$\chi^2_{D.F.}$
Fit0	-49.5500	N/A	N/A	4264	0.2	1.5	37.4
Fit1	-49.8830	3.47×10^{-8}	N/A	4295	1.2	7.2	38.5
Fit2	-49.8938	4.18×10^{-18}	N/A	4287	1.2	7.1	41.6
Fit3	-49.8596	3.60×10^{-21}	-0.01	4250	1.3	7.8	36.9
Fit4	-49.8830	4.08×10^{-04}	-0.01	4272	0.2	1.5	37.1
Fit5	-49.8961	3.47×10^{-21}	-0.01	4240	1.3	7.7	40.5

$\chi^2_{D.F.}$ values of approxiamtely 1 were calculated when both statistical and systematic error estimates were taken into account. The reason for only using the $\sigma^{Stat.}$,statistical error, for calculating $\chi^2_{D.F.}$ in Table 5.6 was to maintain consistency in the data analysis for the numerous experiments to be discussed. In Experiments 2 - 4, when the estimate for $\sigma^{Syst.}$, systematic error, was used in the calculation of $\chi^2_{D.F.}$, values less than 1 were calculated. $\chi^2_{D.F.}$ values less than 1 are a strong indication that the error

is being over estimated. However, the square root of $\chi^2_{D.F.}$ using only the statistical error can be used to estimate the amount of systematic error not accounted for in calculation in $\chi^2_{D.F.}$. The square root of the $\chi^2_{D.F.}$ values calculated in Experiment 1 indicate that the overall error is 6 times greater than that of the statistical error. In Experiement 1 the ratio of the mean $\sigma^{Syst.}$ to $\sigma^{Stat.}$ is approximately 6, which is consistent with the large $\chi^2_{D.F.}$ values calculated using only $\sigma^{Stat.}$.

5.6.3 Experiment 2: Purdue University, Collection Interval: 7-07-18 to 8-26-18

For this experiment, a small reverse voltage of -0.1 V was applied to both the betavoltaic and reference diode.

Environmentals: Experiment 2

Electrical data for both the betavoltaic and the reference diode as well as ambient environmental conditions were captured continuously for a period of 51 days at a rate of 1.4 Hz and 0.14 Hz respectively. The mean and one root-mean-square (RMS) standard deviation for the measured environmental parameters are given in Table 5.7. A Pearson correlation between each parameter and betavoltaic current was calculated, and is presented in the table.

Data Analysis: Experiment 2

The betavoltaic data collected during this experiment are shown in Fig. 5.35, which has the raw betavoltaic current measurements, a 0.5 hour binned average, and the projected betavoltaic current using the accepted half-life of 4500 days, both currents starting from the initial measured I_{rad}. The binned data were used for fitting purposes and half-life determinations.

Table 5.7.
Electrical and environmental parameters and their associated RMS variations over the 51 day data collection for Experiment 2.

Parameter	Unit	$\bar{x}$	σ	Pearson Coeff.
BV Voltage	(V)	-0.10	5.0×10^{-6}	0.646
Ref. Diode Current	(nA)	-0.91	0.003	0.401
BME Temperature	(°C)	26.77	0.03	0.617
BME Pressure	(Pa)	945	3	-0.011
1 BME Rel. Humidity	(%)	1.03	0.11	0.999
AC Line Voltage	(VAC)	120.0	0.70	0.315
AC Line Frequency	(Hz)	60.04	0.02	-0.074

Table 5.8.
Observed and projected current summary for Experiment 2

Data	Initial (nA)	Final (nA)	Delta (pA)	Percent of Initial (%)	-0.1 V/R_{SH} (pA)
Observed	-48.499	-48.073	-426	0.88	-333
Projected	-48.498	-48.119	-379	0.78	-333

The same fits used in Experiment 1, were explored in Experiment 2 except for Fit4. Fit4 sets the humidity compensation coefficient to 0.1, as well as sets the intial value of I_{rad} to -48.1632 nA. The fits were used to model the measured betavoltaic current from serial number 18. Current measurements were also taken on reference B, however these data are not utilized in the data fitting process.

$$Fit4 = -48.1632 * \exp[-\lambda t] + C_1(\exp[\frac{e(V)}{k_{\mathrm{B}}T}] - 1) + \frac{V}{.3} + .1 \times h \tag{5.24}$$

The data fits used a non-linear least squares fit curve fitting function as previously mentioned.

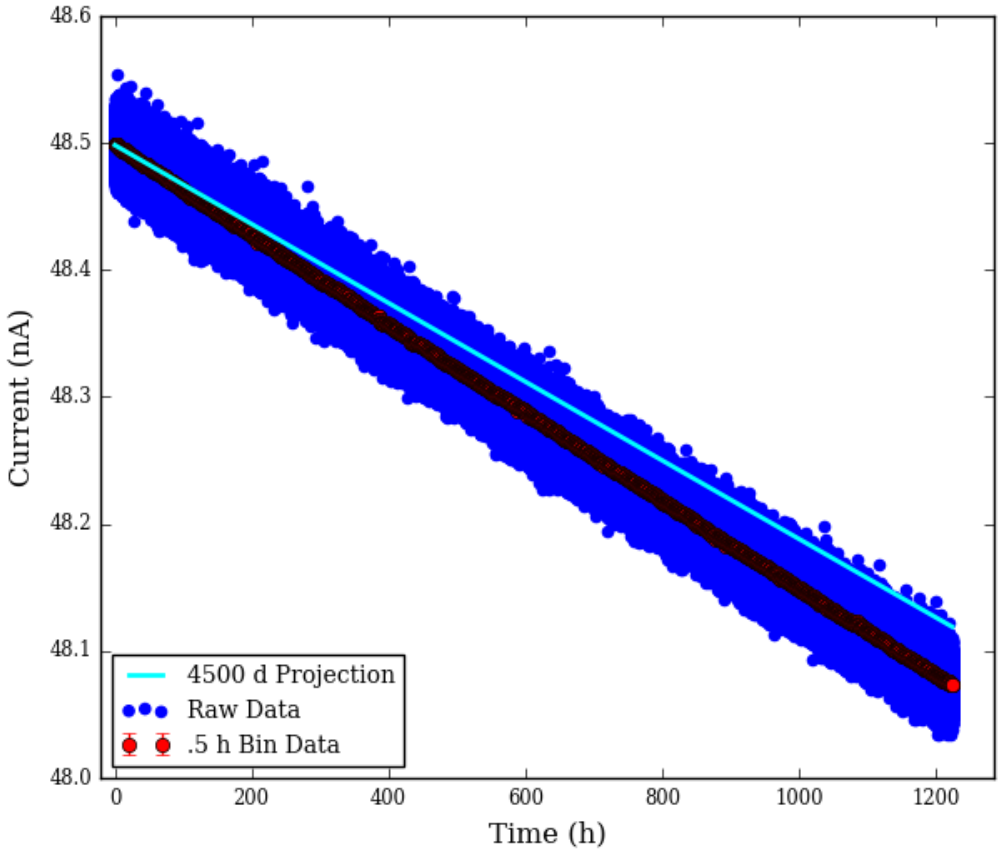

Figure 5.35. Measured BV Current, binned BV current, and projected BV current using accepted tritium half-life for Experiment 2

$\chi^2_{D.F.}$ values of approxiamtely 0.3 were calculated when both statistical and systematic error estimates were taken into account. $\chi^2_{D.F.}$ values less than 1 are a strong indication that the error is being over estimated. The square root of the $\chi^2_{D.F.}$ values calculated in Experiment 2 indicate that the overall error is 3 times greater than the statistical error. In Experiement 2 the ratio of the mean $\sigma^{Syst.}$ to $\sigma^{Stat.}$ is approximately 7. Though these two numbers differ by at least factor of 2, it is consistent with the fact that the calculated $\sigma^{Syst.}$ is an overestimate.

Table 5.9.
Parameter bounds were used in the fitting of Experiment 2 data. These bounds leverage the measurements taken on the reference diode, which serve as an upper bound on I_{dark} contribution to the measured betavoltaic current of serial number 18.

Fit	C_0 (nA)	λ	C_1 (nA)	C_2 (nA/%RH)
Fit0	N/A	N/A	N/A	N/A
Fit1	-50 to -45	0 to ∞	0 to 1	N/A
Fit2	-50 to -45	0 to ∞	0 to 1	N/A
Fit3	-50 to -45	0 to ∞	0 to 1	-1 to 1
Fit4	-48.1632*	0 to ∞	0 to 1	0.1*
Fit5	-50 to -45	0 to ∞	0 to 1	-1 to 1

Table 5.10.
Fit parameters results and tritium half-life determinations for Experiment 2. Statistical and systematic error values for the half-life are reported. The reported $\chi^2_{D.F.}$ value was calculated with the estimated value for statistical error.

Fit	C_0 (nA)	C_1 (nA)	C_2 (nA/%RH)	$t_{1/2}$ (d)	$\sigma^{Stat.}t_{1/2}$ (d)	$\sigma^{Syst.}t_{1/2}$	$\chi^2_{D.F.}$
Fit0	-48.4969	N/A	N/A	4009	0.2	1.2	12.0
Fit1	-48.1632	6.25×10^{-4}	N/A	3982	61.4	451	12.1
Fit2	-47.1541	1.0	N/A	3894	61.2	451	11.7
Fit3	-47.2455	1.0	0.07	4208	70.9	526	9.4
Fit4	-48.1632*	1.0	0.1	4405	0.2	1.5	9.7
Fit5	-47.2047	1.0	0.06	4146	69.6	516	9.7

5.6.4 Experiment 3: Purdue University, Collection Interval: 9-10-18 to 9-22-18

For this experiment, a small reverse voltage of -0.001 V was applied to both the betavoltaic and reference diode. This value was chosen in order to operate both devices in a stable condition, but also to enhance I_{rad} while minimizing I_{dark}. This experiment ended after 13 days due to an unexpected power outage.

Environmentals: Experiment 3

Electrical data for both the betavoltaic and the reference diode as well as ambient environmental conditions were captured continuously for a period of 13 days at a rate of 1.4 Hz and 0.14 Hz respectively. The mean and one root-mean-square (RMS) standard deviation for the measured environmental parameters are given in Table 5.11. A Pearson correlation between each parameter and betavoltaic current was calculated, and is presented in the table.

Table 5.11.
Electrical and environmental parameters and their associated RMS variations over the 13 day data collection for Experiment 3.

Parameter	Unit	$\bar{x}$	σ	Pearson Coeff.
BV Voltage	(V)	-0.001	2.0×10^{-5}	
Ref. Diode Current	(nA)	-0.024	0.003	-0.935
BME Temperature	(°C)	26.81	0.007	0.444
BME Pressure	(Pa)	947	3	-0.232
BME Rel. Humidity	(%)	1.35	0.02	0.992
AC Line Voltage	(VAC)	121.3	1.8	-0.174
AC Line Frequency	(Hz)	60.03	0.01	-0.121

Data Analysis: Experiment 3

The betavoltaic data collected during this experiment can seen in Figure 5.36, which has the raw betavoltaic current measurements, a .5 hour binned average, and the projected betavoltaic value using the accepted half-life of 4500 days. The word projected is used given that the initial current measurements recorded by the setup serve as the initial value for I_{rad} and then the accepted value half-life value of tritium

is used to project the expected observed current reduction over the course of the experiment. The binned data was used for fitting purposes and half-life determinations.

Table 5.12.
Observed and projected current summary for experiment 3

Data	Initial (nA)	Final (nA)	Delta (pA)	Percent of Initial (%)	-0.001 V/R_{SH} (pA)
Observed	-47.812	-47.705	107	0.22	-3.33
Projected	-47.811	-47.716	95	0.20	-3.33

The same fits used in Experiment 1, were explored in Experiment 2 except for Fit4. Fit4 sets the humidity compensation coefficient to 0.012, as well as sets the intial value of I_{rad} to -48.8086 nA. These fits were used to model the measured betavoltaic current from serial number 18. Current measurements were also taken on reference B, however these data are not utilized in the data fitting process.

$$Fit4 = -48.8086 * \exp[-\lambda t] + C_1(\exp[\frac{e(V)}{k_{\mathrm{B}}T}] - 1) + \frac{V}{.3} + 0.012 \times h \tag{5.25}$$

Table 5.13.
Parameter bounds were used in the fitting of Experiment 3 data. These bounds leverage the measurements taken on the reference diode, which serve as an upper bound on I_{dark} contribution to the measured betavoltaic current of serial number 18.

Fit	C_0 (nA)	λ	C_1 (nA)	C_2 (nA/%RH)
Fit0	N/A	N/A	N/A	N/A
Fit1	-50 to -45	0 to ∞	0 to 1	N/A
Fit2	-50 to -45	0 to ∞	0 to 1	N/A
Fit3	-50 to -45	0 to ∞	0 to 1	-1 to 1
Fit4	-47.8086*	0 to ∞	0 to 1	0.012*
Fit5	-50 to -45	0 to ∞	0 to 1	-1 to 1

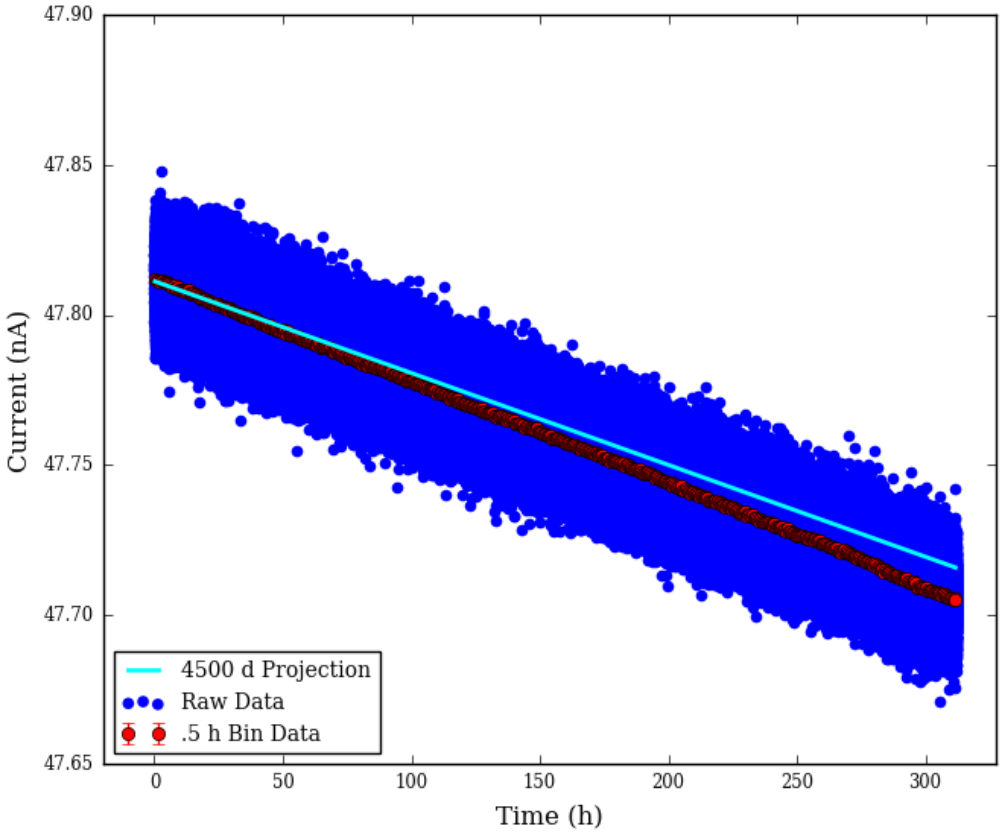

Figure 5.36. Measured BV Current, binned BV current, and projected BV current using accepted tritium half-life for Experiment 3.

$\chi^2_{D.F.}$ values of approxiamtely 0.04 were calculated when both statistical and systematic error estimates were taken into account. $\chi^2_{D.F.}$ values less than 1 are a strong indication that the error is being over estimated. The square root of the $\chi^2_{D.F.}$ values calculated in Experiment 3 indicate that the overall error is 1.8 times greater than the statistical error. In Experiement 3 the ratio of the mean $\sigma^{Syst.}$ to $\sigma^{Stat.}$ is approximately 9. Though these two numbers differ by at least factor of 4, it is consistent with the fact that the calculated $\sigma^{Syst.}$ is an over estimate.

Table 5.14.
Fit parameters results and tritium half-life determinations for Experiment 3. Statistical and systematic error values for the half-life are reported. The reported $\chi^2_{D.F.}$ value was calculated with the estimated value for statistical error.

Fit	C_0 (nA)	C_1 (nA)	C_2 (nA/%RH)	$t_{1/2}$ (d)	$\sigma^{Stat.}t_{1/2}$ (d)	$\sigma^{Syst.}t_{1/2}$	$\chi^2_{D.F.}$
Fit0	-47.8119	N/A	N/A	4046	1.2	10.7	3.3
Fit1	-47.8086	2.32×10^{-12}	N/A	4045	1.4	11.9	3.3
Fit2	-47.8079	5.89×10^{-14}	N/A	4045	1.4	11.9	3.3
Fit3	-47.7747	1.27×10^{-11}	-0.03	3974	10.7	94.3	3.3
Fit4	-47.8086*	9.93×10^{-25}	0.012	4076	1.3	10.9	3.4
Fit5	-47.7741	8.78×10^{-14}	-0.03	3975	10.7	94.3	3.2

5.6.5 Experiment 4: Purdue University, Collection Interval: 9-27-18 to 10-20-18

This experiment is a continuation of Experiment 3. A small reverse voltage of -0.001 V was applied to both the betavoltaic and reference diode. This experiment ran for approximately 24 days.

Environmentals

Electrical data for both the betavoltaic and the reference diode as well as ambient environmental conditions were captured continuously for a period of 24 days at a rate of 1.4 Hz and 0.14 Hz respectively. The mean and one root-mean-square (RMS) standard deviation for the measured environmental parameters are given in Table 5.15. A Pearson correlation between each parameter and betavoltaic current was calculated, and is presented in the table.

Table 5.15.
Environmental parameters and associated variations over a 12.5 day data collection.

Parameter	Unit	$\bar{x}$	σ	Pearson Coeff.
BV Voltage	(V)	-0.001	2.2×10^{-6}	-0.088
Ref. Diode Current	(nA)	-0.027	0.001	0.950
BME Temperature	(°C)	26.84	0.017	0.830
BME Pressure	(Pa)	948	5	0.095
BME Rel. Humidity	(%)	1.4	0.02	0.693
AC Line Voltage	(VAC)	119.9	0.4	-0.006
AC Line Frequency	(Hz)	60.03	0.01	0.643

Data Analysis

The betavoltaic data collected during this experiment can seen in Figure 5.37, which has the raw betavoltaic current measurements, a 0.5 hour binned average, and the projected betavoltaic value using the accepted half-life of 4500 days. The word projected is used given that the initial current measurements recorded by the setup serve as the initial value for I_{rad} and then the accepted value half-life value of tritium is used to project the expected observed current reduction over the course of the experiment. The binned data was used for fitting purposes and half-life determination.

Table 5.16.
Observed and projected current summary for experiment 4

Data	Initial (nA)	Final (nA)	Delta (pA)	Percent of Initial (%)	-0.001 V/R_{SH} (pA)
Observed	-47.672	-47.475	197	0.41	-3.33
Projected	-47.672	-47.495	176	0.37	-3.33

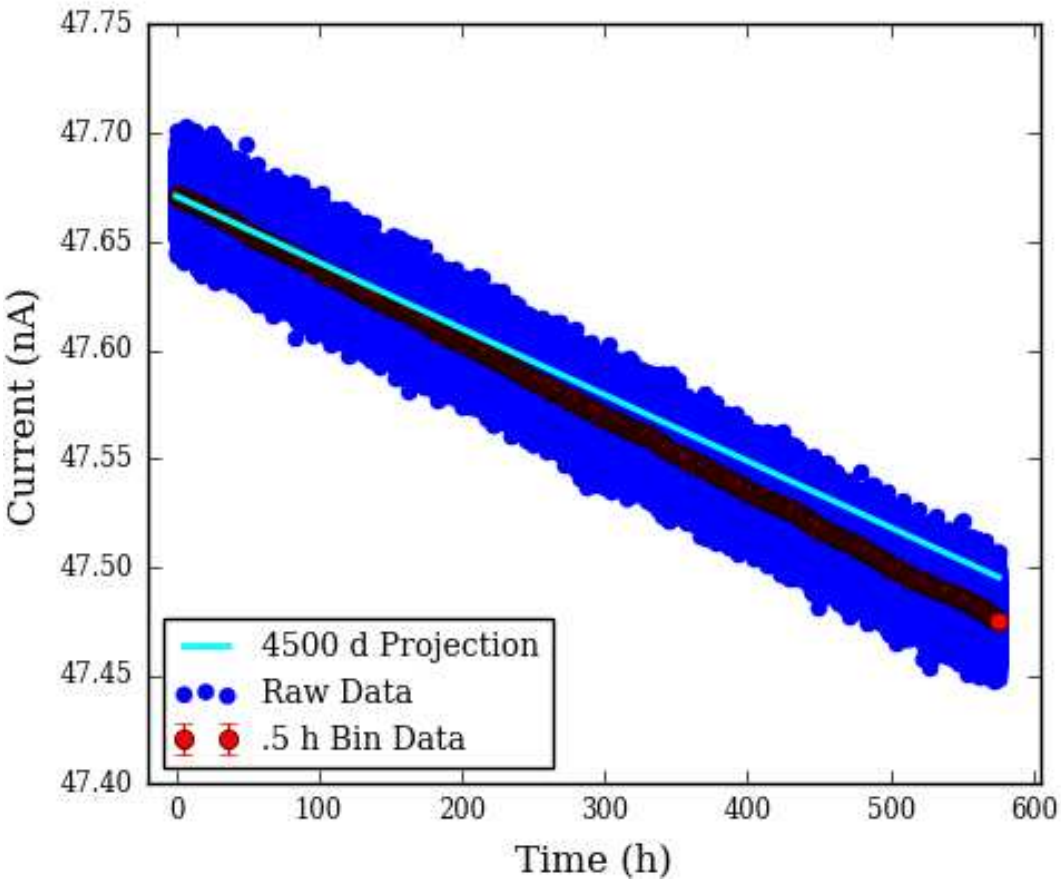

Figure 5.37. Measured BV Current, binned BV current, and projected BV current using accepted tritium half-life for Purdue 12.5 day experiment

The same fits used in Experiment 1, were explored in Experiment 4 except for Fit4. Fit4 sets the humidity compensation coefficient to 0.012, as well as sets the intial value of I_{rad} to -47.6845 nA. These fits were used to model the measured beartvoltaic current from serial number 18. Current measurements were also taken on reference B, however these data are not utilized in the data fitting process.

$$Fit4 = -47.6845 * \exp[-\lambda t] + C_1(\exp[\frac{e(V)}{k_{\text{B}}T}] - 1) + \frac{V}{.3} + 0.012 \times h \qquad (5.26)$$

Table 5.17.
Electrical and environmental parameters and their associated RMS variations over the 24 day data collection for Experiment 4.

Fit	C_0 (nA)	λ	C_1 (nA)	C_2 (nA/%RH)
Fit0	N/A	N/A	N/A	N/A
Fit1	-50 to -45	0 to ∞	0 to 0.03	N/A
Fit2	-50 to -45	0 to ∞	0 to 0.03	N/A
Fit3	-50 to -45	0 to ∞	0 to 0.03	-1 to 1
Fit4	-47.6845*	0 to ∞	0 to 0.03	0.012*
Fit5	-50 to -45	0 to ∞	0 to 0.03	-1 to 1

Table 5.18.
Fit parameters results and tritium half-life determinations for Experiment 4. Statistical and systematic error values for the half-life are reported. The reported $\chi^2_{D.F.}$ value was calculated with the estimated value for statistical error.

Fit	C_0 (nA)	C_1 (nA)	C_2 (nA/%RH)	$t_{1/2}$ (d)	$\sigma^{Stat.}t_{1/2}$ (d)	$\sigma^{Syst.}t_{1/2}$	$\chi^2_{D.F.}$
Fit0	-47.6718	N/A	N/A	4034	0.5	4.6	5.20
Fit1	-47.6673	0.03	N/A	4033	0.6	5.2	5.19
Fit2	-47.6667	0.03	N/A	4033	0.6	5.5	5.18
Fit3	-47.6536	0.03	-0.01	4020	0.9	7.5	4.75
Fit4	-47.6845*	2.97×10^{-20}	0.012	4050	0.5	4.7	6.98
Fit5	-47.6529	0.03	-0.04	4020	0.9	7.5	4.74

$\chi^2_{D.F.}$ values of approximately 0.07 were calculated when both statistical and systematic error estimates were taken into account. $\chi^2_{D.F.}$ values less than 1 are a strong indication that the error is being over estimated. The square root of the $\chi^2_{D.F.}$ values calculated in Experiment 4 indicate that the overall error is 2.2 to 2.6 times greater the statistical error. In Experiement 4 the ratio of the mean $\sigma^{Syst.}$ to $\sigma^{Stat.}$ is approx-

imately 9. Though these two numbers differ by at least factor of 4, it is consistent with the fact that the calculated $\sigma^{Syst.}$ is an overestimate.

6. SUMMARY DISCUSSION: SYSTEMATIC ERROR, ADVANTAGES TO APPROACH, AND METHODOLOGY REFINEMENT

6.1 Discussion of Experimental Results

The data captured from all four experiments were analyzed via six different parametric fits described previously. Fit0 is a simple expontential ignoring I_{dark} contributions, whereas Fit1 does include the I_{dark} term. Fit2 is an attempt to capture the temperature dependence of R_{SH}, which had minimal impact on the calculated half-life values. Half-life determinations from Fit0, Fit1, and Fit2 are comparable for all four experiments, and converge as bias voltage approaches zero. The last three fits used in the analyses attempt to take into account current loss due to humidity. Additional analysis was conducted in which we determined a value of 0.1 $nA/\%RH$ as a correction coefficient for accounting for humidity effects, persumably due to parasitic leakage paths caused by ionic contamination over the surface of the betavoltaic package. This analysis consisted of detrending both betavoltaic current and humidity, and using diurnal oscillations present in both data sets as means to estimate a correction coefficient. By applying this term to the fit for Experiment 2, a value of $4405^{\sigma_{stat.}\pm 0.2d}_{\sigma_{sys.}\pm 1.5d}$ with a $\chi^2_{D.F.}$ value of 9.7 was determined for the half-life of tritium, a value within approximately 2% of the accepted value. Values of $4076^{\sigma_{stat.}\pm 1.3d}_{\sigma_{sys.}\pm 2.4d}$ and $4050^{\sigma_{stat.}\pm 0.5d}_{\sigma_{sys.}\pm 1d}$ with $\chi^2_{D.F.}$ values of 3.4 and 6.98 were calculated in Experiments 3 and 4 respectively. These fits used a humidity correction coefficient of 0.012 $nA/\%RH$, which is roughly a factor of 10 smaller than that used in Experiment 2. The bias voltage between these sets of experiments was reduced by a factor of a 100. Fit3, Fit4, and Fit5 provide comparable results as well. Given the comparable results of Fit0, Fit1, and Fit2 and the comparable results of Fit3, Fit4, and Fit5, the six pa-

rameteric fits effectively reduce to two: an exponential fit with and without humidity compensation.

The residuals from all four experiments can be seem in Fig. 6.1, Fig. 6.2, Fig. 6.3, and Fig. 6.4. These residulas are representative for all six parametric fits. Given the obvious structure still present in the residuals from the fits in all four of experiments, indicate a need for model refinement. Systematics sources or error and or variation are likely to be contributing to this structure. Future efforts and models need to account for these systematics.

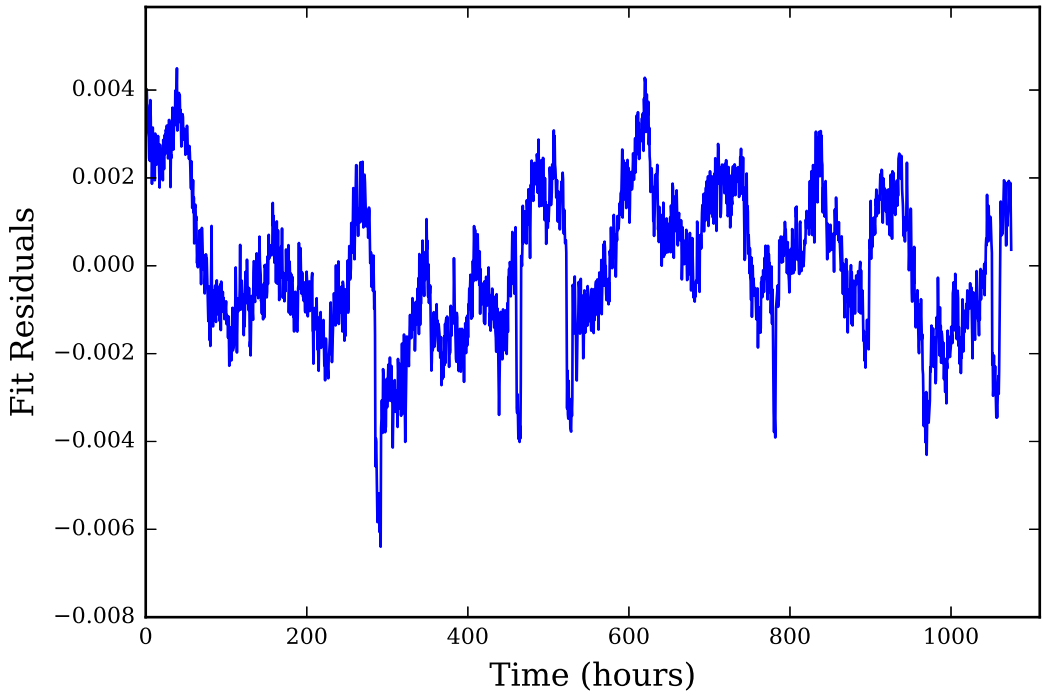

Figure 6.1. Fit0 current residuals in nanoamperes for Experiment 1.

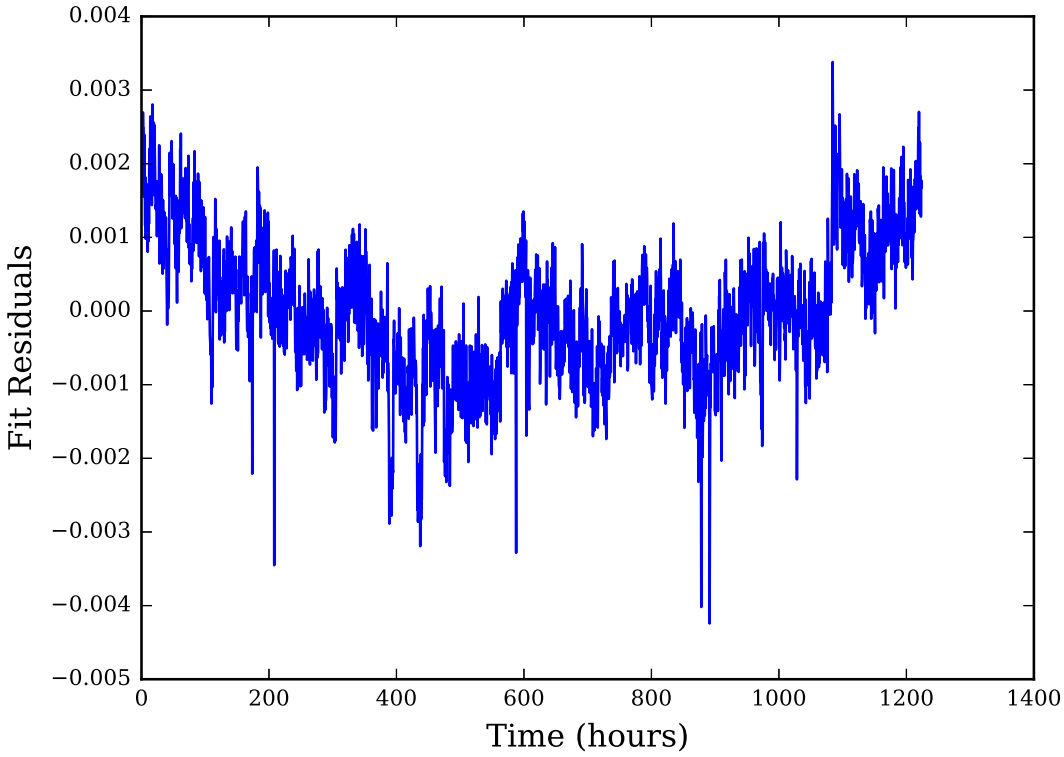

Figure 6.2. Fit0 current residuals in nanoamperes for Experiment 2.

6.1.1 Bias Dependence

Table 6.1 and Fig. 6.5 summarize the calculated half-life values for tritium via the measurement of betavoltaic currents. These results indicate that values within 10% to 5% of the canonical value of 4500 days can be achieved with this method. The amount of scatter within these results clearly indicate that all sources of systematic error have not been identified or addressed. Fig.6.6 illustrates the relative environmental variation amoung the four experiments. The amount of environmental variation appears to decrease for subsequent experiments. It is important to note that Experiments 1 and 2 ran for over 40 days, and that Experiments 3 and 4 ran for 13 and 24 days repsectively. Given that Experiments 3 and 4 ran for a shorter time

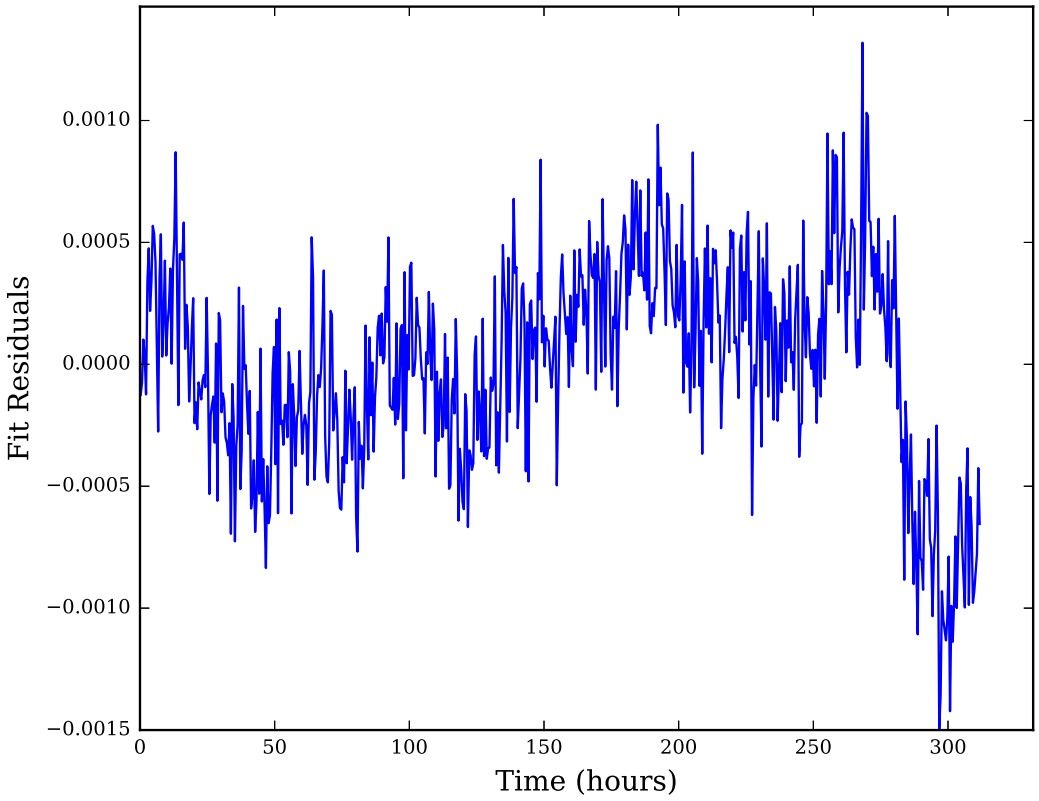

Figure 6.3. Fit0 current residuals in nanoamperes for Experiment 3.

period may account for the precieved reduction in environmental variability. Humidity is one possible source of systematic error that needs to be addressed in future experiments. Experiment 2, where the variation in humidity was greatest, yielded the closest value to the accepted half-life value of tritium. The variable impact of humidty on the calculated half-life values is cause for reservation with respect to the ability to accurately compensate for the associated induced systematic error. Future experiments in which the impact of humidity is further mitigated are warranted.

The half-life value calculated in Experiment 1 without compensating for humidity with a forward bias of 0.1 Volts is the next best result. This result in conjuncion with

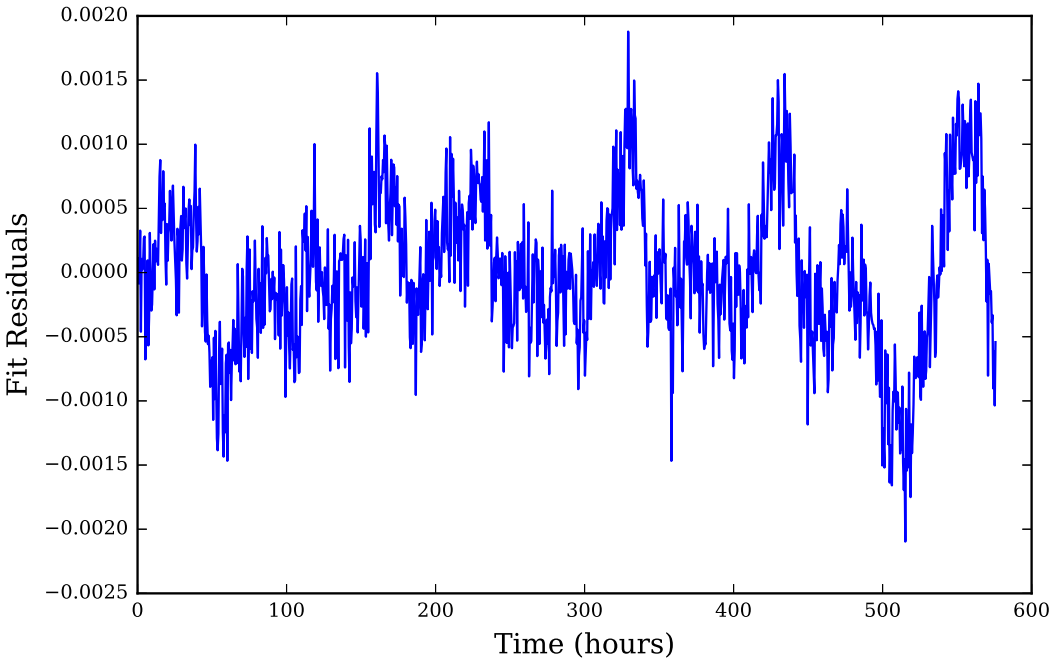

Figure 6.4. Fit0 current residuals in nanoamperes for Experiment 4.

a possible trend observed in Fig. 6.5 of improved accuracy at forward bias warrants conducting repeated experiments at forward bias. Experiment 1 also appears to have the most overall environmental varaibility. Finally, it is important to note that the orientation of the betavoltaic devices within the betavoltaic printed circuit board was rotated 180 degrees between Experiments 1 and 2. The programmed bias for the betavoltaic was -0.1 Volts. The reported polarity of the betavoltaic current by the Keithley 2634b in Experiment 1 was postive when a negative value was expected, and a negative value was reported for a reverse biased reference diode. Upon roation of the device, the Keithley immediately reported a negative value for the measured current. This result is consistent with the betavoltaic being forward biased in Experiment 1, i.e. a negative program voltage being applied as a reversed bias. This is another

aspect of Experiment 1 that warrants a repeated experiment to varify the forward bias result.

Table 6.1.
Tritium half-life values for all four experiments. Estimated error values less then 1 were rounded up to unity as a conservative estimate for error. The square root of the calculated $\chi^2_{D.F.}$ value times the estimated statistical error was reported as an estimate for systematic error.

Fit	Fit1 (days)	$\chi^2_{D.F.}$	Fit4 (days)	$\chi^2_{D.F.}$
Exp. 1	$4295^{\sigma_{stat.}\pm 1d}_{\sigma_{sys.}\pm 7.2d}$	38.5	$4272^{\sigma_{stat.}\pm 1d}_{\sigma_{sys.}\pm 1d}$	37.1
Exp. 2	$3982^{\sigma_{stat.}\pm 61d}_{\sigma_{sys.}\pm 180d}$	12.1	$4405^{\sigma_{stat.}\pm 1d}_{\sigma_{sys.}\pm 2d}$	9.7
Exp. 3	$4045^{\sigma_{stat.}\pm 1d}_{\sigma_{sys.}\pm 3d}$	3.3	$4076^{\sigma_{stat.}\pm 1d}_{\sigma_{sys.}\pm 3d}$	3.4
Exp. 4	$4033^{\sigma_{stat.}\pm 1d}_{\sigma_{sys.}\pm 1d}$	5.2	$4050^{\sigma_{stat.}\pm 1d}_{\sigma_{sys.}\pm 1d}$	4.7

Another source of systematic error that may account for the discrepancy between the results reported here and that of the canonical value, is that of tritium desorption from metal tritides. In the construction of a betavoltiac device, a thin metal film is applied to the semiconductor substrate and then exposed to tritium gas at elevated temepratures which facilitates chemical bonding to the metal. This tritiated metal film and substrate are then placed on the semiconductor diode with the metal film surface facing the semiconductor junction (89; 90). Desorption of tritium from titanium tritide and scandium tritide have been reproted in the literature with effective tritium desoprtion decay constants of approximately 2.5×10^{-6} per hour and 1.2×10^{-7} per hour respectively (87; 88). Assuming these rates would manifest as additional decays and having the effect of artificially shortening the measured half-life, these rates potentially represent 28% to 2% systematic error. These data indicate the desorption of tritium can potentially contribute to the lower half-lives calculated in this effort. It was assumed that scandium was used in the fabrication of the betavoltaics used in

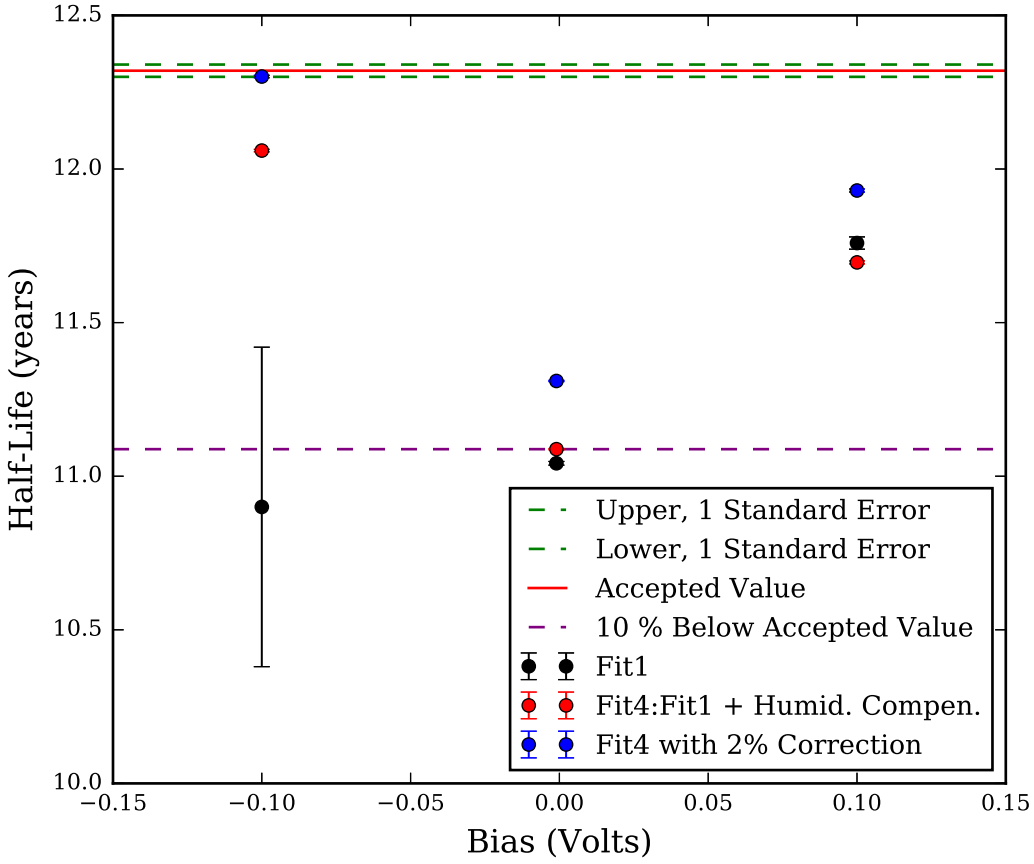

Figure 6.5. Derived tritium half-life from betavoltaic current fits verus applied bias. There is significant scatter within the data. However, values within 5 % of the accepted value appear to obtained utilizing this method.

this work. Table 6.2 presents the tritium half-lives calculated in this work with a 2% tritium desorption correction.

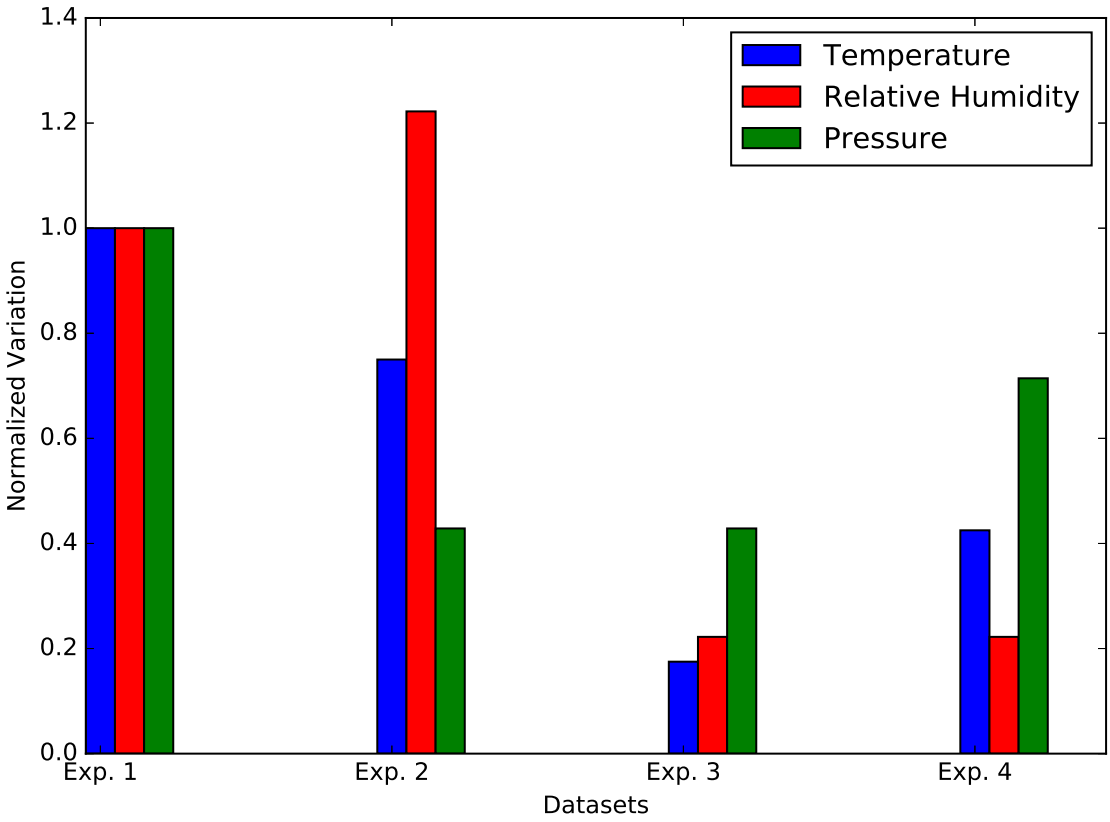

Figure 6.6. Standard deviations for temperature, pressures, humidity for all four experiments normalized to Experiment 1. This approach provides means to compare the relative environmental stability for all four experiments.

6.1.2 Half-Life Convergence

The required data collection and time required for the derived half-life value to stabilize for all four experiments can be seem in Fig. 6.7, Fig. 6.8, Fig. 6.9, and Fig. 6.10. These results indicate that the derived value for the tritium half-life converges after approximately 30 days or less. This is an important result in the context of the time required to obtain a half-life value as well as using betavoltaics to monitor nuclear decay parameters. First, previous efforts to determined the half-life of tritium

Table 6.2.
Tritium half-life values for all four experiments with a 2% correction for tritium desorption.

Fit	Fit1 (days)	$\chi^2_{D.F.}$	Fit4 (days)	$\chi^2_{D.F.}$
Exp. 1	$4381^{\sigma_{stat.}\pm 1d}_{\sigma_{sys.}\pm 7.2d}$	38.5	$4357^{\sigma_{stat.}\pm 1d}_{\sigma_{sys.}\pm 1d}$	37.1
Exp. 2	$4062^{\sigma_{stat.}\pm 61d}_{\sigma_{sys.}\pm 180d}$	12.1	$4493^{\sigma_{stat.}\pm 1d}_{\sigma_{sys.}\pm 2d}$	9.7
Exp. 3	$4126^{\sigma_{stat.}\pm 1d}_{\sigma_{sys.}\pm 3d}$	3.3	$4158^{\sigma_{stat.}\pm 1d}_{\sigma_{sys.}\pm 3d}$	3.4
Exp. 4	$4114^{\sigma_{stat.}\pm 1d}_{\sigma_{sys.}\pm 1d}$	5.2	$4131^{\sigma_{stat.}\pm 1d}_{\sigma_{sys.}\pm 1d}$	4.7

were conducted over periods spanning from years to decades. This method and these results indicate the potential to be significantly more efficient. Second, this result potentially indicates that experiments targeted at monitoring time dependence can leverage the inherent stability of this approach.

6.2 Potential Advantages to Tritium Half-Life Monitoring Using Betavoltaics

A value of $4295^{\sigma_{stat.}\pm 1d}_{\sigma_{sys.}\pm 7.2d}$ days for the half-life of tritium derived from data collected in Experiment 1 is a value within 5% of the accepted value of 4500 days. In order to place this effort into a historical context, the values for the tritium half-life obtained from previously reported values since 1950 are plotted in Fig. 6.11 and listed in Table 6.3. With the assumption that future investments and resources will be made and applied to improve the overall accuracy of this method and to characterize sources of systematic error inherent in the approach, three are several advantages to using betavoltaics for measuring and monitoring nuclear decays parameters:

1. Given that this approach is measuring a macroscopic current composed of a myriad of interactions all happening coincidentally, this approach has an intrinsic insensitivity to dead time and pile up effects that plague detector based detection schemes. This approach therefore facilitates the use of large sources.

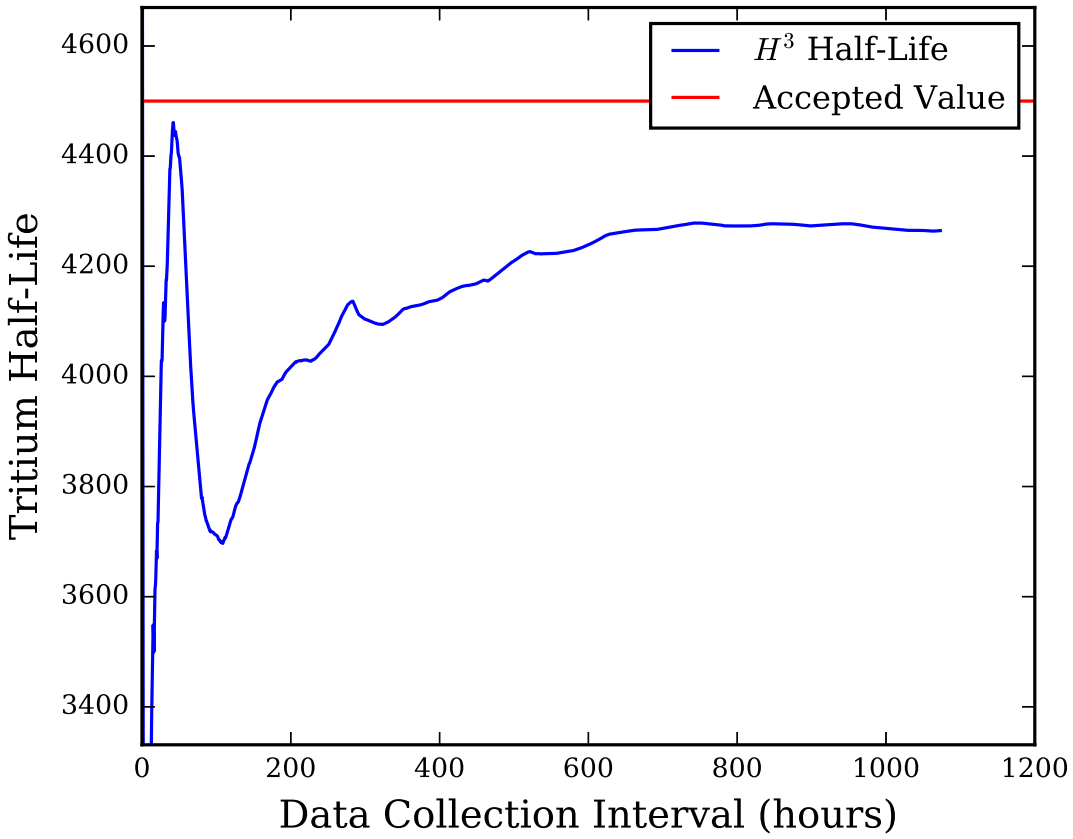

Figure 6.7. Derived tritium half-life versus data collection period for Experiment 1. This graph illustrates the data collection and time required for the derived half-life value to stabilize. The data for Experiment 1 converges to tritium half-life value of 4265 days after approximately 34 days.

2. The size of the betavoltaic devices lend themselves to being isolated from environmental conditions. The compact nature of these devices leads itself to applications where are large network of portable sensors are dispsersed over a large geographical area.

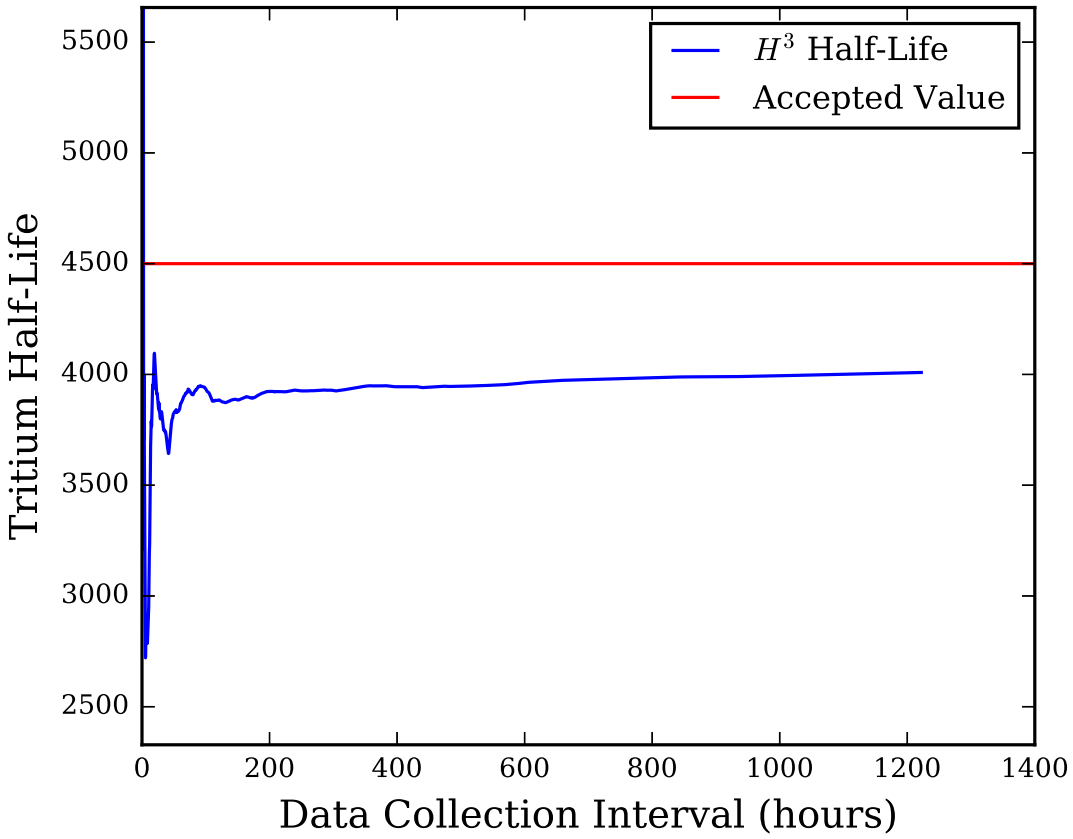

Figure 6.8. Derived tritium half-life versus data collection period for Experiment 2. This graph illustrates the data collection and time required for the derived half-life value to stabilize. The data for Experiment 2 converges to tritium half-life value of 4009 days after approximately 17 days.

3. The inherent stability of these devices and the potential ability to determine nuclear decay parameters of long lived radioisotopes efficienctly is another advantage over detector based techniques.

4. In the event that representative reference diodes can be obtained, measurement of both reference diodes and betavoltaics in parallel allow for the isolation physical mechanisms associated with nuclear decay.

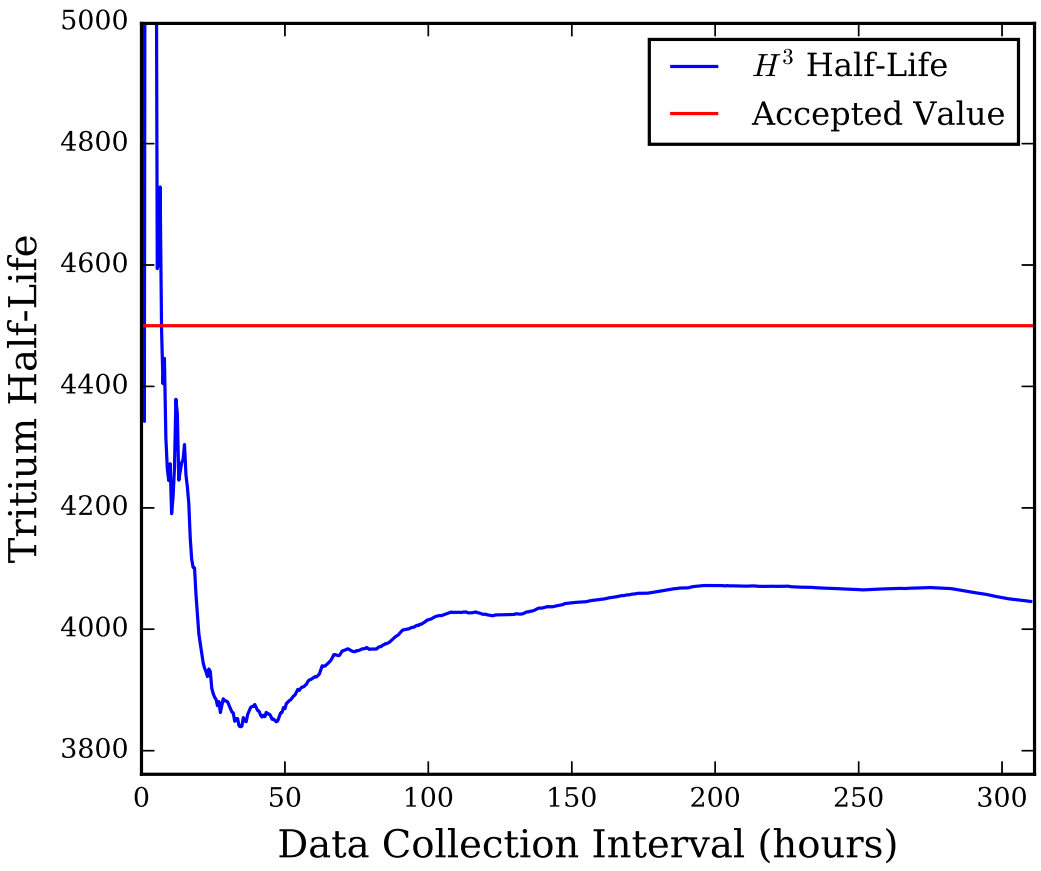

Figure 6.9. Derived tritium half-life versus data collection period for Experiment 3. This graph illustrates the data collection and time required for the derived half-life value to stabilize. The data for Experiment 3 converges to tritium half-life value of 4046 days after approximately 8 days.

5. I_{dark} is likely to be independent of the amount of tritium present in the betavoltaic device in the absence of any β induced degradation effects. Therefore, doubling the amount of tritium in a betavoltaic device doubles I_{dark} and thus doubles the signal to noise ratio of I_{rad} to I_{dark}.

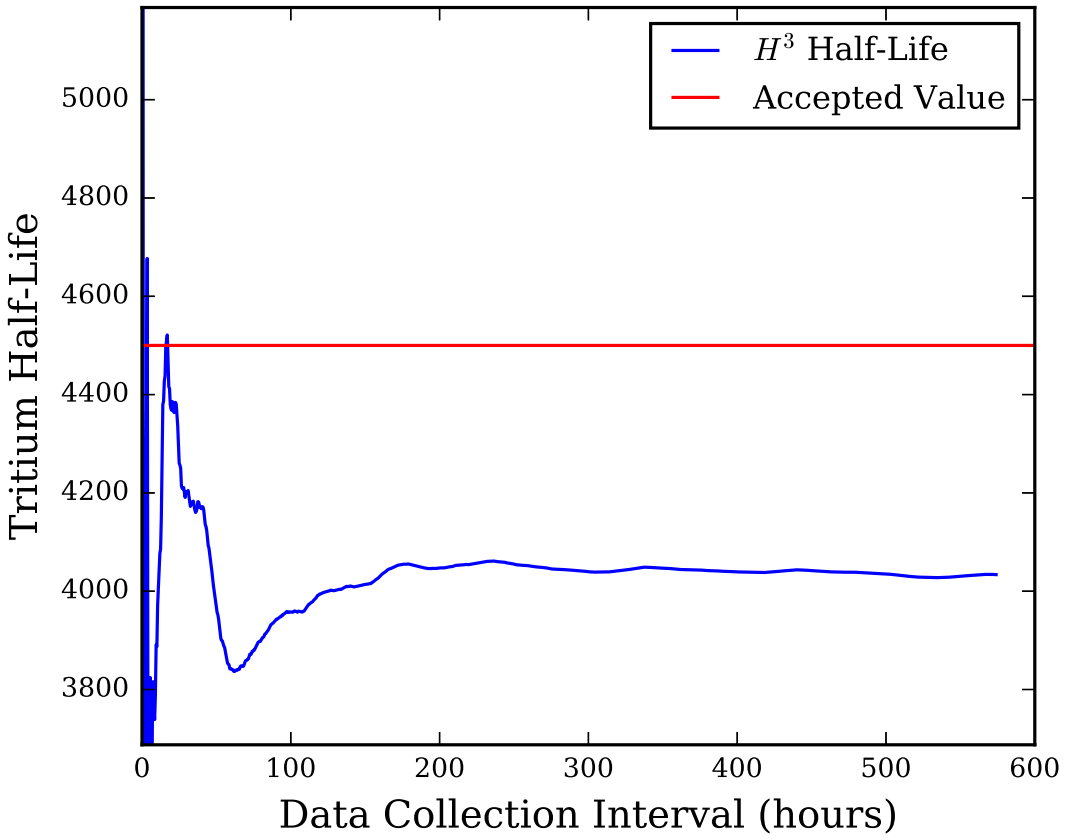

Figure 6.10. Derived tritium half-life versus data collection period for Experiment 4. This graph illustrates the data collection and time required for the derived half-life value to stabilize. The data for Experiment 4 converges to tritium half-life value of 4034 days after approximately 8 days.

6.3 Methodology Refinement

There are numerous aspects to this experimental setup that could be implemented in order to improve the overall setup stability and accuracy of future half-life determinations. The following discussion highlights these aspects, which focus on the betavoltaic device procurement process and the experimental setup.

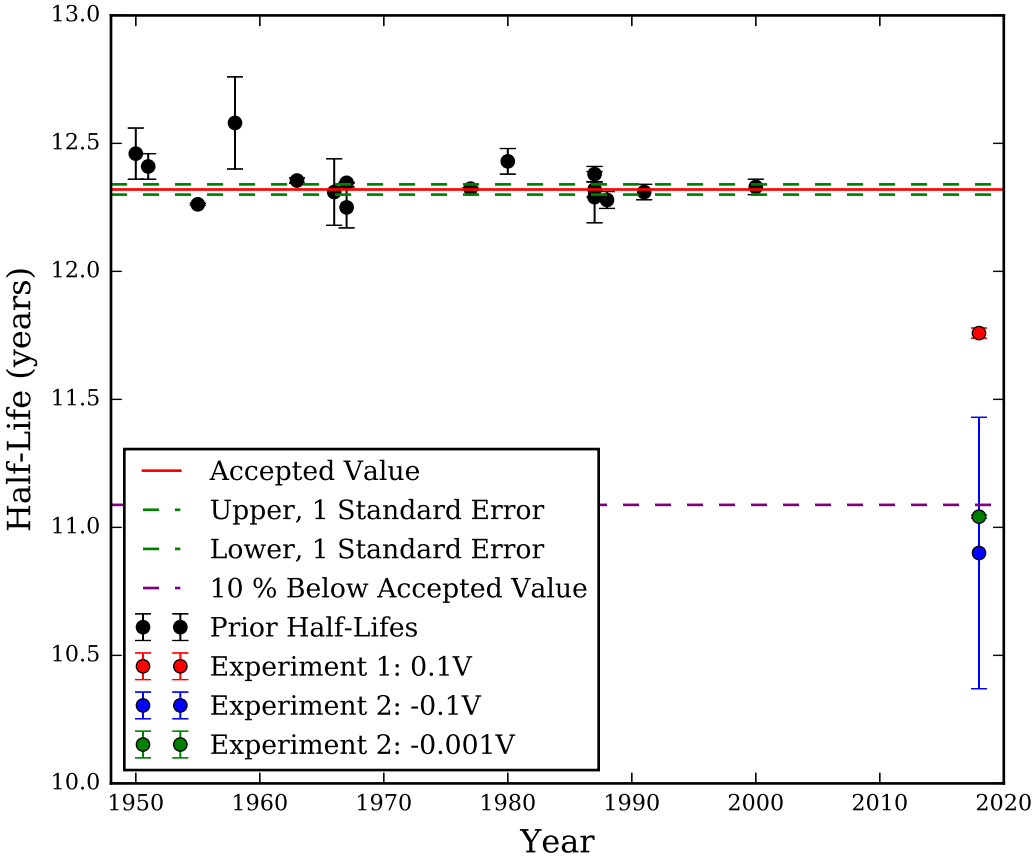

Figure 6.11. Measured tritium half-lives since 1950, and the calculated value from Experiment 1.

6.3.1 Device Requirements and Procurement Process

This work has highlighted the importance of characterizing the behavior of the semiconductor diode used in the fabrication of betavoltaic. Efforts were taken to obtained as much information and data on the procured betavoltaic devices prior to and post tritiation. These efforts can best to described as ad hoc requests for specific information on a as needed basis. There was no agreed upon device specifications prior to procurement of the devices from City Labs. Nor was there a list of

Table 6.3.
Reported Tritium Half-Life Values Since 1950.

Date	Author(s)	Measurement Method	Half-Life (yr)	Uncertainty (yr)	Data Collection Period
1950	Jenks, et al. (62)	Helium-3 collection	12.46	0.10	206 days
1951	Jones (63)	Beta counting	12.41	0.05	N/A
1955	Jones (64)	Helium-3 collection	12.262	0.004	578 days, 893 days
1958	Popov, et al. (65)	Calorimetry	12.58	0.18	390 days
1963	Eichelberger, et al. (66)	Calorimetery	12.355	0.010	4 years
1966	Merritt and Taylor (67)	Beta counting	12.31	0.13	13 years
1967	Jordan et al.(68)	Calorimetry	12.346	0.002	6 years
1967	Jones (69)	Helium-3 collection	12.25	0.08	450 to 800 days
1977	Rudy and Jordan (70)	Calorimetry	12.3232	0.0043	16 years
1980	Unterweger, et al. (71)	Beta counting	12.43	0.05	18 years
1987	Budick, et al. (72)	Bremsstrahlung counting	12.29	0.10	320 days
1987	Oliver, et al. (73)	Helium-3 collection	12.38	0.03	1 to 2 years
1987	Simpson (74)	Beta counting	12.32	0.03	5.5 years
1988	Akulov, et al. (75)	Helium-3 collection	12.279	0.033	846 days
1991	Budick, et al. (76)	Bremsstrahlung counting	12.31	0.03	5.5 years
2000	Unterweger and Lucas (77)	Beta counting	12.33	0.03	38 years
2005	Akulov and Mamyrin (78)	Helium-3 collection	12.264	0.018	?
2018	This work	Betavoltaic current	11.759	0.020	45 days

technical information such as I-V curves to be provided upon receipt of the devices. Future procurements should address this issue via specific contract language and/or a memorandum of understanding (MoU). This contract language and/or MoU should attempt to incorporate as many of the following recommendations, and the entire list should be considered during negotations prior to procurement. It is important to note that in order to successfully execute these recommendations, coordination and negotiations with the manufacturer prior to device fabrication is required.

1. The highest short circuit current possible should be pursued. This equates to maximizing amount of tritium present in the device in order to increase the signal to noise ratio of I_{rad} to I_{dark}.

2. Diode Selection and Chacterization Process:

Step 1. Identify four diodes whose I-V curves and measured R_{SH} values are within a specified range prior to tritiation. This range would have to be negotiated with the manufacturer. Ideally, four diodes whose R_{SH} values are all within 1% of one-another may serve as an initial target, as well as having R_{SH} values as high as possible.

Step 2. Four diodes are to be characterized prior to tritation. A minimum of 5 I-V curves is to be taken for each diode over the range of -0.3 to 1 volts. Temperature and humidity at the time of measurement for each I-V curve is to be recorded. The test equipement used to take electrical measurements and monitor environmental conditions as well any associated configuration parameters are to be recorded. I-V curves, environmental data, electrical and environmental setup, and configuration information are to be provided upon receipt of the devices. Access to this data for review prior to selectrion and triation would be ideal.

Step 3. Two of the four diodes are selected for tritiation. This procedure assumes a 100% yield from the triation process. This, howeve,r is unlikely to be the case. The number of devices needed to undergo Steps 1 and 2 to ensure four functional devices will have to be negotiated with the manufacturer.

Step 4. Repeat Step 2.

Optional Provide printed circuit board cards (2x) to manufacturer for population of betavoltaics. This would facilitate the removal of DIP sockets from the electrical confirguration. I-V curves post population are to be provided in order to confirm device functionality and that no damage was done to the devices during the population process.

The intent of this procedure is to ensure representative reference diodes are procured. These reference diodes potentially provide an effective method to isolate

I_{rad}. This concept was explored in this work, but not implemented due to disimiliarity of the reference diodes procured.

6.3.2 Setup Refinement

Numerous aspects of the overall experimental setup can be improved upon. These aspects include both electrical measurement and environmental mitigations.

1. Electrical Measurement

   Measurement Instrumentation A Keithley 2634B was implemented in this setup, which provides roughly an accuracy of 70 pA at 100 nA. A Keithley 6487 picoammeter, an instrument designed for sub nanoampeter, could be implemented in future experiments. The 6487 has comparable resolution and accuracy as that of the 2634B at a third of the price. This would faciliate the monitoring of another betavoltaic and reference diode pair.

   Triaxial Cable Type and Length The cables used in this experiment were standard 7078-TRX ten foot triaxial cables. These are small diameter cables. The small diameter increases shunt capacitance, which is unwanted. Ultra low noise, low capacitance cables could be implemented in future experiments. Keeping cable lengths to a minimum is another method by which shunt capacitance can be reduced. Shunt capacitance reduction would decrease the time required for the setup to stabilize upon power cycling as well as reduce delay and settling time for I-V sweeps.

   I-V Sweep Parameter Optimization The I-V curve sweep parameters for this setup are not optimal. Futher work could be done to optimize these parameters for repeatability and resolution. As perviously stated the reduction of shunt capacitance will aid the refinement of the I-V sweep data.

Auxiliary Power Supply (APS) During the course of this effort, several power outages occured which caused breaks in the data aqusition as well as destabilization of the setup. An APS was implemented in the experimental setup, however it was not sufficient to provide AC power for more than a few hours. An APS that could provide A 3000VA APS can be purchased for less than $1500 dollars. This investment would increase the ability for continous data acquistion in the event of facility power loss. The APS would provide the added benefit of AC power filtering.

2. Environmental Mitigations

Humidity Humidity was mitigated in this setup by the use of dessicant. A hermetic container with electrical feedthroughs should be considered for future experiments. The betavoltaic devices as well as the DUT board could be populated in a dry nitrogen glove box and dessicant packages could be added to the container volume prior to closure. Another alternative is the container, in additional to electrical feedthroughs, could be designed to be continously purged with dry nitrogen at positive pressure. This approach would greatly reduce the effects of parasitic leakage paths due to the combination of surface contamination and moisture. In conjunction with the implementation of either a hermetic chamber or continous dry nitrogen purging, an electrical surface decontamination process shoud be implemented. All surfaces including the DUT board, electrical interconnects, and the betavoltaic devices should never be handled without latex gloves. Prior to assembling the final configuration for electrical measurement and monitoring, all electrical surfaces should be wipe down with isopropanol in order to remove any surface contamination.

Temperature Temperature variations could be further mitigated by the implementation of a hermetic chamber and a galden bath. Galden is a

proprietary, high performance, inert, polyether fluid used in temperature management applications. This fluid in conjuntion with a precision temperature bath could be implemented in future experimental setups to control the temperatue to with 0.005 °C. This approach would require the use of a hermetic chamber. Monitoring of the galden fluid would need to be addressed in order to compensate for evaporation, or a closed temperature control system could be designed.

Pressure Ambient pressure of the experiment was not mitigated in this setup but only monitored. The implementation of a hermetic, rigid container would provide the additional benefit of ambient pressure stability.

REFERENCES

REFERENCES

Röntgen, W. (1896). On a New Kind of Rays. *Science*, 3(59), 227-231.

Becquerel, H., (1896) Sur les radiations emises par phosphorescence. *Comptes Rendus* Acad. Sci. Paris, t. 122, p. 420-421.

Chayut, Michael. (1991). J. J. Thompson: The Discovery of the Electron and the Chemists. *Annals of Science*, 48(6), 527-545.

L'Annunziata, M., & Ebrary, Inc. (2007). *Radioactivity Introduction and History.* Burlington: Elsevier Science.

E. Rutherford. Uranium radiation and the electrical conduction produced by it. *Philosophical Magazine*, xlvii:109163, January 1899.

E. Rutherford. A radioactive substance emitted from thorium compounds. *Philosophical Magazine*, xlix:114, January 1900.

E. Rutherford. The magnetic and electric deviation of the easily absorbed rays from radium. *Philosophical Magazine*, v:177187, February 1903.

E. Rutherford and F. Soddy. The cause and nature of radioactivity - part i.*Philosophical Magazine*, iv:370396, September 1902.

E. Rutherford and F. Soddy. The cause and nature of radioactivity - part ii. *Philosophical Magazine*, iv:569585, November 1902.

E. Rutherford and F. Soddy. The radioactivity of uranium. *Philosophical Magazine*, v:441445, April 1903.

E. Rutherford and F. Soddy. A comparative study of the radioativity of radium and thorium. *Philosophical Magazine*, v:445457, April 1903.

E. Rutherford and F. Soddy. Condensation of the radioactive emanations. *Philosophical Magazine*, v:561576, May 1903.

E. Rutherford and F. Soddy. Radioactive change. *Philosophical Magazine*, v:576591, May 1903.

E. Rutherford, H. Geiger, and H. Bateman. The probability variations in the distribution of particles. *Philosophical Magazine*, xx:698707, October 1910.

Rutherford, E., Chadwick, J., & Ellis, C. (1951). *Radiations from Radioactive Substances* (Re-issue of the edition of 1930. Reprinted with corrections.. ed.). Cambridge [England]: University Press.

J. Buncher. *Phenomenology of Time-Varying Nuclear Decay Parameters* Ph.D. thesis, Purdue University, 2010.

E. D. Falkenberg. Radioactive Decay Caused by Neutrinos? *Apeiron*, 8:32-45, 2001.

S. E. Shnoll, V. A. Kolombet, E. V. Pozharskii, T. A. Zenchenko, J. M. Zvereva, A. A. Konradov. Realization of discrete states during fluctations in macroscopic processes. *Physics-Uspekhi*, 41:1025-35, 1998.

D. P. Veprev, V. I. Muromtsev. Evidence of solar influence on tritium decay rate. *Astropart. Phys.,* 36:26-30, 2012.

Lobashev, Aseev, Belesev, Berlev, Geraskin, Golubev, Kazachenko, Kuznetsov, Ostroumov, Rivkis, Stern, Titov, Zadorozhny, and Zakharov. "Direct Search for Mass of Neutrino and Anomaly in the Tritium Beta-spectrum." *Physics Letters B* 460.1 (1999): 227-35.

Lobashev, V. M. "Direct Search for the Neutrino Mass in the Beta Decay of Tritium: Status of the Troitsk -Mass Experiment." *Physics of Atomic Nuclei* 63.6 (2000): 962-69.

T. Adams. *Hydrogen Loading System Development and Evaluation of Tritiated Substrates to Optimize Performance in Tritium Based Betavoltaics.* Ph.D. thesis, Purdue University, 2014.

Neudeck, G. (1983). *The PN junction diode* (Repr. with corrections.. ed., Modular series on solid state devices ; v. 2). Reading, Mass.: Addison-Wesley.

Pierret, R. (1983). *Semiconductor Fundamentals* (Repr. with corrections.. ed., Modular series on solid state devices ; v. 1). Reading, Mass.: Addison-Wesley.

D. O'Keefe, B.L. Morreale, R.H. Lee, J. Buncher, J.H. Jenkins, E. Fischbach, T. Gruenwald, D. Javorsek, and P.A. Sturrock. Spectral content of 22 Na/ 44 Ti decay data: Implications for a solar influence. *Astrophysics and Space Science*, 2013, 344(2), 297-303.

Jere H. Jenkins, Ephraim Fischbach, John B. Buncher, John T. Gruenwald, Dennis E. Krause, Joshua J. Mattes. Evidence of Correlations Between Nuclear Decay Rates and Earth-Sun Distance. *Astropart. Phys.*, 2010, Vol.32 (1), p.42-47

P. A. Sturrock, E. Fischbach, and J.H. Jenkins. Further evidence suggestive of a solar influence on nuclear decay rates. *Solar Physics*, 272(1):1-10, 2011.

P. A. Sturrock, J. B. Buncher, E. Fischbach, J. T. Gruenwald, D. Javorsek, J. H. Jenkins, R. H. Lee, J. J. Mattes, and J. R. Newport. Power Spectrum Analysis of BNL Decay-Rate Data. *Astropart. Phys.*, 34:121-127, 2010.

J. Heim. *The Determination of the Half-Life* ^{32}*Si and Time Varying Nuclear Decay.* Ph.D. thesis, Purdue University, 2015.

J. Nistor. *Direct and Indirect Searches for Anomalous Beta Decay.* Ph.D. thesis, Purdue University, 2015.

Jere H. Jenkins, Kevin R. Herminghuysen, Thomas E. Blue, Ephraim Fischbach, Daniel Javorsek, Andrew C. Kauffman, Daniel W. Mundy, Peter A. Sturrock, and Joseph W. Talnagi. Additional experimental evidence for a solare influence on nuclear decat rates. *Astropart. Phys.*, 37:81-88, 2012.

Jere H. Jenkins and Ephraim Fischbach, Perturbation of nuclear decay rates during the solar flare of 2006 December 13. *Astropart. Phys.*, 31(6):407-411, 2009.

Jenkins, Jere H., Ephraim Fischbach, Peter A. Sturrock, and Daniel W. Mundy. "Analysis of Experiments Exhibiting Time-Varying Nuclear Decay Rates: Systematic Effects or New Physics?" (2011). Web.

K J Ellis. "The Effective Half-life of a Broad Beam 238 Pu/Be Total Body Neutron Irradiator." *Physics in Medicine and Biology* 35.8 (1990): 1079-087. Web.

Parkhomov, A. G. "Researches of Alpha and Beta Radioactivity at Long-term Observations." (2010). Print.

Parkhomov, A. G. "Periods Detected During Analysis of Radioactivity Measurements Data." (2010). Web.

Baurov, Yu. A., Yu. G. Sobolev, V. F. Kushniruk, A. N. Kuznetzov, and A. A. Konradov. "Experimental Investigation of Changes in Beta-decay Count Rate of Radioactive Elements." (1999). Web.

Schrader, H. "Half-life Measurements of Long-lived RadionuclidesNew Data Analysis and Systematic Effects." *Applied Radiation and Isotopes* 68.7 (2010): 1583-590. Print.

Sturrock, Parkhomov, Fischbach, and Jenkins. "Power Spectrum Analysis of LMSU (Lomonosov Moscow State University) Nuclear Decay-rate Data: Further Indication of R-mode Oscillations in an Inner Solar Tachocline." *Astropart. Phys.* 35:755-758, 2012.

Jenkins, Fischbach, Javorsek, Lee, and Sturrock. "Concerning the Time Dependence of the Decay Rate of 137Cs." *Applied Radiation and Isotopes* (2012): Applied Radiation and Isotopes. Web.

Siegert, Schrader, and Schtzig. "Half-life Measurements of Europium Radionuclides and the Long-term Stability of Detectors." *Applied Radiation and Isotopes* 49.9 (1998): 1397-401. Web.

Steinitz, Piatibratova, and Kotlarsky. "Possible Effect of Solar Tides on Radon Signals." *Journal of Environmental Radioactivity* 102.8 (2011): 749-65. Web.

Sturrock, P.A., Steinitz, G., Fischbach, E., Javorsek, D., and Jenkins, J.H. "Analysis of Gamma Radiation from a Radon Source: Indications of a Solar Influence.(Report)." *Astropart. Phys.* 36.1 (2012): 18. Web.

Sturrock, P., A. Buncher, J. Fischbach, B. Gruenwald, E. Javorsek, T. Jenkins, D. Lee, H. Mattes, and R. Newport. "Power Spectrum Analysis of Physikalisch-Technische Bundesanstalt Decay-Rate Data: Evidence for Solar Rotational Modulation." *Solar Physics* 267.2 (2010): 251-65.

"Dr. Tesla Writes of Various Phases of his Discover," *New York Times*, 6 February 1932, p. 16, col. 8.

T. Mohsinally. *An Investigation Into The Phenomenological Realtion Between Solar Activity and Nuclear Beta-Decay Rates* Ph.D. thesis, Purdue University, 2015.

Knoll, G. (2010). *Radiation detection and measurement* (4th ed.). Hoboken, N.J.: John Wiley.

MAESTRO-32, MCA Emulator for Microsoft Windows 2000 Professional and XP Professional. Version 6.0. USA: Advanced Measurement Technologies Inc., 2006.

Brookhaven National Laboratory, and United States. Dept. of Energy. Office of Scientific Technical Information. *NNDC (National Nuclear Data Center) On-line Services Documentation*. Upton, N.Y. : Oak Ridge, Tenn.: Brookhaven National Laboratory ; Distributed by the Office of Scientific and Technical Information, U.S. Dept. of Energy, 1987. Print.

Saint-Gobain Ceramics and Plastics Inc, *NaI(Tl) and Polysin NaI(Tl) Sodium Iodide Scintillation Material*, http://www.crystals.saint-gobain.com/sites/imdf.crystals.com/files/documents/sodium-iodide-material-data-sheet.pdf

L. L. Lucas and M. P. Unterweger, J. Res. Natl. Inst. Stand. Technol., **105**, 541 (2000).

C. R. Rudy and K. C. Jordan, *Tritium Half-Life, Progress Report MLM-2458*, U.S. Department of Energy, Mound Laboratory, Miamisburg, Ohio, December 1977, pp. 2-10.

B. M. Oliver, M. M. Bretscher, H. Farrar IV, Mass Spectrometric Determination of the Absolute Tritium Activities of NBS Tritiated Water Standards, Appl. Radait. Isot. **40**, 199 (1989).

B. Budick and H. Lin, Bull. Am. Phys. Soc. **32**, 1063 (1987).

J. J. Simpson, Phys. Rev. C **35**, 752 (1987).

S. M. Sze, *Physics of Semiconductor Devices* (Wiley, New York, 1981).

G. C. Messenger and M. S. Ash, *The Effects of Radiation on Electronic Systems* (Van Nostrand Reinhold, New York, 1986).

T. Ma and P. Dressendorfer, *Ionizing radiation effects in MOS devices and circuits* (New York: Wiley, 1989).

Keithley Instruments, Inc. *Low Level Measurements Handbook* 4th edition. (1992).

E. Jones, E. Oliphant, P. Peterson, et al., *SciPy: Open Source Scientific Tools for Python, 2001-*, http://www.scipy.org.

J. J. More, B. S. Garbow, and K. E. Hillstrom, *User Guide for MINPACK-1*, (R102 in the SciPy 0.13.0 Reference Guide Bibliography, 1980).

G. H. Jenks, F. H. Sweeton, and J. A. Ghormley, Phys. Rev. **80**, 990 (1950).

W. M. Jones, Phys. Rev **83**, 537 (1951).

W. M. Jones, Phys. Rev. **100**, 124 (1955).

M. M. Povov, I. V. Gagarinskii, M. D. Senin, I. P. Mikhalenko, and I. M. Morozov, Atomnaya Energiya **4**, 296 (1958). English translations: Soviet J. At. Energy **4**, 393-396 (1958) and J. Nucl. Energy **9**, 190-193 (1959).

J. F. Eichelberger, G. R. Grove, and L. V. Jones, *Half-Life of Tritium*, Progress Report MLM-1160, U.S. Department of Energy, Mound Laboratory, Miamisburg, Ohio, June 1963, pp. 5-6.

J. S. Merritt and J. G. V. Taylor, *Half-Life of* ^3H, Report AECL-2510, Atomic Energy of Canada Limited, Chalk River Laboratory, Chalk River, Ontario (1966) p.28.

K. C. Jordan, B. C. Blanke, and W. A. Dudley, J. Inorg. Nucl. Chem. **29**, 2129 (1967).

P. M. S. Jones, J. Nucl. Mater. **21**, 239 (1967).

C. R. Rudy and K. C. Jordan, *Tritium Half-Life*, Progress Report MLM-2458, U.S. Department of Energy, Mound Laboratory, Miamisburg, Ohio, June 1977, pp. 2-10.

M. P. Unterweger, B. M. Coursey, F. J. Schima, and W. B. Mann, Int. J. Appl. Radiat. Isot. **31**, 611 (1980).

B. Budick and H. Lin, Bull. Am. Phys. Soc. **32**, 1063 (1987).

B. M. Oliver, H. Farrar IV, and M. M. Bretscher, Appl. Radait. Isot. **38**, 959 (1987).

J. J. Simpson, Phys. Rev. C **35**, 1063 (1987).

Y. A. Akulov, B. A. Mamyrin, L. V. Khabarin, V. S. Yudenich, and N. N. Ryazantseva, Pis'ma Zh. Tekh. Fiz. **14**, 940-942 (1988). English translation: Sov. Tech. Phys. Lett. **14**, 416 (1988).

B. Budick, J. Chen, and H. Lin, Phys. Lett. **14**, 416 (1991).

M. P. Unterweger and L. L. Lucas, Appl. Radiat. Isot. **52**, 527 (2000).

Yu. A. Akulov and B. A. Mamyrin, Phys. Lett. B **600**, 41 (2004).

Yu. A. Akulov and B. A. Mamyrin, Phys. Lett. B **610**, 45 (2005).

https://www.pveducation.org/pvcdrom/solar-cell-operation/shunt-resistance

Singh, P., and Ravindra, N., Analysis of series and shunt resistance in silicon solar cells using single and double exponential models. Emerging Materials Research, 1(1), 33-38, (2012).

Priyanka, Lal, and Singh., A new method of determination of series and shunt resistances of silicon solar cells. Solar Energy Materials and Solar Cells, 91(2), 137-142, (2007).

Banerjee, S., and Anderson, W., Electron irradiation effects on the shunt resistance of silicon solar cells. Solar Cells, 20, 315-321, (1987).

Gao, Luo, Zhang, Wang, and Fu., Demonstration, radiation tolerance and design on a betavoltaic micropower. Energy, Energy, (2013).

Breitenstein, O, Rakotoniaina, J.P., Al Rifai, M. H., and Werner, M., *Shunt Types in Crystalline Silicon Soalr Cells*, Prog. Photovolt: Res. Appl. 12:529-538, (2004).

Olsen, L. (1993). Review of betavoltaic energy conversion. NASA. Lewis Research Center, Proceedings of the 12th Space Photovoltaic Research and Technology Conference (SPRAT 12), (Ogy conference (sprat 12)), 256-267.

Bower, K. (2002). Polymers, phosphors, and voltaics for radioisotope microbatteries. Boca Raton, Fla.: CRC Press.

Liu, B., Chen, Kherani, Zukotynski, and Antoniazzi. (2008). Betavoltaics using scandium tritide and contact potential difference. Applied Physics Letters, 92(8), .

Phone conversation with Dr.Thomas Adams, Purdue University, November 2, 2018.

Phone conversation with Dr. Peter Cabauy, City Labs Inc., October 29, 2018.

P. Cabauy, inventor; City Labs Inc, assignee. *Tritium direct conversion semiconductor device having active area*, US grant 9711250B2, June 6, 2013.

P. Cabauy, L. Olsen, P. Noren, inventors; City Labs Inc, assignee. *Tritium direct conversion semiconductor device*, US grant 8487507B1, December 14, 2008.

VITA

VITA

Matt and his family currently reside in Bloomington Indiana.